WISSENSCHAFTSZENTRUM WEIHENSTEPHAN FÜR

ERNÄHRUNG, LANDNUTZUNG UND UMWELT

Lehrstuhl für Ernährung und Immunologie

Tissue-specific overexpression of UPR-related C/EBP homologous protein impairs mucosal repair in *Chop*$^{IEC\ Tg/Tg}$ mice

Nadine Waldschmitt

Vollständiger Abdruck der von der Fakultät Wissenschaftszentrum Weihenstephan für Ernährung, Landnutzung und Umwelt der Technischen Universität München zur Erlangung des akademischen Grades eines

Doktors der Naturwissenschaften

genehmigten Dissertation.

Vorsitzender:		Univ.-Prof. Dr. M. Schemann
Prüfer der Dissertation:	1.	Univ.-Prof. Dr. D. Haller
	2.	Univ.-Prof. Dr. M. Gerhard

Die Dissertation wurde am 12.02.2014 bei der Technischen Universität München eingereicht und durch die Fakultät Wissenschaftszentrum Weihenstephan für Ernährung, Landnutzung und Umwelt am 27.06.2014 angenommen.

Für meine Eltern Elisabeth und Thomas Waldschmitt

Die höchste Form des Glücks ist ein Leben mit einem gewissen Grad an Verrücktheit

Erasmus von Rotterdam

ZUSAMMENFASSUNG

Chronisch entzündliche Darmerkrankungen (CED) sind immunvermittelte Erkrankungen des Gastrointestinaltrakts, welche durch komplexe Interaktion verschiedener Faktoren wie genetische Prädisposition und Umwelteinflüsse charakterisiert sind. Die Störung der Integrität intestinaler Epithelzellen ist einer der kritischen Faktoren für die Entstehung von CED. Im Hinblick auf epitheliale Dysfunktion konnten in Epithelzellen spezifische, zelluläre Stressantworten, sogenannte „unfolded protein responses“ (UPR), des endoplasmatischen Retikulums (ER) und des Mitochondriums detektiert werden, die mit der Entstehung von CED assoziiert scheinen. Diese Signalwege werden durch Akkumulation ungefalteter Proteine im ER beziehungsweise Mitochondrium aktiviert und führen in weiterem Verlauf zur Expression von „C/EBP homologous protein“ (CHOP), einem Transkriptionsfaktor, der stark mit der Induktion von Apoptose assoziiert erscheint. Bisher konnte kein funktioneller Zusammenhang zwischen UPR-vermittelter CHOP Expression und CHOP-induzierter epithelialer Apoptose in CED gezeigt werden. In der vorliegenden Arbeit sollten die Folgen einer erhöhten CHOP Expression in einer gewebsspezifischen Auflösung untersucht werden. Hierfür wurden transgene *Chop*$^{IEC\ Tg/Tg}$ Mäuse generiert, welche CHOP im Darmepithel überexprimieren.

Es konnte gezeigt werden, dass eine erhöhte Expression von CHOP die Proliferationskapazität von Dickdarmepithelzellen negativ beeinflusst. Dieser Effekt schien unabhängig von Apoptose zu sein, konnte jedoch einer durch CHOP-induzierten Verzögerung der Zellzyklus-Progression zugeordnet werden. Des Weiteren konnte festgestellt werden, dass die durch CHOP reduzierte Zellproliferation mit einer verminderten Zellmigration einherging. Obwohl *Chop*$^{IEC\ Tg/Tg}$ Mäuse diesen Effekt unter normalen Bedingungen kompensieren konnten, konnte bei mechanischer Schädigung der Mukosa eine verringerte Regenerationsfähigkeit des Dickdarmepithels beobachtet werden. Darüber hinaus zeigten sich *Chop*$^{IEC\ Tg/Tg}$ Mäuse anfälliger gegenüber einer Dextran Natriumsulfat (Dextran Sodium Sulphate, DSS)-induzierten Kolitis, die sich bereits in der frühen Entzündung durch verstärkte Immunzellinfiltration manifestierte und sich des Weiteren in der Regenerationsphase durch eine verzögerte Heilung der Mukosa auszeichnete.

Zusammenfassend deuten unsere Ergebnisse darauf hin, dass eine verstärkte Expression von CHOP im Darmepithel das Risiko für die Entstehung von CED erhöht. Im Hinblick auf mögliche Therapieansätze sollte beachtet werden, dass CHOP als potentielles Zielprotein nicht nur Mechanismen der Apoptose beeinflusst, sondern vielmehr die Proliferation und damit die Regenerationsfähigkeit des Epithels limitiert.

ABSTRACT

Inflammatory bowel diseases (IBD) are immune-mediated disorders of the gastrointestinal tract that are characterized by complex interactions of different factors, including genetic predisposition and environmental impacts. The disruption of intestinal epithelial integrity is one of the crucial factors considering causative triggers of IBD. With regard to epithelial dysfunction, specific cellular stress responses of the endoplasmic reticulum (ER) and the mitochondrion, also known as unfolded protein responses (UPR), could be detected in epithelial cells that have been associated with the development of IBD. These signaling pathways are activated upon accumulation of unfolded proteins in ER and mitochondrion, respectively, which subsequently leads to the expression of C/EBP homologous protein (CHOP), a transcription factor highly associated with the induction of apoptosis. Up to now, no functional correlation between UPR-related CHOP expression and CHOP-induced epithelial apoptosis has been shown in the onset of IBD. In this study, we aimed to investigate the consequences of enhanced CHOP expression in a tissue-specific resolution. Therefore, we generated transgenic *Chop*$^{IEC\ Tg/Tg}$ mice that conditionally overexpress CHOP in intestinal epithelial cells (IECs).

It has been shown that enhanced expression of CHOP negatively affected the proliferative capacity of colonic epithelial cells. This effect was most likely independent of apoptosis, but was rather associated with a CHOP-induced delay in cell cycle progression. Furthermore, it has been demonstrated that CHOP-induced decrease in cell proliferation was correlated with reduced cell migration. Even though *Chop*$^{IEC\ Tg/Tg}$ mice were able to compensate this effect under normal conditions, transgenic mice exhibited an impaired regenerative ability of the colonic epithelial lining in response to mechanically induced mucosal tissue damage. In addition, *Chop*$^{IEC\ Tg/Tg}$ mice were more susceptible to Dextran Sodium Sulphate (DSS)-induced colitis that already became evident in early inflammation due to enhanced immune cell infiltration and was further characterized by delayed mucosal healing during recovery.

In conclusion, our data suggest that high expression of CHOP in the intestinal epithelium increases the risk of IBD. With regard to potential therapeutic approaches, it should be considered that targeting CHOP protein not only affects mechanisms of apoptosis, but rather limits the proliferative capacity and regenerative ability of intestinal epithelial lining.

TABLE OF CONTENTS

1 Introduction

Since decades scientists dedicated their work to the examination of molecular regulation patterns that cause the development and maintenance of diseases. Much knowledge was gained from intensive studies of pathological findings, thereby translating the disease-phenotype into susceptibility loci [1, 2]. The decoding of the human genome opened the door for genome wide association studies (GWAS) that allow the investigation of patient cohorts for unknown genetic variants [3-5]. Although GWAS successfully identified novel genetic risk loci and new molecular markers for diagnostic application, the etiology of complex disorders remains elusive [6, 7]. It is largely unknown to which extend genetic predispositions do impact on inherited risk, as distinct environmental factors contribute to the outcome of disease-phenotypes [8, 9]. Therefore, studies with genetically modified animal models provide important insights into the architecture of complex mechanisms by elucidating the gene-gene and gene-environment interactions, respectively [10, 11].

Complex diseases, such as chronic illness has become more prevalent in the developing world [12-14]. Among those, IBD have been observed with steadily rising incidence rates in North America and Western Europe strongly associated with environmental triggers resulting from modern lifestyle, such as diet, changes in enteric microbiota, smoking, and stress [14-17]. The understanding of how these environmental factors do implicate in inherited genetic risk will hopefully lead to new therapeutic approaches to decrease the burden of chronic diseases.

1.1 Inflammatory bowel diseases

IBD including the major subtypes Crohn's disease (CD) and ulcerative colitis (UC) are chronic relapsing, immune-mediated disorders of the gastrointestinal tract that are triggered by complex interactions of genetic predisposition and environmental factors (Figure 1) [18-22]. The precise etiology of IBD is still unknown, but GWAS with IBD patients as well as experimental studies with human samples and genetically engineered mouse models identified distinct genetic susceptibility loci for CD and UC, respectively, that affect the maintenance of gut homeostasis [23-29].

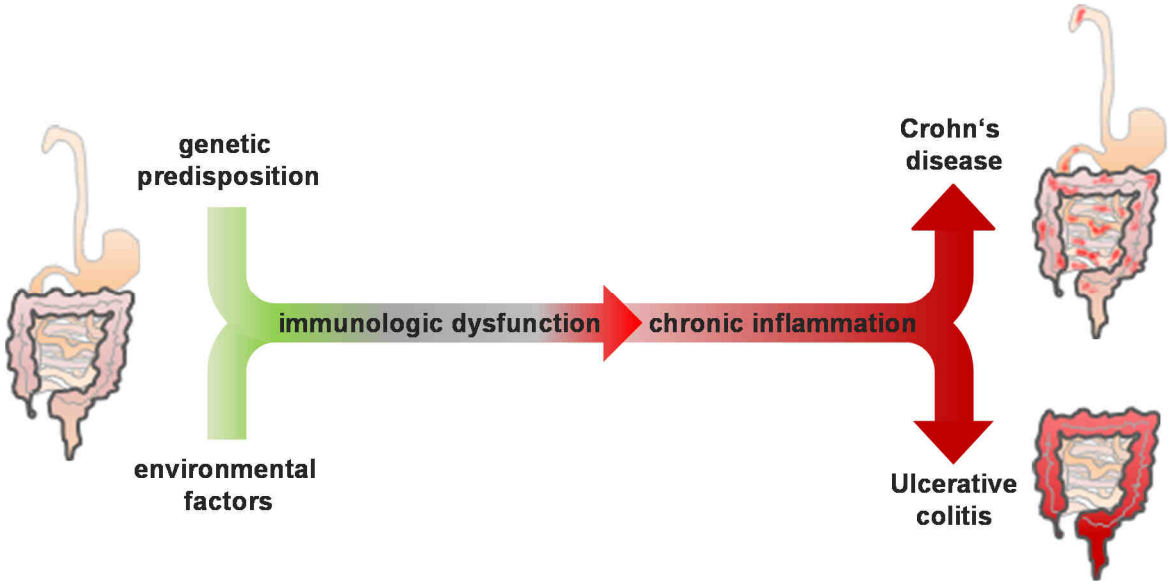

Figure 1. Disease-phenotype of the IBD subtypes CD and UC.

The development of IBD is triggered by complex interactions of genetic predisposition and environmental factors, thus leading to sustained immunologic dysfunction that drives the disease-phenotype of CD and UC. Chronic inflammation appears in any part of the gastrointestinal tract in CD, while it is restricted to the colon in UC. Here, colitis usually starts in the rectum and spreads proximally in severe UC.

Up to now, 163 IBD loci have been reported to influence innate and adaptive immune mechanisms relevant for intestinal barrier functions and microbial defense [27, 28, 30-36]. Even though there is considerable overlap in the susceptibility loci between CD and UC (110 out of 163), the two forms of IBD distinguish in the immune-mediated response to environmental factors, including commensals and pathogens (Figure 2) [33, 37]. Immunologic dysfunction may be further triggered by disease-specific epithelial cell responses, such as autophagy, apoptosis/necroptosis, ER stress, and oxidative stress [28, 36, 38, 39]. In this regard, changes in epithelial integrity, including intestinal permeability, epithelial cell proliferation or apoptosis, cellular redox equilibrium, and alterations in synthesis and secretion of antimicrobial substances are frequently associated with sustained UPR of the ER and mitochondria (mt) [28, 40-42].

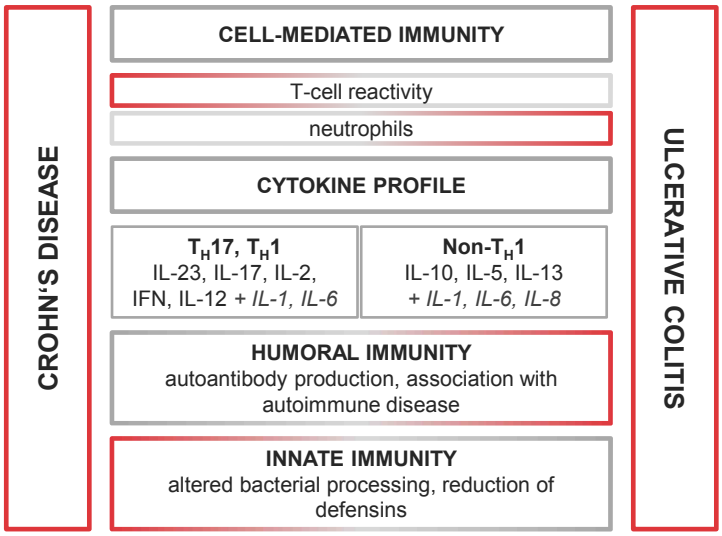

Figure 2. Contribution of immune and inflammatory response to CD and UC.

Cell-mediated, humoral, and innate immune responses distinctly influence the disease-phenotype of CD and UC. T-cell reactivity is enhanced in CD, but either normal or decreased in UC. Here, enhanced neutrophil infiltration could be observed. Regarding the cytokine profile, CD is characterized by T_H17 response including the increased expression of interleukin (IL)-23, IL-17, IL-2, IFN, IL-12, but also other cytokines, such as IL-1 and IL-6, respectively. Cytokines, such as IL-10, IL-5, IL-13 are prominent in UC defining a non-T_H1 T-cell response. Humoral immune response could be observed in UC indicating an autoimmune responsiveness. Disturbances of innate immune mechanisms have been implicated in CD showing an altered processing of intracellular bacteria as well as decreased synthesis of defensins.

1.2 Unfolded protein responses

Both unicellular and multicellular organisms are highly dependent on molecular mechanisms that allow a fast adaptation to environmental changes to enhance cell survival. In this context, the intestinal homeostasis is highly dependent on the maintenance of intestinal epithelial integrity. The intestinal epithelial layer comprises distinct cell types, such as absorptive epithelial cells, enteroendocrine cells, Goblet cells, Paneth cells, and stem cells whose optimal cell function is steadily challenged by external environmental factors, including diet and the microbiota [43]. In particular, the capacity to adapt to high levels of protein demand often decides cell fate, consequently affecting whole tissue homeostasis [44-46]. The UPR describes a physiological process contributing to the protein folding capacity of eukaryotic cells [47]. Herein, protein folding is supported by heat-shock proteins (HSP), also called chaperones, that bind to unfolded polypeptides enhancing their stabilization during protein structure formation [48]. Several protein families, such as specifically modified membrane proteins as well as secretory proteins, are synthesized along the ER and Golgi apparatus network [49]. In the cytoplasmic compartment protein folding is facilitated by HSP70, while structure formation in the ER is promoted by glucose-regulating peptide (GRP) 78 [50, 51]. Both HSP70 and GRP78 are ubiquitously expressed, but are associated with other proteins

defining a sensing complex for unfolded proteins. HSP70 forms complexes with the transcription factor heat shock factor (HSF) 1, while GRP78 is associated with the three ER transmembrane proteins activating transcription factor (ATF) 6, PKR-like ER kinase (PERK), and inositol requiring enzyme 1 (IRE1) [50, 51]. In case of enhanced protein demand mis- and malfolded proteins can aggregate in the cytoplasm and the ER, respectively. Consequently, chaperones dissociate from their binding partners to support protein refolding. The release of the sensor proteins HSF1, ATF6, PERK, and IRE1 initiates the signaling cascade of the cytosolic UPR and the ER UPR, respectively [50-52]. Subsequently, specifically activated transcription factors facilitate the restoration of cellular homeostasis inducing the expression of UPR-related genes, such as chaperones (Figure 3) [53].

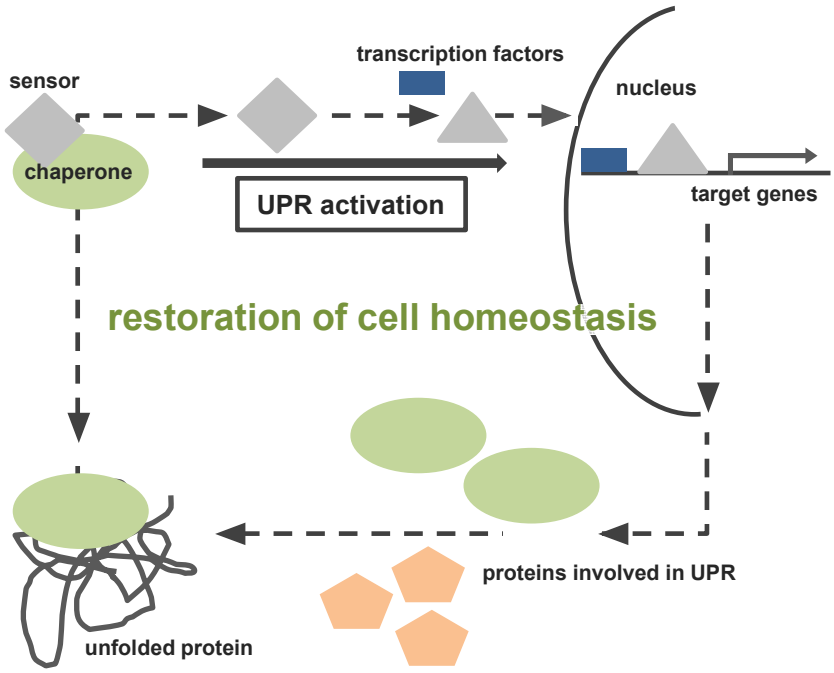

Figure 3. Model of UPR in restoration of cell homeostasis.
Under physiological conditions, specific sensors for incompletely folded proteins form inactive complexes with associated chaperones. Upon accumulation of malfolded protein aggregates chaperones dissociate from their binding partners supporting protein structure formation. The release of the sensor proteins initiates a signaling cascade termed as UPR. The UPR leads to the activation and/or synthesis of specific transcription factors that in turn induce the expression of UPR-related genes, such as chaperones, to restore cellular homeostasis.

When the accumulation of mis- and malfolded proteins exceeds the cellular protein folding capacity, sustained UPR activation aims towards apoptosis to eliminate unhealthy cells [54, 55]. In this context, unresolved UPR signaling might cause defective apoptosis strongly associated with the pathophysiology of IBD [56].

1.3 UPR in IBD-associated processes

It is well known that ER stress plays a critical role in the pathogenesis of various diseases, such as diabetes, Alzheimer's disease, IBD, and cancer [28, 57-61]. GWAS with IBD patients have identified several ER stress-related genes, such as *cytoplasmic polyadenylation element binding protein 4* (*CPEB4*), *ORM1-like 3* (*ORMDL3*), *serine incorporator 3* (*SERINC3*), and *X-box binding protein 1* (*XBP1*) as genetic factors that may affect the risk of IBD by deregulating ER UPR and apoptotic signaling under inflammatory conditions [26, 28, 36, 62, 63]. While dysfunction in the UPR-related XBP1 has been linked to the development of enteric inflammation, consequences of deregulated ORMDL3 (ER Ca^{2+} homeostasis), CPEB4 (polyadenylation and translation of proteins), and SERINC3 (ER-Golgi stress) in IBD remain elusive [28, 63-66]. However, ER stress signaling has been observed in underlying mechanisms of IBD implicating in goblet cell homeostasis, Paneth cell function, autophagy, and T_H17 cell-driven immune responses (Figure 4) [28, 39, 67-70].

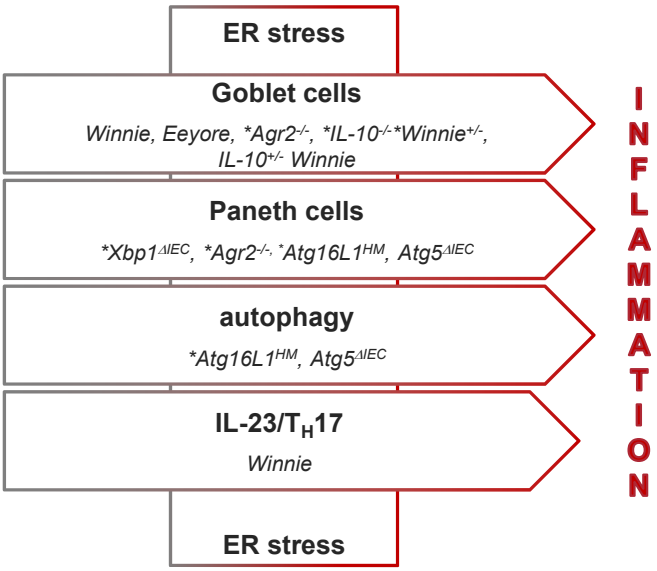

Figure 4. ER stress-associated processes in intestinal inflammation.
ER stress signaling has been found in IBD-associated processes using genetically modified mice with defects in goblet cell homeostasis, Paneth cell function, and autophagy. Genes identified as genetic risk variants for IBD are labeled with *.

With regard to corresponding mouse models, ER stress in goblet cells has been linked to spontaneously developing colitis in Mucin 2 (MUC2)-deficient mice (*Winnie, Eeyore, IL-10$^{-/-}$Winnie$^{+/-}$, IL-10$^{+/-}$ Winnie*) [68, 71, 72]. Furthermore, ER stress signaling has been observed in mice coping with spontaneous enteritis induced by disruption of goblet cell and Paneth cell function (*Agr2$^{-/-}$*, *Xbp1$^{\Delta IEC}$*) [28, 73]. Of note, Paneth cell depletion has been further described in mouse models with defects in signaling pathways of autophagy. In this context,

signs of ER stress have been evaluated in intestinal inflammation in mice harbouring an IEC-specific deletion of *autophagy protein 5* (*Atg5*$^{\Delta IEC}$) and hypomorphic mutation in *autophagy-related protein 16-1* (*Atg16L1*^{HM}), respectively [74, 75].

It was previously reported that IEC-specific ER UPR further interrelates with IBD-associated mtUPR (Figure 5) [40].

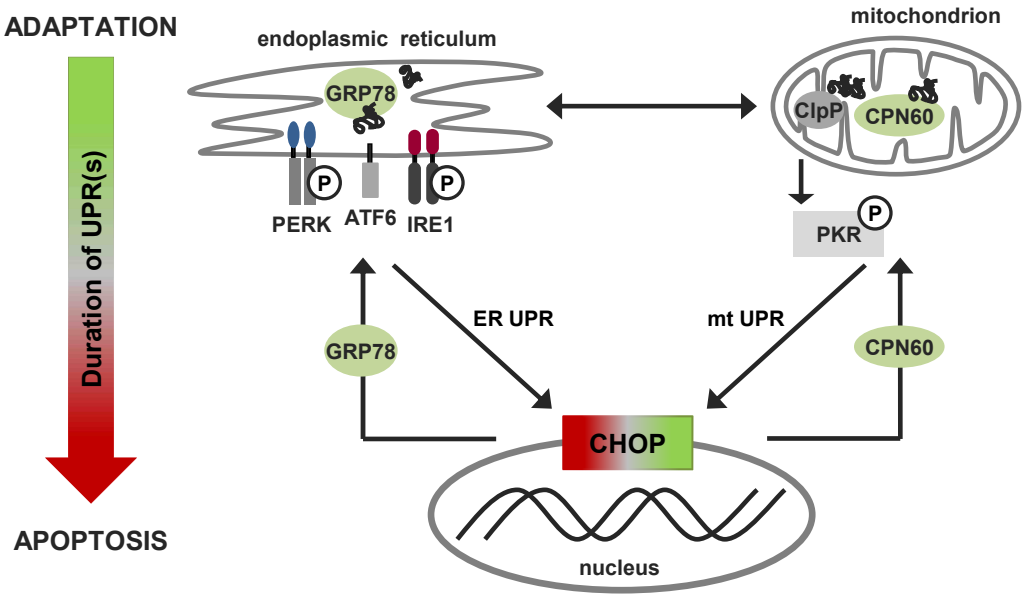

Figure 5. ER and mtUPR converge at the level of CHOP expression.
Both ER and mtUPR are initiated by aggregates of unfolded proteins leading to specific downstream signaling that is mediated by the ER-associated ER stress transducers PERK, ATF6, and IRE1 as well as mtUPR-dependent activation of PKR, respectively. Upon ER and mtUPR, the expression of chaperones, such as GRP78 and CPN60, is enhanced supporting adaptation by increasing the protein folding capacity of the organelles. Herein, the induction of CPN60 is driven by mtUPR-related CHOP protein expression. In contrast, CHOP protein expression appears highly associated with unsolved ER stress that consequently leads to the elimination of the unhealthy cell by initiating pro-apoptotic signaling (adapted from Rath et al., 2012).

The mtUPR is suggested to be activated by increased efflux of peptides into the cytosol promoted by the degradation of unfolded proteins from the mitochondrial matrix through the protease ClpP [76]. As a consequence, mitochondrial chaperones, such as chaperonin 60 (CPN60), are induced, thus promoting mitochondrial protein folding [77]. With regard to UPR signaling, mtUPR and the ER UPR converge at the level of CCAAT/enhancer-binding protein (C/EBP) homologous protein (CHOP) expression - one of the transcription factors highly associated with UPR-mediated apoptosis [55, 78-80]. CHOP, also called growth arrest- and DNA damage-inducible gene 153 (GADD153), is a basic leucine zipper (bZIP) tran-

scription factor rarely expressed under physiological conditions. CHOP is induced in response to stress, including hypoxia, nutrient deprivation, and protein mis- and malfolding in the ER and mitochondria, respectively [40, 81-85]. In the context of UPR, CHOP is reported to initiate cell apoptosis in late ER stress signaling, but, on the contrary, leads to an early increase of CPN60 in mtUPR [78, 79, 86]. Regarding the onset of inflammatory responses the cell-specific functions and consequences of ER UPR and mtUPR in IBD are poorly understood. Accordingly, the significance of CHOP expression in maintaining cellular homeostasis or inflammation-driven tissue pathology is completely unknown.

1.4 CHOP expression in ER UPR

1.4.1 The ER UPR

Being responsible for the correct folding of secretory proteins, membrane proteins, and proteins for the Golgi apparatus, lysosomes and others, as well as post-translational modifications, such as N-glycosylation and intra- and intermolecular disulfide bonds, respectively, the ER strongly contributes to cellular homeostasis by regulating distinct mechanisms to overcome harmful ER stress [87-89]. ER stress is defined as the unhealthy condition that is triggered by an enhanced demand of proteins that exceeds the protein folding capacity of the organelle, thus leading to the accumulation of aggregated proteins negatively influencing the ER function [89-93]. Mis- and malfolded proteins are recognized by the three ER stress transducers ATF6, IRE1, and PERK that initiate a signaling network known as the ER UPR [94-97]. Under physiological conditions, these sensor proteins form inactive complexes with the luminal bound chaperone GRP78 that consequently dissociates from its binding partner when incomplete protein folding leads to ER stress [98-101]. The dissociation of GRP78 results in oligomerization of both transmembrane protein kinases IRE1 and PERK followed by autophosphorylation and specific downstream signaling. In contrast, liberated ATF6 translocates to the Golgi apparatus, where the activated transcription factor nATF6 is released after subsequent proteolysis through the site-1 protease (S1P) and the site-2 protease (S2P). The ER UPR comprises distinct interacting mechanisms to regain organelle and cell homeostasis (Figure 6). First, early ER stress responses diminish the accumulation of malfolded proteins by inducing a PERK signaling-dependent shut-off of protein translation Enhanced degradation of mRNA encoding for various ER-located proteins is further mediated by the PERK-dependent regulated IRE1-dependent decay (RIDD) [94, 102-104]. Second, IRE1α-dependent JUN N-terminal kinase (JNK) pathway enables the activation of autophagy strongly suggested to eliminate protein aggregates and damaged ER, respectively, through the lysosomal pathway [105]. The removal of incompletely folded proteins is further supported

by the ER-associated degradation (ERAD), which is highly associated with mechanisms underlying protein quality control [95, 106, 107].

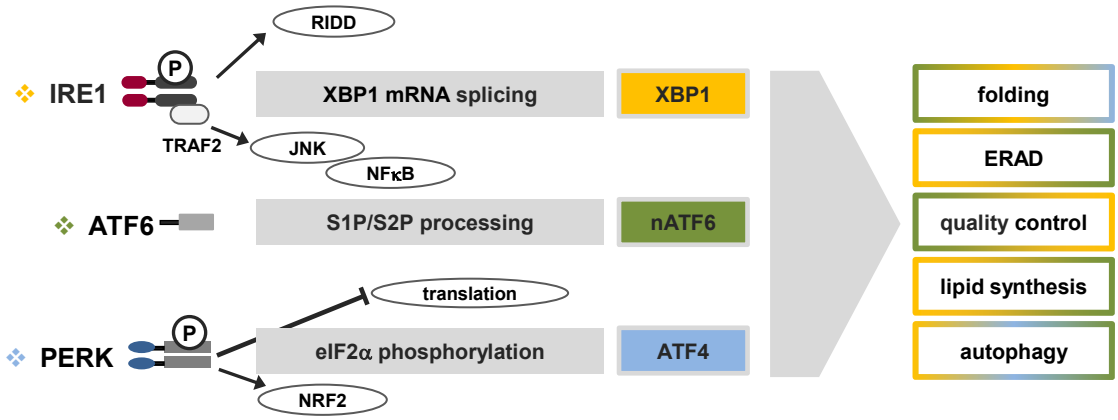

Figure 6. Downstream signaling in ER UPR.

First ER stress responses ameliorate protein load through degradation of mRNA by IRE1-mediated RIDD as well as PERK signaling-dependent translational inhibition. Upon activation and/or synthesis of ER UPR-related transcription factors XBP1, nATF6, and ATF4, the expression of distinct genes is regulated supporting protein folding, ERAD, protein quality control, lipid synthesis, and autophagy.

When ER stress could not be resolved, sustained UPR signaling leads to the expression of pro-apoptotic genes that trigger the elimination of exhausted cells. Herein, the induction of CHOP expression is crucially involved in cell fate [54, 80]. Upon ER stress, CHOP is transcriptionally regulated by the activation of PERK and ATF6, respectively, but also signaling downstream of IRE1 contributes to CHOP expression [102, 108, 109].

1.4.2 Regulation of CHOP expression in ER UPR

In response to ER stress, distinct transcription factors are synthesized or activated along the signaling axis of IRE1, ATF6, and PERK, such as XBP1, nuclear ATF6 (nATF6), and ATF4 [90, 99, 102]. These transcription factors bind to several promoter elements, such as ER stress element (ERSE) I and II, UPR element (UPRE), cAMP response element (CRE), antioxidant response element (ARE), and amino-acid-regulatory element (AARE) I and II, thus driving the expression of UPR-related genes [110-114]. During prolonged ER stress responses, elimination of unhealthy cells is mediated by at least three pro-apoptotic pathways, such as activation of the JNK pathway, activation of ER-associated capsase-12, and transcriptional activation of CHOP [86, 115]. At least one AARE and two ERSE motifs could be identified in the human CHOP promoter, whereas latter reveal high homology with ERSE motifs found in the promoter region of other UPR-related genes, such as GRP78, GRP94, protein disulfide isomerase (PDI), and calreticulin [111, 116-118].

Regarding the three branches of the ER UPR, the PERK pathway appears most relevant in CHOP induction (Figure 7) [102, 119]. The type I transmembrane kinase PERK is activated through the dissociation of GRP78 from its luminal domain [96]. Upon oligomerization and autophosphorylation, activated PERK in turn mediates phosphorylation of substrate proteins, thus initiating distinct signaling pathways that contribute to the resolution of ER stress [95, 120-123]. Herein, eukaryotic initiation factor-2α (eIF2α) is phosphorylated on Ser51 that consequently results in an attenuation of general protein synthesis, even though there is limited translation of several short upstream open reading frames (uORF). Accordingly, ATF4 mRNA is translated due to its small uORF within the 5' untranslated region [124]. The transcription factor ATF4 can bind to the AARE core sequence 5'-AATGCATCA-3' which triggers the expression of CHOP in late ER stress responses [86]. Although both nATF6 and XBP1 have been shown to induce the expression of CHOP in response to ER stress, studies in PERK$^{-/-}$ cells and eIF2α^{S51A} cells, respectively, strongly suggested that CHOP induction is mainly regulated by the PERK/eIF2α pathway [102, 119].

However, induction of CHOP expression through nATF6 and XBP1 is mediated by binding of these transcription factors to the CACG part of the ERSE consensus sequence 5'-CCAAT-N_9-CCACG-3'. In mammalian cells, ATF6 termed for the two isoforms ATF6α and ATF6β, but further represents a group of ATF6 homologues bZIP transcription factors including LUMEN/CREB3, CREB4, OASIS/CREB3L1, BBF2H7/CREB3L2, and CREBH/CREB3L3, respectively, that are similarly processed upon ER UPR [125, 126]. Liberated ATF6 translocates to the Golgi apparatus, where it is transformed into an active bZIP transcription factor nATF6 through proteolytic processing catalyzed by the two proteases S1P and S2P [99]. ATF6-dependent signaling is mediated through the binding of nATF6 to

distinct promoter elements, such as ERSE I and II, UPRE, and CRE. Accordingly, nATF6 induces the expression of genes encoding UPR-related components for protein folding, such as GRP78, and protein degradation, respectively [108, 127]. Activation of CHOP transcription is triggered by both nATF6 dimers and heterodimers formed with constitutively expressed NF-Y that binds to the CCAAR part of the ERSE motif. Furthermore, the activation of the ATF6 branch contributes to CHOP expression by the induction of unspliced XBP1 (XBP1u) transcription, one of the main targets of activated IRE1.

The IRE1 pathway displays the most conserved UPR signaling pathway in eukaryotic cells [90]. Notably, higher eukaryotes possess two forms of IRE1. IRE1α is ubiquitously expressed, while IRE1β appears tissue-specifically expressed in epithelial cells [109, 128-131]. Like PERK, IRE1 is known as an atypical type I transmembrane protein kinase that further reveals endoribonuclease activity [90]. Upon ER stress, GRP78 dissociation uncovers the ER luminal dimerization domain of IRE1 that drives the oligomerization and subsequently the activation of IRE1 by autophosphorylation of the cytosolic RNase domain [132, 133]. The active endoribunuclease converts XBP1u mRNA into the spliced form XBP1s. The removal of a 26 nucleotide intron leads to a frame shift in the coding sequence of XBP1 resulting in the translation of the 54 kDa bZIP transcription factor XBP1 with potential transcriptional activity [51, 64].

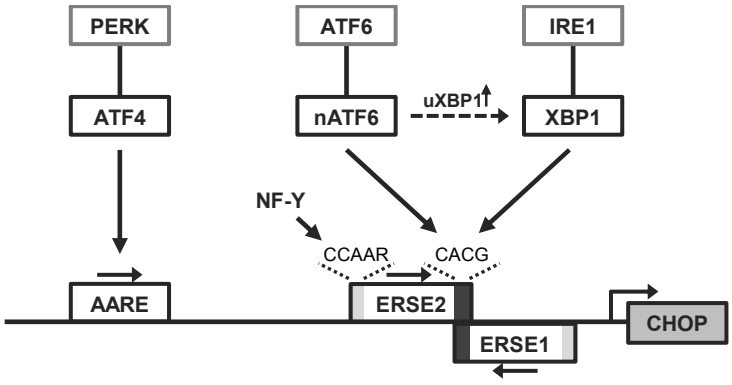

Figure 7. Induction of CHOP mRNA expression during ER UPR according to Oyadomori et al. (2007).

The promoter site of *Chop* presents at least one AARE motif and two ERSE motifs, through which the expression of CHOP is regulated upon ER stress signaling. Binding to the AARE results from activation of the UPR branch PERK/ATF4, while binding to ERSE is promoted by the induction of the ATF6 and IRE1 signaling pathways, respectively. nATF6 binds as dimers and/or heterodimers formed with constitutively expressed NF-Y, while XBP1 exclusively binds to the ERSE motif as heterodimers with NF-Y. Arrows indicate specific binding sites of nATF6/XBP1 (CACG) and NF-Y (CCAAR) within the ERSE motif.

XBP1 can bind to both the ERSE and UPRE sequence 5'-TGACGTGG-3' in interaction with NF-Y, thus leading to the expression of genes encoding for chaperones, such as

GRP78, and genes contributing to ERAD, ER quality control, and membrane biogenesis [110, 134-137]. Even though XBP1/NF-Y complexes reveal low affinity to ERSE motifs, CHOP expression may also occur in response to IRE1 activation [109].

Taken together, the expression of CHOP is strongly suggested to be regulated by the ER UPR branch PERK/eIF2α. In this regard, EIF2α kinases, such as PERK, RNA-activated protein kinase (PKR), general control nonderepressible kinase 2 (GCN2), and heme-regulated inhibitor kinase (HRI), are commonly known to implicate in translational inhibition under stress conditions [96, 138-141]. Of those, PKR has been clearly demonstrated to contribute to ER stress-mediated apoptosis through the activation of the signaling pathway eIF2α/ATF4/CHOP [142]. Most recently, PKR has been shown to impact on intestinal inflammation upon mitochondrial stress signaling. In this context, studies on interrelated signaling pathways revealed that ER UPR and mtUPR converge at the level of CHOP expression [40].

1.5 CHOP expression in mtUPR

In mammalian cell culture, mtUPR can be specifically induced by the transfection of truncated ornithine transcarbamylase (OTCΔ). As a consequence, OTCΔ-driven mtUPR causes the expression of genes encoding mitochondrial *Cpn60* and *Cpn10*, but further leads to the expression of CHOP [78, 143, 144]. CHOP as well as CHOP dimer partner C/EBPβ were found to be regulated by the mtUPR responsive element AP-1, which in turn strongly suggested interrelated mitochondrial and nuclear signaling pathways at the level of JNK2 activation [78]. CHOP/C/EBPβ dimers were shown to induce further mtUPR responsive genes, whereas gene activation seemed to be tightly regulated by conserved mtUPR elements (MURE) flanking corresponding promoter sites [78, 79]. Binding of CHOP to the *Cpn60* promoter contributes to Cpn60 induction [78, 144]. Thus, CHOP expression is strongly suggested to be an early event upon mtUPR, which is in stark contrast to the expression patterns of CHOP in response to ER UPR signaling.

1.6 Molecular features of CHOP

CHOP, also termed GADD153 and DNA-damage-inducible transcript 3 (DDIT3), is a bZIP transcription factor that belongs to the family of C/EBPs [81, 145]. CHOP is a ~29 kDa protein comprising a N-terminal putative transactivation domain and a C-terminal bZIP domain that contains a DNA-binding basic region and a leucine zipper dimerization domain [81, 146]. CHOP is known to be rarely expressed under physiological conditions, but is induced in response to cellular stress, such as hypoxia, nutrient deprivation, as well as ER and mtUPR [81-85, 144]. The expression of CHOP is mainly regulated at the transcriptional level, but mRNA as well as protein levels are tightly controlled by post-transcriptional and post-translational regulation patterns (Figure 8). At the transcriptional level, the induction of CHOP expression correlates with increasing cellular stress. In this context, CHOP expression has been shown to be dependent on stress underlying mechanisms controlling both activation and inhibition of Chop promoter [118, 147]. Post-transcriptional regulation of CHOP expression is mediated by mRNA stability . The highly conserved 5'-untranslated region (UTR) of CHOP mRNA has been implicated in the regulation of CHOP translation, while binding of conserved 3'-UTR to Methionyl-tRNA Synthase pre-mRNA was suggested to impact on the mRNA stability of CHOP [148, 149].

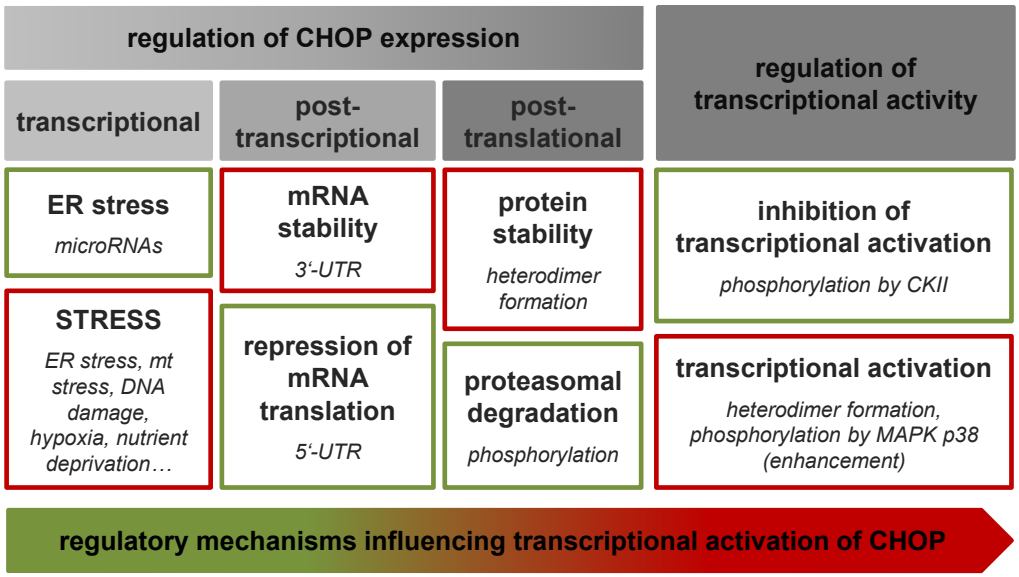

Figure 8. Regulatory mechanisms underlying the expression and transcriptional activation of CHOP.

CHOP expression is regulated at the transcriptional, post-transcriptional, and post-translational level. Transcriptional activation of CHOP protein is mainly mediated by phosphorylation and heterodimer formation. Green labeled regulatory elements lead to the reduction, red labeled elements to an increase of CHOP expression and transcriptional activation, respectively.

Distinct post-translational modifications have been described affecting CHOP protein expression levels as well as its transcriptional activation. In this regard, phosphorylation of CHOP protein appears crucial for both regulation patterns. Inhibitory effects on the transcriptional activation has been shown for CHOP phosphorylation through casein kinase II (CKII) [150]. In contrast, phosphorylation of CHOP on serine-residues 79/82 (human) and 78/81 (rodents) by p38 mitogen activated protein (MAP) kinase has been demonstrated to enhance the transcriptional activation of CHOP protein upon ER stress **[151]**. The transcriptional activation of CHOP is further dependent on heterodimer formation, which in turn protects CHOP against proteasomal degradation [81, 152-157]. CHOP protein constitutively undergoes polyubiquitination that is triggered by phosphorylation of the N-terminal portion [153]. Polyubiquitination and subsequent degradation by the proteasome is suppressed by dimer formation with other C/EBPs, whereas formation of CHOP dimers has not been reported so far [152] [146].

However, various regulatory mechanisms seem to limit the expression of CHOP under physiological conditions, while both expression and transcriptional activation are tightly controlled in response to stress. In this regard, CHOP has been strongly suggested to be a key regulator of cell fate.

1.7 Consequences of CHOP protein expression

CHOP has been originally described as a DNA damage-inducible gene highly associated with cell growth arrest [81, 158-160]. Shortly thereafter, CHOP has been linked to ER stress-induced apoptosis upon sustained UPR signaling [54, 108]. In this context, CHOP is suggested to be crucially involved in the interplay between disease-related ER stress and apoptosis in degenerative disorders [60, 161-163]. With regard to intestinal inflammation, down-regulation of CHOP mRNA and protein expression in inflamed mucosal tissue indicated that regulation of CHOP is most likely dissociated from UPR signaling as well as ER stress-mediated apoptosis in UC patients [28, 164, 165]. In contrast to that, studies on complete CHOP knock-out mice (*CHOP*$^{-/-}$) demonstrated that CHOP deficiency leads to protection against intestinal apoptosis associated with reduced inflammation in response to DSS- and 2,4,6-trinitrobenzene-sulfonic acid (TNBS)-induced colitis [166]. Following these discrepancies, recently published data further indicated that CHOP implicates in the protection of hyperoxia-induced lung injury in mice, thus demonstrating that even the effects of enhanced CHOP expression are not restricted to cell death-promoting mechanisms [167]. In this regard, CHOP has been shown to be regulatory involved in mechanisms underlying the proliferative capacity of cells independent of cell death-promoting signals [160, 168].

However, it is worth mentioning that changes in both proliferation and apoptosis have been observed in IECs of UC patients [169, 170]. Even though CHOP expression has not been correlated to epithelial cell-specific proliferation and/or apoptosis so far, it is sufficiently characterized in terms of apoptosis and has been further described in the context of proliferative regulation.

1.7.1 CHOP and apoptosis

Strong evidence accumulated demonstrating a pro-apoptotic role for CHOP protein [54, 171]. Herein, both transcriptional activation and nuclear translocation of CHOP appear dependent on heterodimer formation, but seem rather enhanced by stress-induced protein phosphorylation on serine-residues 78 and 81 through the MAP kinase p38 [81, 151, 155-157]. Dimers are most prominently formed with both isoforms of C/EBPβ - liver activating protein (LAP) and liver inhibitory protein (LIP), but also with C/EBPα and members of the ATF family, including ATF3 and ATF4, which promotes the binding of unique DNA recognition sites inducing the expression of specific genes downstream of CHOP [172]. Genes, such as *Bcl-2*, *Bim*, *Ero1*α, *Gadd34*, *DR5*, and *Trb3*, have been reported to be regulated by CHOP protein, thus driving apoptosis in unhealthy cells (Figure 9) [80, 173-176].

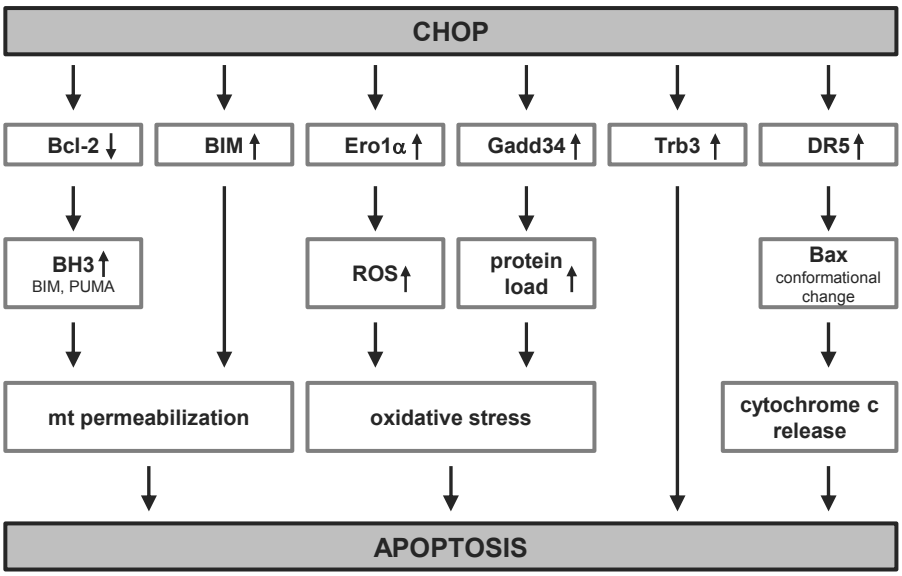

Figure 9. Pro-apoptotic signaling downstream of CHOP.
ER stress-induced CHOP protein expression leads in turn to the regulation of CHOP target genes, such as *Bcl-2*, *BIM*, *Ero1*α, *Gadd34*, *Trb3*, and *DR5*, highly associated with pro-apoptotic signaling.

According studies in mammalian cell lines demonstrated that the presence of CHOP/LIP heterodimers leads to down-regulation of pro-survival Bcl-2 [156, 173]. Although direct implications of CHOP in *Bcl-2* suppression remain elusive, decreased expression of Bcl-2 subsequently results in enhanced levels of BH3-only proteins, such as BIM and PUMA both contributing to mitochondrial permeabilization and apoptosis [177]. Furthermore, up-regulation of BIM has been shown to contribute to ER stress-mediated apoptosis, whereas elevated BIM levels were induced by decreased proteasomal degradation as well as increased gene expression triggered by CHOP-C/EBPα heterodimers [178].

CHOP-mediated apoptosis is widely cited in response to unresolved ER stress, which is further associated with oxidative stress [80]. Under physiological conditions, the oxidative environment of the ER lumen supports post-translational modification of proteins, such as disulfide bond formation. ERO1 proteins, including ERO1α, appear mechanistically involved in maintaining an adequate redox state in the ER lumen [179]. Upon prolonged ER stress, CHOP-induced Ero1α expression might contribute to hyperoxidizing conditions in the ER lumen, thus promoting H_2O_2 leakage into the cytosol and subsequent formation of cytotoxic reactive oxygen species (ROS) [80, 180]. As a consequence, oxidative stress can cause more severe cellular stress and cell death by amplifying CHOP expression in response to enhanced PKR activation [40, 180]. It has been demonstrated that both ER stress as well as ER-related oxidative stress appeared sufficiently decreased upon eIF2α-mediated translation attenuation. Upon UPR signaling, translational inhibition is reversed by GADD34 whose cellular expression is tightly controlled by proteasomal degradation [121, 122, 181]. Thus, CHOP-dependent accumulation of GADD34 highly enhances the protein load subsequently leading to oxidative stress and apoptosis [80, 182].

Further genes that have been described in causing ER stress-mediated cell death are *DR5* and *Trb3*. *DR5* and *Trb3* are expressed in a CHOP-dependent manner when cells were treated with the ER stress inducers thapsigargin and tunicamycin, respectively [175, 176]. Although less is known about the pro-apoptotic mechanisms of Trb3, DR5 is strongly suggested to have an effect on the conformational change of Bax that in turn promotes cell death through the release of apoptogenic proteins including cytochrome c [176, 183, 184].

Under physiological conditions, apoptosis is described as a tightly regulated process that enables tissue regeneration in order to overcome cellular dysfunction [185]. In this regard, the renewal of the intestinal epithelial layer is characterized by strictly controlled proliferative and apoptotic events promoting a balance between turnover and shedding of epithelial cells [186]. As a consequence, both defective apoptosis and/or proliferation could cause an imbalance in tissue regeneration, thus leading to changes in epithelial integrity.

1.7.2 CHOP and proliferation

The intestinal epithelium is renewed every 3-5 days [187]. Self-renewal is organized by stem cell compartments located in the crypts of the small and large intestine, respectively [188] . Intestinal stem cells have been well characterized as crypt base-located Leucine-rich repeat-containing G-protein coupled receptor 5 (Lgr5)-positive cells that give origin to all cell types of the epithelial layer, including absorptive epithelial cells (enterocytes), goblet cells, Paneth cells, and enteroendocrine cells (Figure 10) [43, 188]. In principle, Lgr5-positive cells divide to adjacent transit-amplifying (TA) cells that in turn loose their proliferative capacity during terminal differentiation. Within 3-4 days, mature epithelial cells migrate toward the intestinal lumen, undergo programed cell death, and are finally shed into the lumen the time when dead cells had been replaced by new ones [186]. In contrast to that, cells differentiated into Paneth cells remain located in the crypt base to constitute the niche for Lgr5-positive cells [189].

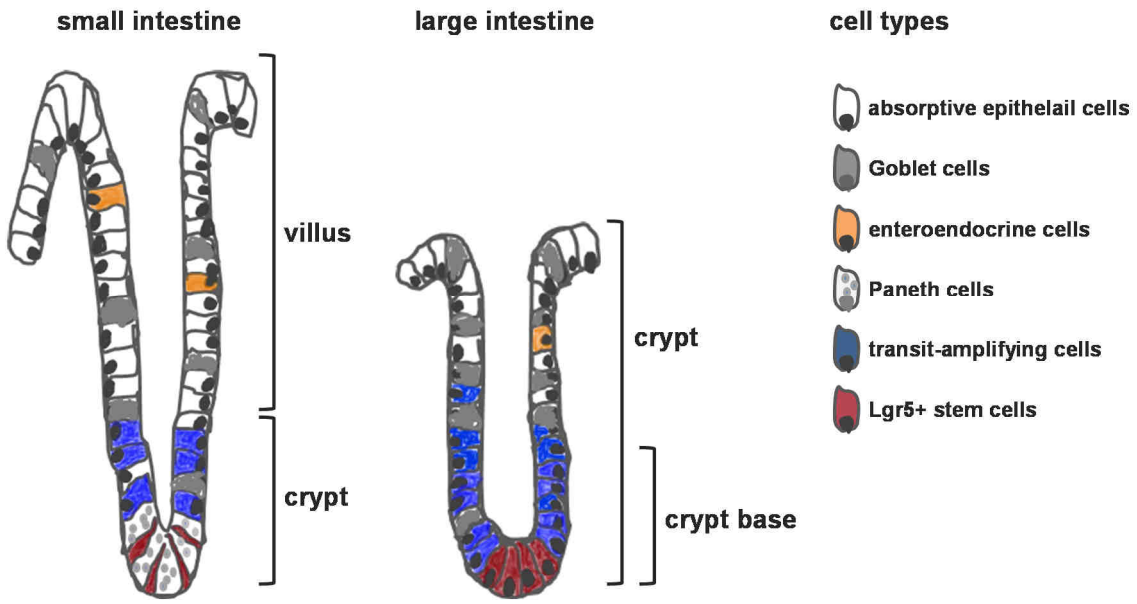

Figure 10. Cell types in small and large intestine.
The intestine comprises distinct cell types, such as crypt base-located stem cells, transit-amplifying cells, and differentiated cells, such as absorptive epithelial cells, enteroendocrine cells, mucus-producing goblet cells, and Paneth cells.

It was recently reported that UPR signaling implicates in the differentiation of IECs [42]. In this context, it has been shown that TA cells contain higher basal mRNA expression levels of ER stress responsive genes than Lgr5-positive stem cells [42, 190]. Increased expression of Grp78, Atf6, Xbp1, Perk, Atf4, and CHOP was highly associated with down-regulation of stem cell marker, such as Ascl2, Oflm4, and Myc. In turn, induction of ER stress in stem cells led to the loss of stemness, which was strongly attributed to signaling downstream of

PERK [42]. In this regard, previous studies demonstrated that ER stress-dependent eIF2α phosphorylation promotes cell cycle arrest by inhibiting the translation of Cyclin D [191-193]. Cell cycle arrest has further been shown to be induced in response to enhanced CHOP protein expression [160]. Although an implication of CHOP in intestinal epithelial stemness and/or proliferative potential of IECs remains elusive, previous studies described a role for CHOP in the inhibition of Wnt/TCF signals [194]. Wnt signaling has been demonstrated to play an essential role in the epithelial stem cell compartment of the intestine [195]. In principle, activation of the canonical Wnt pathway leads to the induction of distinct target genes, such as *c-Myc* and *Cyclin D*, thus supporting cell cycle progression and proliferation, respectively (Figure 11) [196-198].

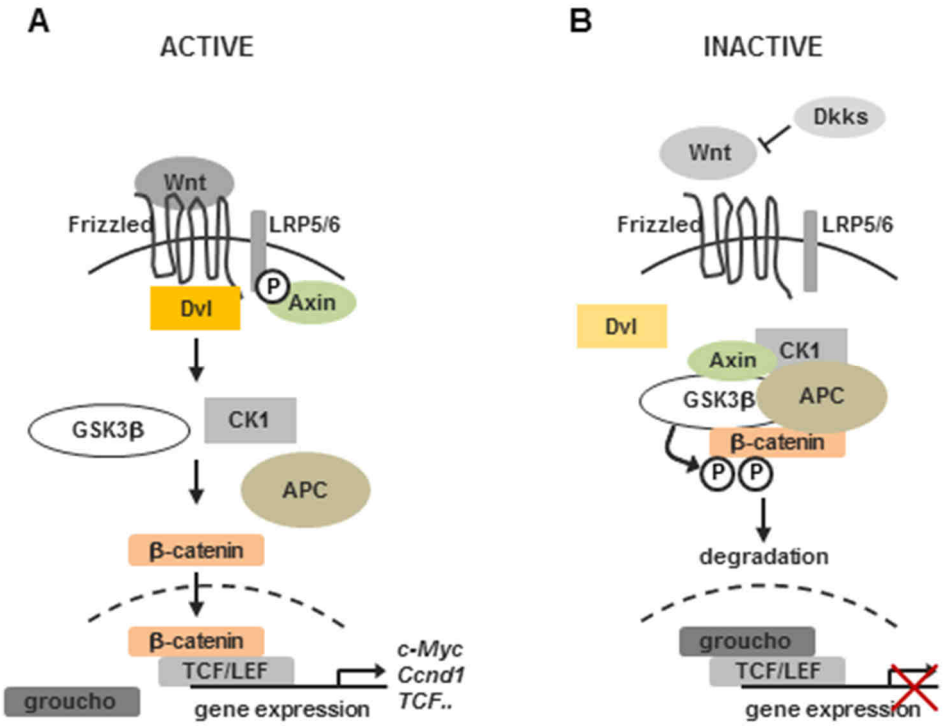

Figure 11. Canonical Wnt signaling leads to the expression of genes promoting cell cycle progression.

(A) Wnt binding to Fizzled receptors initiates a signaling cascade that mediates the stabilization and nuclear translocation of β-catenin. Subsequently, β-catenin forms transcriptionally active complexes with TCF proteins, thus inducing the expression of Wnt target genes, such as c-Myc, Ccnd1, and TCF. (B) In the absence of Wnt binding, β-catenin is phosphorylated by GSK3β, which induces β-catenin degradation through the proteasome. Transcriptional activation of TCF proteins is suppressed by complex formation with groucho.

Wnt binding to membrane-associated Fizzled receptors initiates a signaling cascade that mediates stabilization and nuclear translocation of β-catenin. Nuclear β-catenin forms transcriptionally active complexes with members of the T cell factor (TCF) family, which pro-

motes the expression of Wnt target genes. In the absence of Wnt binding, β-catenin undergoes proteasomal degradation in the cytoplasm, while TCFs form inactive complexes with repressors, such as groucho. Modification of the Wnt signaling cascade through the depletion of TCF4 and β-catenin, respectively, as well as overexpression of Dickkopf (DKK) 1 leads to the loss of proliferative potential of intestinal crypts [195, 199, 200]. Studies in *Xenopus laevis* revealed that high CHOP protein expression inhibited the embryonic development. In this context, CHOP is strongly suggested to impact on Wnt signaling at the level of TCF, thus suppressing the expression of Wnt target genes, including *c-Myc* [194].

Taken together, CHOP is an important regulator of proliferation and apoptosis. Dysregulation of both cellular events have been strongly associated to imbalanced epithelial turnover rates, thus negatively affecting epithelial integrity [201]. In this regard, mechanisms underlying the regulation of CHOP protein expression, including ER stress signaling could be crucially involved in the onset of inflammation, thereby contributing to the disease phenotype of IBD.

2 Study objective

While both ER UPR and mtUPR have been implicated in chronic intestinal inflammation, functional correlation between interrelated signaling pathways and inflammation-related disease susceptibility remains to be elucidated at a tissue-specific level. Despite the fact that ER UPR and mtUPR converge at the level of CHOP expression, the significance of this transcription factor in maintaining cellular homeostasis or promoting inflammation-associated tissue pathology is completely unclear. Since CHOP mRNA and protein expression appears down-regulated under inflammatory conditions in UC, we suggested that UPR-related CHOP expression is regulated in an apoptosis-independent fashion.

Hence, we aim to investigate the functional consequences of enhanced CHOP protein expression in a tissue-specific resolution beyond single cell-mediated effects obtained in cell culture. We generated *Chop*$^{IEC\ Tg/Tg}$ mice overexpressing CHOP protein in the intestinal epithelium that were characterized under normal and disease-related conditions of experimental colitis, thus elucidating the relevance of UPR-related CHOP protein in the disease-conditioning of intestinal inflammation.

3 Material and methods

3.1 Molecular biological methods

Generation of HA-tagged CHOP

The plasmid construct pBluescript containing HA-tagged CHOP was generated by Emanuel Berger. It was provided to Taconic for the generation of the *Chop*$^{Rosa26\ flox/flox}$ mouse model. Total RNA was extracted from C57BL/6N embryo 7.5 dpc (*Macherey*-Nagel GmbH & Co.KG, Düren, Germany) and cDNA library was generated by using SuperScript® Reverse Transcriptase (Life Technologies, Karlsruhe, Germany). Cloning of Gadd153 cDNA was performed by using primer pairs *for_5'-tatcatgttgaagatgagcgggtg-3'*, *rev_5'-caat-gtaccgtc-tatgtgcaagcc-3'* and *for_5'-agaattcaccatggcagctgagtccctgc-3'*, *rev_5'-agcggccgct-gcttggtg-cagg-3'* (Sigma-Aldrich, Taufkirchen, Germany). PCR product and HA-tag oligomer were digested with NotI and ligated using Quick Ligation Kit following manufacturer's instructions (New England Biolabs, Frankfurt, Germany). Ligation product was amplified by using primers *for_5'-agaattcaccatggcagctgagtccctgc-3'*, *rev_5'-aggatccctaagcgtaatctggaa-catcg-tatggg-3'* and inserted into pBluescript xy by using EcoRI and BamHI restriction sites (New England Biolabs, Frankfurt, Germany).

Generation of pcDNA3.1(-)-Hygro-CHOP-HA and mutated plasmid constructs

For mammalian cell culture experiments, CHOP-HA was cut off pBluescript and inserted into pcDNA3.1(-)-Hygro by using EcoRI and BamHI restriction sites. Site-directed mutagenesis of CHOP-HA was performed by overlap extension PCR using Phusion Hot Start II High-Fidelity DNA Polymerase (New England Biolabs, Frankfurt, Germany). PCR reactions were performed using cycle conditions: 1x 3 min at 95°C; 25x 1 min at 95°C, 1 min at 52°C, 1 min at 72°C; 1x 7 min at 72°C. Primers that were used for the generation of CHOP-HA mutants [S14/15A], [S30/31A], [S78/81A], [S14/15A, S30/31A], and [S14/15A, S30/31A, S78/81A] are listed in Table 1.

PCR products were digested using restriction enzymes BamHI and XhoI and ligated with pcDNA3.1(-)-Hygro. Sequencing of plasmid constructs was performed by GATC. Sequence data and alignments are listed in Supplementary materials.

Table 1. Primers used for site-directed mutagenesis of CHOP-HA

construct	primer ID	primer sequence 5'-3'
S14/15A	1392	tcaccttggagacggtggccgcctgggagctggaagcc
	1393	ggcttccagctcccaggcggccaccgtctccaaggtga
S30/31A	1394	gatctgcaggaggtcctggccgcagatgaaattgggggcac
	1395	gtgcccccaatttcatctgcggccaggacctcctgcagatc
S78/81A	1809	acacgcacatcccaagcccctcgcgctccagattccagtcagag
	1810	ctctgactggaatctggagcgcgaggggcttgggatgtgcgtgt
Chop-HA XhoI seq (all)	1377	gtctcgagaccatggcagctgagtc
ATF6-HA (all)	596	agcggccgcacttgggactttgagc

Gene expression analysis

Total RNA was isolated using column-based NucleoSpin® RNAII kit (*Macherey*-Nagel GmbH & Co. KG, Düren, Germany) according to the manufacturer's instructions. Complementary DNA was prepared using random hexamer primers and SuperScript™ First-Strand Synthesis System (Life Technologies GmbH, Karlsruhe, Germany). Quantification of gene expression was performed on LightCycler® 480 System using the Universal ProbeLibrary System (Roche Diagnostics GmbH, Mannheim, Germany) and gene-specific primers (Sigma-Aldrich, Taufkirchen, Germany) (Table 2 and 3).

Table 2. Primer list for qPCR analysis 1

gene	primer ID	primer sequence 5'-3'	probe #
GAPDH	703, 704	tccactcatggcaaattcaa, tttgatgttagtggggtctcg	9
Chop	774, 775	agctagctgtgccactttcc, gggaagcaacgcatgaag	2
endo Chop	664, 665	gatgcacttccttctggaaca, gcgacagagccagaataaca	91
Reg3β	1302, 1303	caccatggaggacaagaatgaagc, ccacagacctggtttgatgcaga	99
Ero1α	874, 875	tcgaagtgcaaaggaaatga, gcgtccagattttcagctct	48
Gadd34	755, 756	agctgaatccaaatcgctgt, tctgtactggaaatgccttcct	6
ATF3	878, 879	gctggagtcagttaccgtcaa, cgcctccttttcctctcat	80
BIM	762, 763	ggagacgagttcaacgaaactt, aacagttgtaagataaccatttgagg	41
Trb3	757, 758	gtcgctttgtcttcagcaact, tcatctgatccagtcatcacg	67
Bcl-2	1052, 1053	gggatgcctttgtggaact, gctgagcagggtcttcagag	2

Table 3. Primer list for qPCR analysis 2

gene	primer ID	primer sequence 5'-3'	probe #
Ki-67	1546, 1547	gctgtcctcaagacaatcatca, ggcgttatcccaggagact	80
Hes1	971, 972	acaccggacaaaccaaagac, cgcctcttctccatgatagg	99
Ccnd	1759, 1760	tttctttccagagtcatcaagtgt, tgactccagaagggcttcaa	72
Myc	1761, 1762	cctagtgctgcatgaggaga, tccacagacaccacatcaattt	77

Microarray analysis

Total RNA was prepared from primary colonic epithelial cells of *Chop*$^{IEC\ Tg/Tg}$ mice and wild-type controls with an age of 12 weeks (n = 8 per group) as well as DSS-treated male mice (3d 2% DSS, 5d 2% DSS plus 5d H_2O, n = 5-6) with column-based NucleoSpin® RNAII kit (*Macherey*-Nagel GmbH & Co. KG, Düren, Germany) according to the manufacturer's instructions. RNA concentration and quality was determined by spectrophotometric analysis (ND-1000, PEQLAB Biotechnologie GmbH, Erlangen, Germany). RNA integrity number (RIN) was >8 for all samples (Agilent bioanalyzer, Alpha Metrix Biotech GmbH, Rödermark, Germany). Labeling of total RNA (100ng) was performed with the Ambion WT Expression kit (Life Technologies, Bleiswijk, The Netherlands), samples were hybridized to Affymetrix GeneChip Mouse Gene 1.1 ST arrays (Affymetrix, Santa Clara CA) and scanned on an Affymetrix GeneTitan instrument. Probes are annotated using up-to-date databases and assigned to unique gene identifiers, in this case Entrez IDs. The probes present on the mouse Gene 1.1 ST arrays represent 21.225 Entrez IDs. Arrays were normalized with the Robust Multi-array Average method. Only probe sets with normalized signal intensities above 20 on at least five arrays, interquartile range > 0.15 and at least 7 probes per probeset were selected for further analysis. Enriched pathways and gene ontology (GO) groups were identified by using the GeneRanker tool in the Genomatix Genome Analyzer. Additional analysis on GO terms was performed by using WEB-based GEne SeT AnaLysis Toolkit [202]. Heat map generation and hierarchical clustering analysis was performed by using MultiExperiment Viewer (TM4 microarray software suite) [203].

3.2 Cell culture methods

Cell lines and media

Cell culture experiments were performed using the colonic epithelial cell line ptk6 (passage 40-50) kindly provided by R. Whitehead (Vanderbilt University, Nashville) [204]. Non-differentiated ptk6 cells were grown in RPMI 1640 medium containing 5% FCS, 1% insulin/transferrin/selenium, interferon-γ (2ng/ml), and 2 mM L-glutamine (all Life Technologies, Karlsruhe, Germany) under a humidified atmosphere and 5% CO_2 at 33°C. For differentiation, ptk6 cells were cultured for at least 5 days in media lacking interferon-γ under a humidified atmosphere and 5% CO_2 at 37°C. Ptk6 cell lines containing mutated plasmid constructs were grown in media additionally supplemented with hygromycin B (500µg/ml).

Transient transfection

Plasmid DNA transfection was performed by using Fugene 6 (Promega, Mannheim, Germany) according to the manufacturer's instructions. Therefore, cells showing 50% confluency were incubated with a mixture containing plasmid DNA and Fugene 6 reagent in a ratio of 1:3 (0.5 µg plasmid DNA per 24-well) for 24h followed by an expression time for 14h. Data are presented giving entire transfection time of 38h.

Generation of polyclonal cell lines ptk6:CHOP-HA, ptk6:S78/81A, ptk6:ctrl

Plasmid DNA transfection was performed by using Fugene 6 (Promega, Mannheim, Germany) according to the manufacturer's instructions. Ptk6 cells were grown in a T-75 flask and transfected with pcDNA3.1(-), pcDNA3.1(-)-CHOP-HA, and pcDNA3.1(-)-S78/81A when cells were grown to 50% confluency. Transfection medium was removed after 48h and selection medium was applied containing hygromycin (500 µg/ml). Polyclonal ptk6 cell line was generated by changing selection medium every 1-3 days until cells were grown to confluency. Newly generated cell lines were at least cultivated for 5 passages before being used in an experiment.

Inhibition of proteasomal degradation by Lactacystine

Non-differentiated ptk6 cell were transiently transfected with pcDNA3.1(-)-CHOP-HA for 24h. Cell medium was changed and proteasome inhibitor Lactacystine (Sigma-Aldrich, Taufkirchen, Germany) was applied in a concentration of 10 µM. After 3h and 6h of incubation cells were lysed in lysis buffer containing 7 mol/L urea, 2 mol/L thiourea, 2% CHAPS, 1% DTT (all from Roth, Karlsruhe, Germany), and protease inhibitor (Roche Diagnostics, Mannheim, Germany) for Western blot analysis.

Determination of cellular proliferation rate by cell proliferation ELISA, BrdU

Determination of cell proliferation was performed by using Cell Proliferation ELISA, BrdU (Roche Diagnostics, Mannheim, Germany). Non-differentiated ptk6 cells were seeded into 96-well plates with 1.000 cells/ml. Cell proliferation was determined for 5 days following the manufacturer's instructions. Doubling time was assessed calculating linear progression of received absorbance.

Transwell experiments

For transwell experiments ptk6 cells were cultivated in media without INF-γ at 37°C. Ptk6 cells ($3x10^5$ cell/ml) were seeded into 0.4 µm polyester Transwell inserts (Costar Corning, Corning, USA). Transepithelial electrical resistance (TEER) was measured using Volt-Ohm-meter by Millipore (Millipore, Schwalbach/TS, Germany) following the manufacturer's instructions.

***In vitro* scratch wound healing assay**

Polyclonal cell lines ptk6:ctrl, ptk6:CHOP-HA, and ptk6:CHOP-HA [S78/81A] ($5x10^4$ cells/ml) were seeded into a 96 well plate and cultivated in media without INF-γ at 37°C to confluent monolayers. Four days after reaching confluency, ptk6 cells were scratched (1 scratch/well) using a 1 ml pipette tip. Cells were washed 2 times with PBS (Life Technologies, Karlsruhe, Germany) to remove cells in supernatants. Scratch size was monitored daily by microscopic analysis using the CKX41-combined DP26 camera system and the cellSens Digital Imaging Software (Olympus, Hamburg, Germany). Scratch closure was determined calculating scratch diameters in percentage to initial scratch size.

Analysis of cell cycle by flow cytometry

Polyclonal cell lines ptk6:ctrl, ptk6:CHOP-HA, and ptk6:CHOP-HA [S78/81A] ($2x10^4$ cells/ml) were seeded into T-25 cell culture flasks (Sarstedt AG & Co., Nümbrecht, Germany) and cultivated in media supplemented with INF-γ at 33°C. When cell monolayers reached 50% confluency, cells were detached using Trypsin/EDTA (Life Technologies, Karlsruhe, Germany) and resuspended by pipetting to single cells. 5 ml of medium was added and cells were centrifuged at 300g for 5 min. Cell pellets were resuspended in 5 ml ice-cold PBS (Life Technologies, Karlsruhe, Germany) and centrifuged at 300g for 5 min. Cell pellets were resuspended in 2 ml ice-cold 70% ethanol and incubated on ice for 1h. Cells were centrifuged at 300g for 5 min and washed twice with 1 ml ice-cold PBS. 100 µl RNase-solution (100 µg/ml in PBS) was added and cells were incubated for 5 min at RT. 800 µl propidium iodide-solution (50 µg/ml in PBS) was added and cells were incubated for additional 15 min at RT and 10 min at 37°C. Afterwards cell suspensions were stored on

ice. Flow cytometry was performed using FACSDiva software (BD Biosciences, Heidelberg, Germany) and cell cycle was analyzed using ModFit LT 3.0 (Verity Software House Inc., Topsham, ME).

3.3 Protein methods

Western blot analysis

Cells were lysed in protein lysis buffer containing 7 mol/L urea, 2 mol/L thiourea, 2% CHAPS, 1% DTT (all from Roth, Karlsruhe, Germany), and protease inhibitor (Roche Diagnostics, Mannheim, Germany). Total protein concentration of ultrasonicated samples was determined by Bradford Assay (Carl Roth GmbH & Co.KG, Karlsruhe, Germany) according to standard protocol. Sample volumes containing 10 µg and 20 µg of protein were diluted with 5x SDS buffer and incubated for 10 min at 95°C. 12.5% reducing sodium dodecyl sulfate polyacrylamide gel electrophoresis (SDS-PAGE) was performed (Biometra, Göttingen, Germany) followed by semi-dry blotting (PEQLAB Biotechnologie GmbH, Erlangen, Germany) using PVDF membranes (Merck KGaA, Darmstadt, Germany). Unspecific binding sites were blocked with 5% milk powder/1xTBS/0.1% Tween-20 (TBST) for 1 hour at RT. Primary antibody (Table 4) was incubated o/n at 4°C and HRP-conjugated secondary antibody was applied for 1h at RT (Table 5). The respective immunoreactive protein was detected by using an enhanced chemiluminescence light-detecting kit (GE Healthcare, Uppsala, Sweden).

Table 4. List of primary antibodies used in Western blotting.

antibody	dilution	ID	company
anti-HA	1:1000	14-6756	eBioscience, Frannkfurt, Germany
anti-CHOP	1:1000	sc-575	Santa Cruz Biotechnology, Heidelberg, Germany
anti-Reg3β	1:1000	AF5110	R&D Systems, Wiesbaden, Germany
anti-P-p38	1:1000	4511	Cell Signaling Technol-ogy, Frankfurt, Germany
anti-β-Actin	1:2000	4970	Cell Signaling Technology, Frankfurt, Germany
anti-CPN60	1:1000	sc-1053	Santa Cruz Biotechnology, Heidelberg, Germany
anti-P-eIF2α	1:1000	7921	Cell Signaling Technol-ogy, Frankfurt, Germany
anti-PKR	1:1000	sc-366777	Santa Cruz Biotechnology, Heidelberg, Germany
anti-P-RelA	1:500	3039	Cell Signaling Technology, Frankfurt, Germany
anti-GRP78	1:4000	G9043	Sigma-Aldrich, Taufkirchen, Germany
anti-cleaved Caspase3	1:1000	9661	Cell Signaling Technology, Frankfurt, Germany

Table 5. List of secondary antibodies used in Western blotting

antibody	dilution	ID	company
anti-sheep	1:2000	-----	Jackson ImmunoResearch, Hamburg, Germany
anti-rabbit	1:4000	-----	Dianova, Hamburg, Germany
anti-goat	1:2000	-----	Dianova, Hamburg, Germany

Protein dephosphorylation

Cells were lysed in native cell lysis buffer (#9803, Cell Signaling Technology, Frankfurt, Germany) supplemented with 1mM PMSF. Approximate protein concentration was determined by Bradford protein assay. For dephosphorylation, 15 µg of native protein was treated with alkaline phosphatase (AP) for 15, 30, and 60 min, and with and without AP for 90 min following the manufacturer's instructions (New England Biolabs, Frankfurt, Germany).

3.4 Histological methods

Histology and tissue staining

Freshly isolated intestinal tissue was fixed in 4% neutral buffered formalin for one to two days, dehydrated through a series of graded alcohol and xylene and embedded in paraffin (Leica Microsystems GmbH, Nussloch, Germany). Hematoxylin & eosin (H&E) staining and alcian blue staining were performed on 5 µm-thick tissue sections (Leica Microsystems GmbH, Nussloch, Germany) by using standard protocols. For morphological analysis, villus height, crypt depth, total epithelial area, and mucus area of 15-20 villi and/or crypts, respectively, was measured for each section using the LAS software (Leica Microsystems GmbH, Nussloch, Germany) and means were calculated. Mucus area is given as percentage of total epithelial area.

For immunohistochemistry (IHC), 5 µm-thick paraffin sections were applied onto poly-L-lysine coated slides and incubated overnight at 37°C. After rehydration, antigen retrieval was performed in 10 mM sodium citrate buffer (pH 6.0) by steaming sections in a microwave oven (900 Watt) for 23 min. Slides were rinsed with H_2O and endogenous peroxidases were blocked for 10 min using 3% hydrogen peroxide (Fluka, Sigma-Aldrich, Taufkirchen, Germany). Tissue sections were washed twice in H_2O for 5 min each and rinsed with PBST. Unless indicated otherwise, individual slides were washed 3 times with PBS for 5 min between each step. 5% BSA/PBS block was done for 30 min at RT. Primary antibodies against cleaved Caspase 3 (1:50, #9661, Cell Signaling Technology, Frankfurt, Germany), Ki-67

(1:100, ab15580, Abcam, Cambridge, UK), and CD19 (1:50, M-20, Santa Cruz Biotechnology, Heidelberg, Germany) were directly applied and incubated overnight at 4°C. Secondary anti-rabbit antibody (1:200, Dianova, Hamburg, Germany) was applied for 1 hour at RT and subsequently stained using 3.3'-diaminobenzidine solution (Sigma-Aldrich, Taufkirchen, Germany) with hematoxylin (Medite GmbH, Burgdorf, Germany) used as a counterstain. In addition, stainings for CD3 (1:300, RM-9107-S0, NeoMarkers/Lab Vision Corporation, CA, US), Ly6G (1:600, 551459, BD Pharmigen, Heidelberg, Germany), B220 (1:3000, 553084, BD Biosciences, Heidelberg, Germany), F4/80 (1:120, T-2006, BMA Biomedicals AG, Augst, Switzerland), and MHCII (1:500, NBP1-43312, Novus Biologicals, CO, US) were performed on 2 µm-thick tissue sections according to the staining protocol mentioned above. Notably, antigen retrievel for both B220 and CD3 as well as Ly6G was performed in EDTA buffer (1 mM EDTA, 0.05 % Tween 20, pH 8.0) by steaming sections in a microwave oven for 20 and 30 min, respectively. Antigen retrieval of tissue sections used for F4/80 and MHCII staining, respectively, were incubated with proteinase K for 10 min following standard protocol. Microscopic analyses were performed by using the LMD 6000 and the Leica Application Suite (LAS) software (Leica Microsystems GmbH, Nussloch, Germany) as well as by using the Olympus BX53 and Olympus cellSens Dimension 1.7 software (Olympus, Hamburg, Germany).

Immunofluorescence staining (IF) was performed following the protocol provided by Cell Signaling Technology. Primary antibodies (4°C, o/n) anti-E-Cadherin (1:100, ab76055, Abcam, Cambridge, UK), anti-Reg3β (1:50, AF5110, R&D Systems, Wiesbaden, Germany), anti-Ki-67 (100, ab15580, Abcam, Cambridge, UK), anti-CD19 (1:50, M-20, Santa Cruz Biotechnology, Heidelberg, Germany), and anti-Vimentin (1:50, #3932, Cell Signaling Technology, Frankfurt, Germany) were applied on paraffin sections, anti-HA-tag antibody was used for cryosections (1:4000, ab9110, Abcam, Cambridge, UK). Fluorescently labeled secondary antibodies anti-rabbit (A11012, Life Technologies, Karlsruhe, Germany), anti-mouse (A11001, Life Technologies, Karlsruhe, Germany), and anti-sheep (Jackson ImmunoResearch, Hamburg, Germany) were incubated for 1 hour at RT. Tissue sections were covered using mounting solution with DAPI (BIOZOL Diagnostica, Eching, Germany). TUNEL assay was performed using ApoBrdU DNA Fragmentation Assay Kit according to the manufacturer's instructions (K401-60, BioVision, Heidelberg, Germany). For positive controls, 5 µm-thick tissue sections were treated with DNaseI (*Macherey*-Nagel GmbH & Co. KG, Düren, Germany) for 15 min immediately after antigen retrieval. Further steps were done following the manufacturer's instructions. Microscopic analysis was performed by using the confocal laser scanning biological microscope FV10i (Olympus, Hamburg, Germany) and Volocity 3D Imaging Software (Perkin Elmer, Rodgau, Germany).

Histopathological analysis

Histological scoring was performed on H&E stained tissue sections by blindly assessing the degree of inflammation as described by Katakura et al. [205]. Colonic tissue sections were scored for epithelial damage [0 = normal; 1 = hyperproliferation, irregular crypts, and goblet cell loss; 2 = mild to moderate crypt loss (10-50%); 3 = severe crypt loss (50-90%); 4 = complete crypt loss, surface epithelium intact; 5 = small- to medium-sized ulcer (<10 crypt widths); and 6 = large ulcer (≥10 crypt widths)] and infiltration of inflammatory cells [mucosa (0 = normal, 1 = mild, 2 = modest, 3 = severe), submucosa (0 = normal, 1 = mild to modest, 2 = severe), and muscle/serosa (0 = normal, 1 = moderate to severe)]. Calculated mean scores ranged from 0 (not inflamed) to 12 (massively inflamed).

Laser capture microdissection

Freshly isolated intestinal tissue was immediately embedded in Tissue-Tek® (Weckert Labortechnik, Kitzingen, Germany). Serial frozen sections were cut into 10 µm size and applied onto RNase-free PET membrane slides (Leica Microsystems GmbH, Nussloch, Germany) followed by H&E staining using truncated standard protocol (70% ethanol for 1 min, DEPC water for 30 sec, hematoxylin for 20 sec, DEPC water for 30 sec, NH_4OH (0.1%) for 30 sec, eosin (2%) for 10 sec, 96% ethanol for 30 sec, and 100% ethanol for 30 sec). A total area of 2,000,000 μm^2 was microdissected from epithelium, lamina propria, and muscularis, respectively, by using the UV laser-cutting system LMD 6000 and the LAS software (Leica Microsystems GmbH, Nussloch, Germany). Microdissected tissue was lysed in 50 µl RLT buffer supplemented with 1 mM mercaptoethanol and total RNA was prepared using RNeasy Micro Kit (Qiagen, Hilden, Germany) according to manufacturer's instructions.

3.5 Animal experimentation

All animal procedures were approved and performed according to institutional guidelines for the Bavarian Animal Care and Use Committee (AZ 55.2-1-54-2531-164-09, AZ 55.2-1-54-2532-160-12, AZ 55.2-1-54-2532-165-12).

Generation of *Chop*$^{Rosa26\ flox/flox}$ wild-type controls

C57BL/6N mice were used for knock-in mutagenesis to generate the *Chop*$^{Rosa26\ flox/flox}$ strain that was purchased from Taconic. Therefore, a construct containing the CMV early enhancer/chicken β-actin (CAGGS) promoter and the coding sequence for murine CHOP protein with HA tagged to the C-terminus was introduced into Rosa26 locus. The promoter-associated floxed STOP sequence inhibits the expression of the transgene. Genotyping was performed by amplification of genomic DNA using primers *for_5'-cacacgcacatccca-*

aagc-3', *rev_5'-ctggaacatcgtatgggtaagc-3'* for modified Rosa26 locus, and *for_5'-catgtctttaatctacctcgatgg-3'*, *rev_5'-ctcttccctcgtgatctgcaactcc-3'* for wild-type allele. Notably, construct generation was performed by Emanuel Berger (see "Generation of HA-tagged CHOP") who additionally organized, supervised, and managed the generation of transgenic mice.

Generation of homozygote *Chop*$^{IEC\ Tg/Tg}$ mouse model

Homozygous *Chop*$^{flox/flox}$ females were mated with males expressing Cre recombinase under control of a 9kb regulatory region of mouse villin promoter (*vil-Cre*) [206]. The F1 offspring was genotyped for *vil-Cre* by amplification of genomic DNA using primers *for_5'-caagcctggctcgacggcc-3'*, *rev_5'-cgcgaacatcttcaggttct-3'* (Sigma-Aldrich, Taufkirchen, Germany). Mice were intercrossed avoiding double-positive *vil-Cre* mating pairs. The progeny of the F2 generation was genotyped for transgenic mice homozygous for *Chop-HA* with *vil-Cre* expression (*Chop*$^{IEC\ Tg/Tg}$). *Chop*$^{Rosa26\ flox/flox}$ and *Chop*$^{IEC\ Tg/Tg}$ mice were intercrossed, thus breeding for adequate wild-type controls (WT) and conditionally CHOP-HA overexpressing mice (TG). Mice were housed in specific pathogen free (SPF) facility and fed with standard diet V1124-300 (Ssniff, Soest, Germany) (Supplementary materials).

Isolation of intestinal epithelial cells

The dissected intestine was inverted, rinsed twice with cold PBS, and placed in ice-cold DMEM with 10% FCS and 1 mM DTT (all from Life Technologies, Karlsruhe, Germany). After vigorous shaking for 1 min, the intestine was incubated for 20 min at 37°C with shaking (180 rpm). After vortexing for 1 min, the intestinal tissue was transferred into PBS containing 1.5 mM EDTA (Life Technologies, Karlsruhe, Germany) for further incubation on a shaker (10 min, 37°C, 180 rpm). Meanwhile, the first fraction was centrifuged for 5 min. Centrifugation steps were continuously performed at 300g and 4°C unless otherwise mentioned. The cell pellet was resuspended in 5 ml of fresh DMEM supplemented with 10% FCS and stored on ice. After vortexing for 1 min, the intestine was removed from PBS/EDTA solution and the cell suspension was centrifuged for 5 min. The cell pellet was pooled with former isolated IECs and purified by centrifugation through a 20/40 discontinuous Percoll gradient (GE, Healthcare, Uppsala, Sweden) for 30 min at 600g. IECs were resuspended in 1 ml of fresh DMEM with 10% FCS, separated in two volumes and pelleted for 5 min. The cell pellets were lysed in RA1 buffer for RNA extraction (*Macherey*-Nagel GmbH & Co. KG, Düren, Germany) and protein lysis buffer containing 7 mol/L urea, 2 mol/L thiourea, 2% CHAPS, 1% DTT (all from Roth, Karlsruhe, Germany), and protease inhibitor (Roche Diagnostics, Mannheim, Germany).

Isolation of small intestinal epithelial cells from villus tip to the crypt

Dissected intestine was inverted, rinsed twice in 6 ml of cold PBS, and incubated in citrate buffer containing 96 mM NaCl, 1.5 mM KCl, 27 mM sodium citrate, 8 mM KH_2PO_4, 5.6 mM Na_2HPO_4, pH 7.3 (all from Roth, Karlsruhe, Germany) for 15 min at 37°C. Thereafter, tissue was incubated in PBS containing 1.5 mM EDTA, 0.5 mM DTT, 1 mg/ml BSA for 10, 10, 6, 5, 5, 9, 10, 15, 25, and 30 min at 37°C with shaking (180 rpm). Tissue was transferred into a new tube after each incubation step. Fractions were split in two volumes and immediately centrifuged at 300 g and 4°C. Cell pellets were lysed in RA1 buffer for RNA extraction (*Macherey*-Nagel GmbH & Co. KG, Düren, Germany) and protein lysis buffer containing 7 mol/L urea, 2 mol/L thiourea, 2% CHAPS, 1% DTT (all from Roth, Karlsruhe, Germany), and protease inhibitor (Roche Diagnostics, Mannheim, Germany). Fractions 1 and 2 are defined to contain IECs from villus tip. To detect fractions containing IECs from crypt region, fractions 3 to 10 were analyzed for Ki-67 and Hes1 mRNA expression.

***Citrobacter rodentium* infection**

Female mice with the age of 8-10 weeks were inoculated orally with $2x10^9$ colony-forming units (CFU) of *Citrobacter rodentium* ICC169 as previously described [207]. Changes in body weight, clinical condition of mice and bacterial load of RF-*C. rodentium* in fecal pellets were monitored every 2-3 days. Mice were sacrificed by cervical dislocation. Both colon weight and length was determined to express colonic weight/length ratio in milligram (mg) per millimeter (mg). Whole colonic tissue was fixed in 4% neutral buffered formalin for paraffin embedding. Alcian blue staining was performed and crypt depth, total epithelial area, and mucus area was assessed in distal colon using the LAS software (Leica Microsystems GmbH, Nussloch, Germany) as described in Histological methods. Mucus area was calculated as percentage of total epithelial area.

DSS-induced colitis

2% DSS solution was prepared in a total volume of 2l (~ 150 ml per mouse) one week before starting the experiment. 40 g of DSS (MW 36,000-50,000, MP Biomedicals, Eschwege, Germany) was solved in 2l veH_2O subsequently followed by sterile filtration. Solution was stored at 4°C. *Chop*$^{IEC\ Tg/Tg}$ mice and wild-type controls (n = 5-6 per group) with an age of 12 weeks received 2% (w/v) DSS ad libitum for 3 and 7 days, respectively. Examination of epithelial repair in experimental colitis was performed providing 2% (w/v) DSS ad libitum for 5 days followed by a period of 5 days for recovery (n = 6 per group). Body weight was daily monitored and disease activity was assessed as further described in Animal experimentation. Mice were sacrificed by CO_2. Spleen weight was determined to ex-

press spleen/body weight ratio and colon length and weight was assessed to calculate colonic weight/length ratio. The colon was opened longitudinally and carefully cut into two pieces. One half was used for IEC isolation and the other one was fixed in 4% neutral buffered formalin for paraffin embedding.

Determination of disease activity index

The disease activity index (DAI) was assessed according to the scoring criteria as described in Murthy et al. [208]. Scores of body weight changes (0-4), stool consistency (0-4), and rectal bleeding (0-4) were calculated to a total score (0-12) and presented as sum ±SD (Table 6).

Table 6. Scoring criteria for disease activity index

score	weight loss (%)	stool consistency*	rectal bleeding
0	None	normal	negative
1	1-5		
2	6-10	loose	gross bleeding
3	11-15		gross bleeding >1d
4	>15	diarrhea	gross bleeding >2d

* normal = well formed pellets; loose = pasty stool, but clean anus; diarrhea = liquid stool that sticks to the anus

In vivo wound healing assay

Colonic mucosal lesions with a diameter of 800 µm were induced in transgenic mice and wild-type controls (n = 6 per group) as previously described [209]. Wound healing was monitored by video colonoscopy (KARL STORZ GmbH & Co.KG, Tuttlingen, Germany) on days 0, 1, 2, 3, and 5 and assessed by calculating wound size relative to original wound diameter. Mice were sacrificed by cervical dislocation at days 3 and 5 (n = 3 per group and day) and colonic tissue containing wound region was fixed in 4% neutral buffered formalin for paraffin embedding.

In vivo BrdU labeling

Chop$^{IEC\ Tg/Tg}$ mice and wild-type controls with an age of 12 weeks were intraperitoneal-injected with BrdU labeling reagent following the manufacturer's instructions (Life Technologies, Karlsruhe, Germany). Mice (n = 5) were sacrificed on days 1 and 3 post injection by cervical dislocation. Intestinal tissue was fixed in 4% neutral buffered formalin for paraffin embedding. Immunohistological detection of BrdU-positive cells was performed by using the BrdU In-situ Detection Kit following the manufacturer's instructions (BD Biosciences,

Heidelberg, Germany). IHC double staining for BrdU and Ki-67 was performed following the manufacturer's instructions. Ki-67 positive cells were detected by using HRP-Green Solution Set (2 components) (life sciences GmbH & Co.KG, Bremerhaven, Germany).

3.6 Statistical analysis

Statistical computations were performed by using SigmaPlot 11.0 (Systat software, Erkrath, Germany). Statistical significance was assessed by Student's t-test, non-parametric rank-sum test, and two-way ANOVA (TWA) with genotype and DSS treatment as main factors followed by Holm-Sidak test. $P < .05$, $P < .01$, and $P < .001$ was considered statistically significant.

4. Results

4.1 Basic characterization of *Chop*$^{IEC\ Tg/Tg}$ mice

4.1.1 Generation of new mouse model *Chop*$^{IEC\ Tg/Tg}$

Transgenic mice that reveal high expression of HA-tagged CHOP protein restricted to the intestinal epithelial layer were generated by crossbreeding female wild-type controls *Chop*$^{Rosa26\ flox/flox}$ with males expressing villin promoter-driven Cre recombinase (Figure 12) [206].

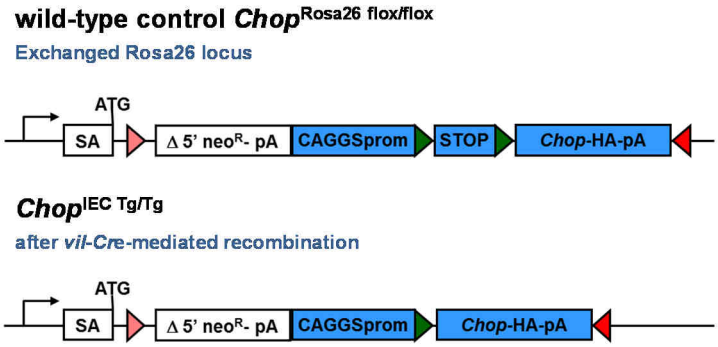

Figure 12. Generation of new mouse model *Chop*$^{IEC\ Tg/Tg}$.
Wild-type controls *Chop*$^{Rosa26\ flox/flox}$ were mated with Villin-Cre positive mice. Cre recombinase-mediated removal of promoter-associated floxed STOP sequence resulted in CAGGS promoter-driven high expression of the HA-tagged transgene CHOP-HA.

Homozygote *Chop*$^{IEC\ Tg/Tg}$ mice were generated following the breeding scheme shown in Figure 13. Genotyping was performed by using primer pairs for Villin-Cre and Rosa26 locus, respectively and offspring were intercrossed avoiding double-positive *vil-Cre* mating pairs. Animals used in experiments derived from breeding of homozygote *Chop*$^{Rosa26\ flox/flox}$ and *Chop*$^{IEC\ Tg/Tg}$ mice with *Chop*$^{Rosa26\ flox/flox}$ mice as adequate wild-type controls. The analysis of numbers of pregnancies and pups per mouse, respectively, indicated that genetic modification of mice did not affect breeding capacity when compared to C57BL/6N mice.

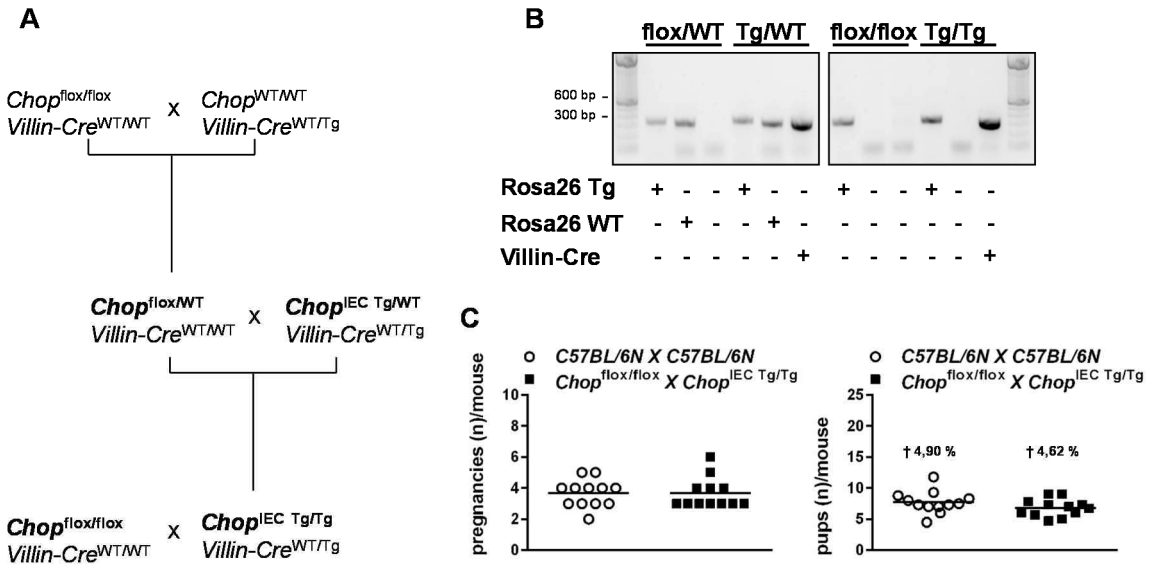

Figure 13. Breeding scheme for *Chop*$^{IEC\ Tg/Tg}$ mice and adequate wild-type controls.

(A) Breeding scheme for the generation of homozygote transgenic mice and adequate wild-type controls. Wild-type controls *Chop*$^{Rosa\ 26\ flox/flox}$ are refered as *Chop*$^{flox/flox}$ (B) Genetic background of progenies was determined by genotyping for both modification of Rosa26 locus and presence of *vil-Cre*. Mice were selected for following breeding avoiding double-positive *vil-Cre* mating pairs. (C) Analysis of breeding capacity for homozygote transgenic mice and adequate C57BL/6N wild-type controls. Number of pregnancies and litter size of mating pairs (n = 12) were assessed over 6 month of breeding. Data are plotted as means. Lethality was assessed calculating numbers of death pubs as percentage to total numbers of progenies.

4.1.2 Transgenic mice reveal high CHOP expression in intestinal epithelial cells

IEC-specific expression of transgenic CHOP with HA-tag fused to the C-terminus was shown by determining mRNA expression of Chop in cell isolates derived from lasermicrodissected intestinal epithelium, lamina propria, and muscularis of transgenic mice and wild-type controls (Figure 14). Transgenic mice displayed high expression of Chop-HA on mRNA and protein level in the intestinal epithelium (Figure 15). Regarding qPCR analysis using IEC isolates (n = 5) from small and large intestine, respectively, Chop-HA mRNA expression revealed 18- to 52-fold increase of transgenic Chop over endogenous Chop. Since transgenic CHOP protein is HA-tagged, both antibodies anti-CHOP and anti-HA were used in Western blot analysis.

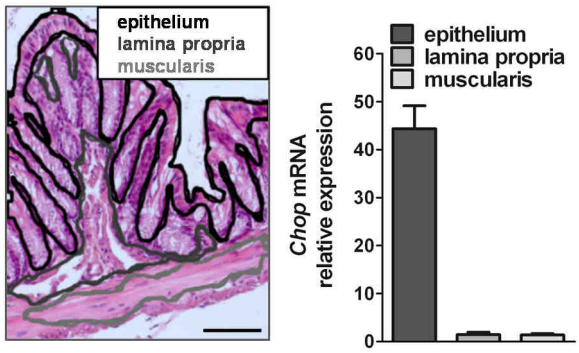

Figure 14. Analysis of intestinal epithelial cell-restricted mRNA expression of Chop-HA.

Tissue-specific mRNA expression of transgenic Chop was assessed by qPCR using isolates of microdissected cells derived from the intestinal epithelium, lamina propria, and muscularis of *Chop*$^{IEC\ Tg/Tg}$ mice and wild-type controls (n = 3). Scale bar represents 100 µm.

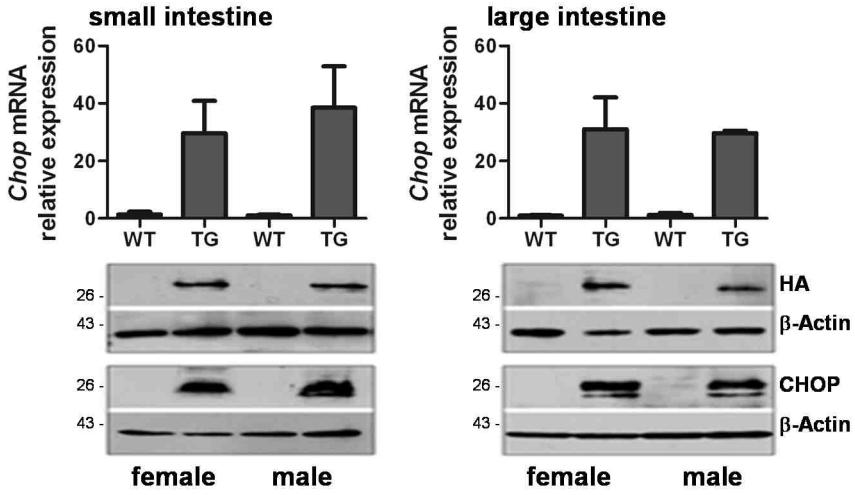

Figure 15. Transgene expression in IEC isolates from small and large intestine of *Chop*$^{IEC\ Tg/Tg}$ mice and wild-type controls.

IECs were isolated from small and large intestine of 12 week old transgenic mice and wild-type controls (n = 3). Chop mRNA was determined by qPCR using intron-spanning primer pair. Data are plotted as means ± SD. Pooled protein lysates were analyzed by Western blotting applying antibodies against CHOP protein and HA-tag.

Chop$^{IEC\ Tg/Tg}$ mice showed high CHOP-HA protein expression in small and large intestine, respectively. Detected protein bands differ in molecular weight from ~26 to ~30 kDa, suggesting transgenic CHOP-HA to be post-translationally modified. The transgene is broadly expressed on both vertical and horizontal axis of the intestine (Figure 16). Immunofluorescense staining of colonic tissue sections indicated nuclear translocation of the HA-tagged transgene. Analysis of CHOP-HA protein expression along the intestine was performed by Western blotting using IEC isolates from the distinct intestinal sections.

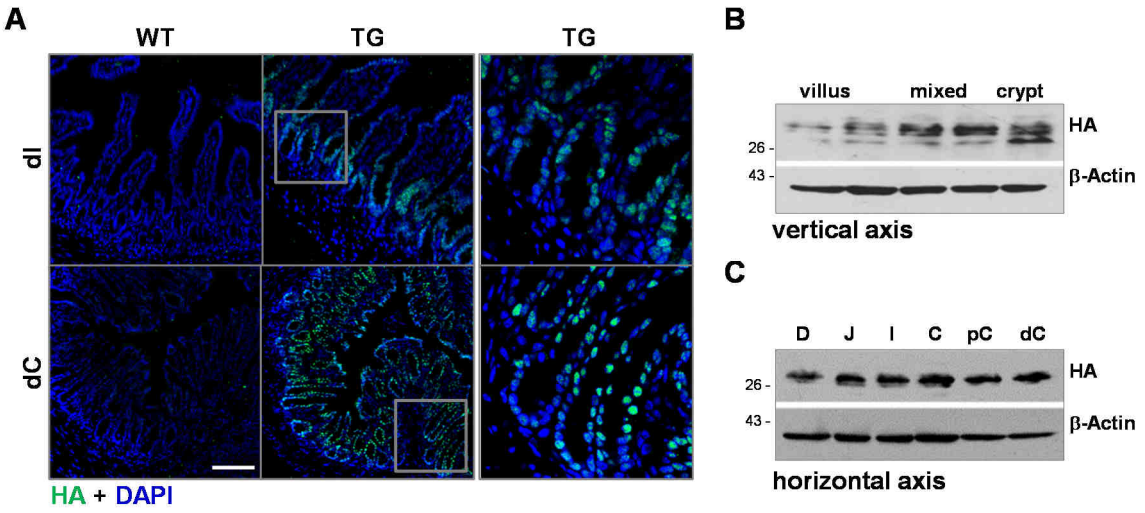

Figure 16. Expression of CHOP-HA on vertical and horizontal axis of the intestine.

(A) Transgene expression was analyzed on 5 µm-thick colonic tissue section using anti-HA antibody. DAPI was applied for nuclear staining. Scale bar represents 100 µm. (B) Jejunal IECs were isolated from villus tip to the crypt and Western blot analysis was performed by using anti-HA antibody. (C) Total IEC isolates from intestinal sections duodenum, jejunum, ileum, cecum, proximal colon, and distal colon were analyzed by Western blotting using anti-HA antibody. Western blot data (B, C) represent results of 3 independent experiments

Transgene expression along the vertical axis was determined by Western bot analysis using jejunal epithelial cells from the villus and the crypt region. Therefore, 10 fractions containing jejunal IECs isolated from villus tip to the crypt were analyzed by qPCR for crypt markers including Ki-67 and Hes1 (Figure 17).

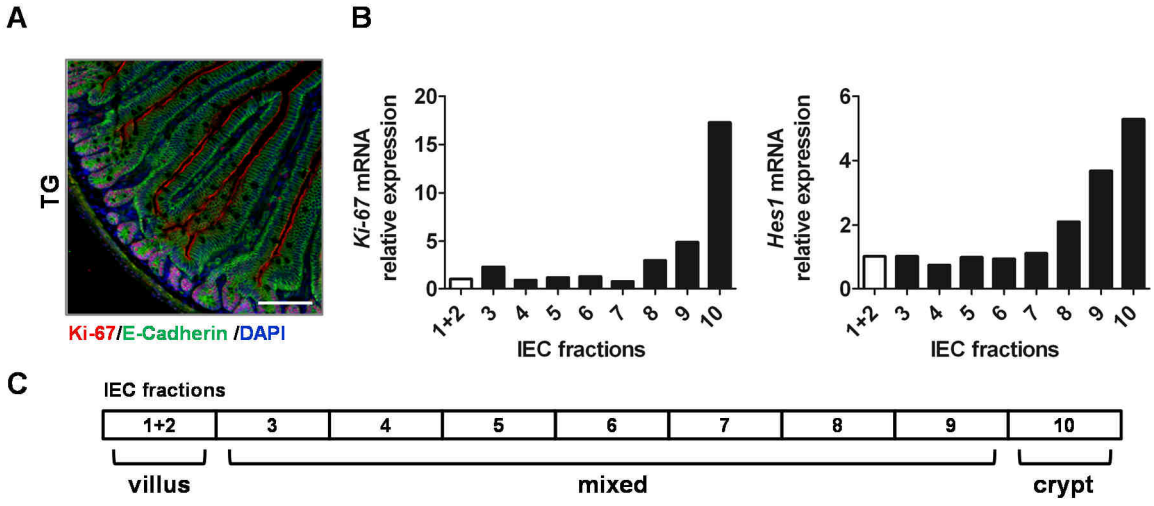

Figure 17. Characterization of IEC fraction isolated from villus tip to the crypt.

(A) IF of Ki-67 on jejunal tissue section of transgenic mice. Scale bar represents 100 µm. Luminal red lining displays unspecific staining. (B) IEC fractions were analyzed for Ki-67 and Hes1 mRNA expression. Expression levels were calculated relative to fractions 1+2. (C) IEC fractions were characterized as fractions containing epithelial cells derived from villus tip and crypt region, respectively, according to the results obtained from qPCR for Ki-67 and Hes1 mRNA expression

Both Ki-67 and Hes1 mRNA expression was enhanced in fractions 8 to 10 with highest expression levels in fraction 10. With regard to jejunal tissue sections stained against Ki-67, proliferative cells could be specifically detected in crypt regions. Accordingly, fraction 10 has been defined to contain IECs derived from crypts, while epithelial cells isolated from villus tip have been regarded in fractions 1 and 2. Fractions 3 to 9 have been considered as mixed cell population. Taken together, *Chop*$^{IEC\ Tg/Tg}$ mice show high expression levels of nuclear located transgenic CHOP that is broadly expressed in IECs along the vertical and horizontal axis of the intestine.

4.1.3 *Chop*$^{IEC\ Tg/Tg}$ mice do not spontaneously develop intestinal inflammation

12 weeks old *Chop*$^{IEC\ Tg/Tg}$ mice and wild-type controls were examined by chromoendoscopy using methylene blue for mucosal tissue staining. Following the colonoscopic evaluation, *Chop*$^{IEC\ Tg/Tg}$ mice appeared disease-free (Figure 18), which could further be confirmed at the histological level regarding histopathological parameters, such as crypt loss and inflammatory cell infiltration (Figure 19).

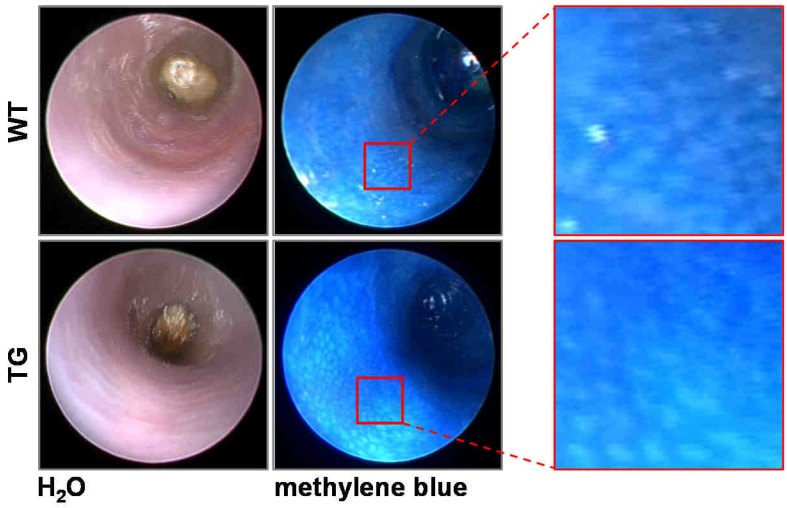

Figure 18. Chromoendoscopic evaluation of *Chop*$^{IEC\ Tg/Tg}$ mice.

Colonoscopy was performed in transgenic mice and controls before and after methylene blue was instilled into the colon. Colonic mucosa was evaluated for vascular structures, colonic crypt structures, and changes in mucus production.

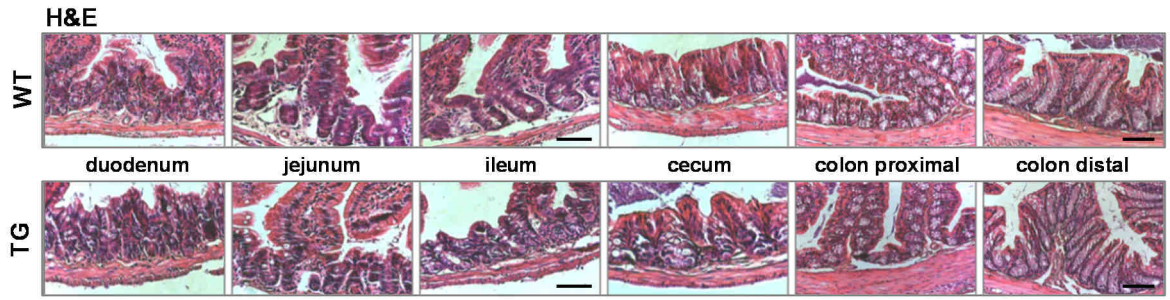

Figure 19. H&E stained intestinal sections of *Chop*$^{IEC\ Tg/Tg}$ mice.

Tissue sections from duodenum, jejunum, ileum, cecum, proximal colon, and distal colon of transgenic mice and wild-type controls were stained with hematoxylin and eosin. Scale bar represents 50 µm for small intestinal sections, 100 µm for cecum and colon

Furthermore, alcian blue-stained intestinal tissue sections from transgenic mice and wild-type controls with an age of 12, 24, 36, and 52 weeks were examined for morphological changes evaluating villus height, crypt depth, as well as mucus area. In addition, total numbers of apoptotic IECs per mm^2 (cleaved Caspase 3) as well as proliferative cells per crypt (Ki-67) were assessed by IHC and IF (Figure 20 and Figure 21). As already indicated by the macroscopic observations, enhanced CHOP protein expression did not affect histometric characteristics, while numbers of both apoptotic and proliferative cells remained comparably to wild-type controls.

In conclusion, high CHOP protein expression does not lead to spontaneously developed inflammation of the intestine.

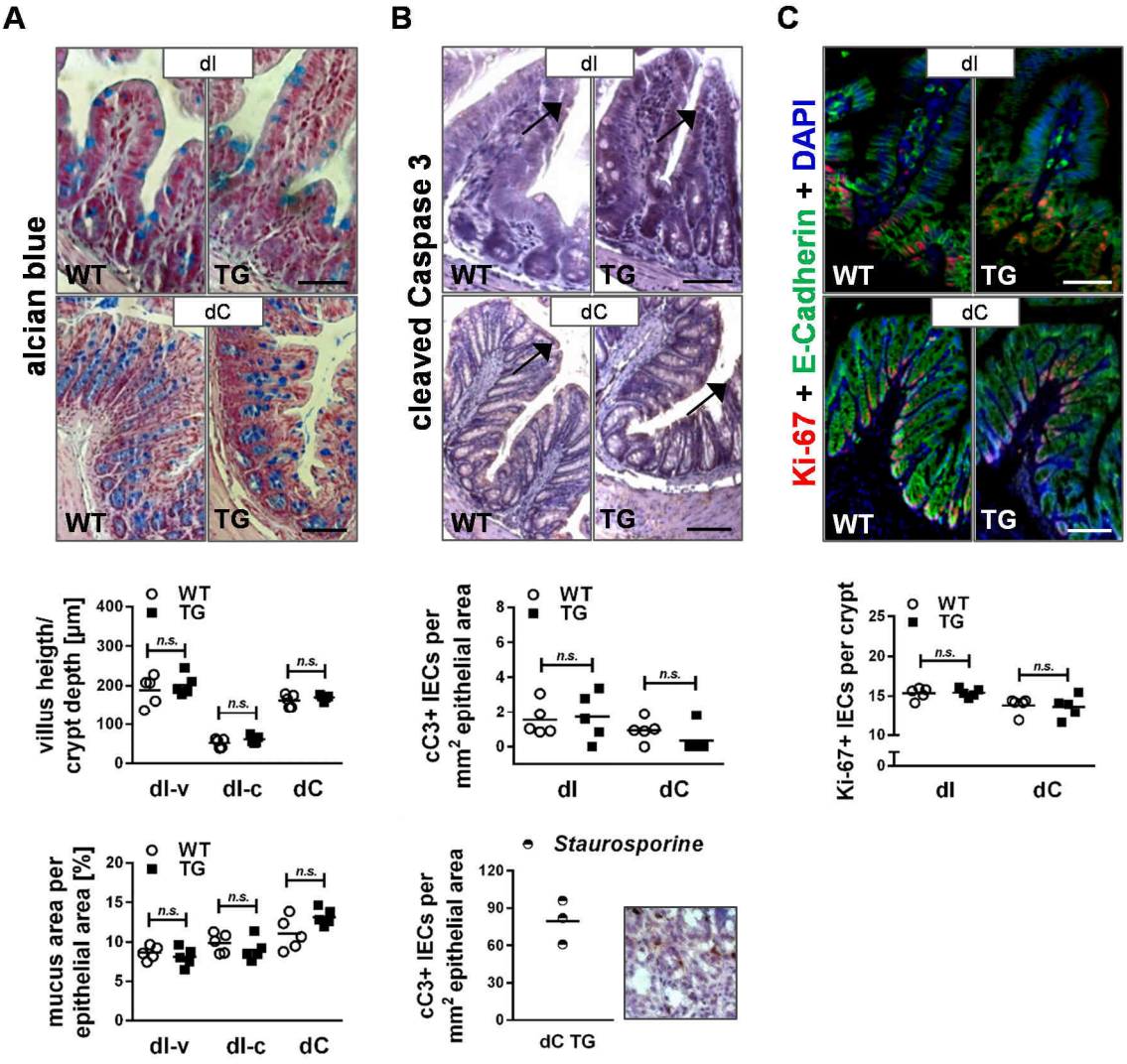

Figure 20. Epithelial cell morphology of *Chop*$^{IEC\ Tg/Tg}$ mice with an age of 12 weeks.

(A) Morphology of distal ileum (dI) and distal colon (dC) (n = 5) was analyzed using 5 µm-thick, alcian blue-stained tissue sections evaluating villus height, crypt depth, total epithelial area, and mucus area of 15-20 villi and/or crypts per animal, respectively, and means were calculated. Mucus area was assessed as percentage of total epithelial area. (B) Caspase 3 cleavage was considered as an apoptotic marker. Numbers of apoptotic cells were assessed in a total epithelial area of 1 mm^2 (see arrows). CC3 positive control staining was performed on 5 µm tissue sections derived from distal colon of transgenic mice treated *ex vivo* with 1 µM staurosporine for 2 h at 37° C. (C) Proliferative cells were detected by applying anti-Ki-67 antibody. For each tissue section, total numbers of Ki-67 positive cells were determined in 15-20 crypts and means were calculated. Data are plotted as numbers of proliferative cells per crypt. All data sets were analyzed by non-parametric rank-sum test, $P < .05$ was considered statistically significant. Scale bars represent 50 µm (dI) and 100 µm (dC).

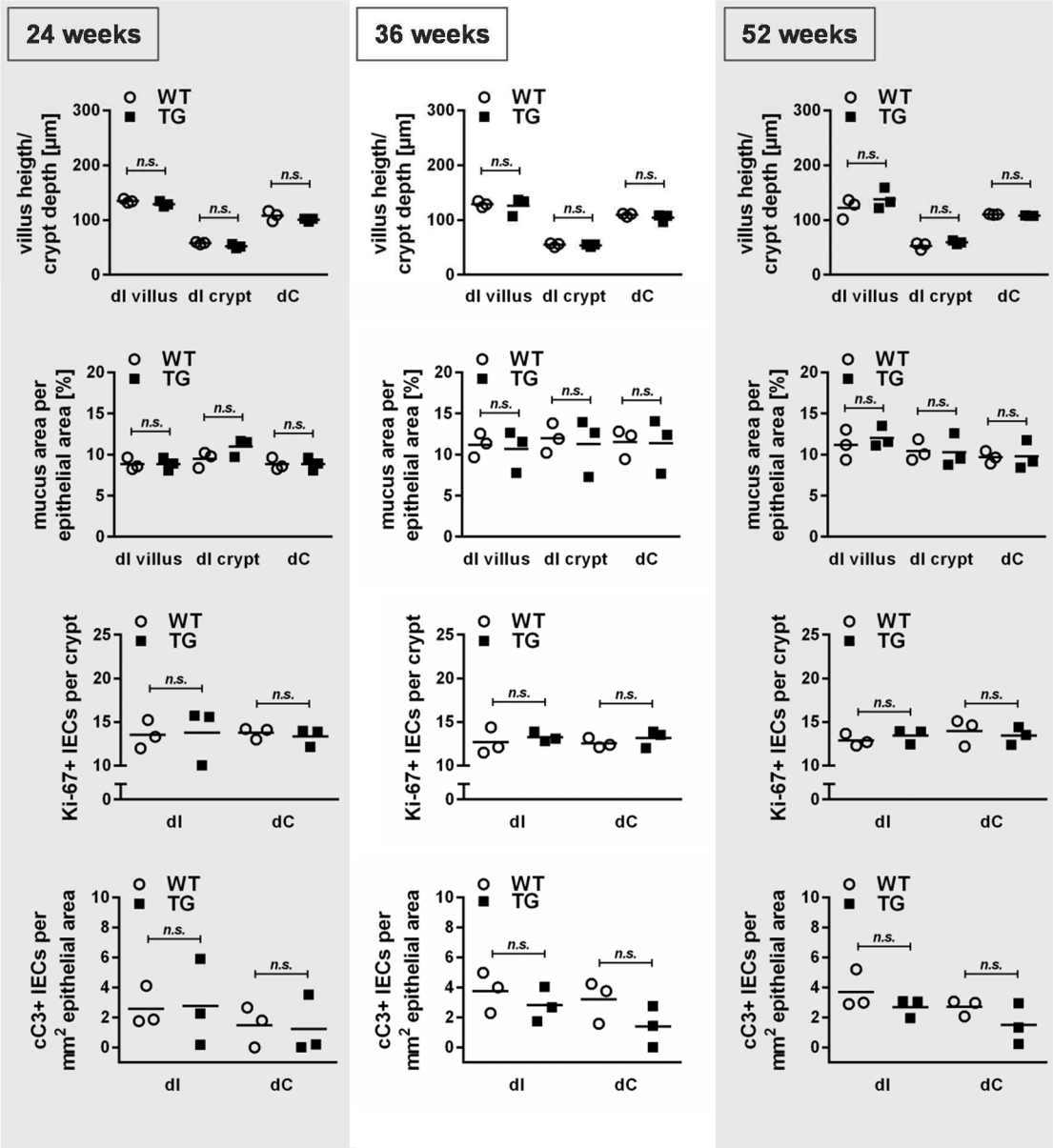

Figure 21. IEC morphology of transgenic mice with an age of 24, 36, and 52 weeks.

Analysis of epithelial cell morphology of 24, 36, and 52 weeks old transgenic mice and wild-type controls (n = 3) was performed as mentioned for mice with an age of 12 weeks. All data sets were analyzed by non-parametric rank-sum test, $P < .05$ was considered statistically significant.

4.1.4 Protein overexpression does not induce unspecific stress signaling

Transgene overexpressing animal models have been frequently criticized to induce cellular stress responses in an unspecific manner. Since CHOP-HA has been shown highly expressed in IECs, transgene-driven protein overload-dependent activation of stress-related signaling pathways was analyzed (Figure 22). Western blotting of both phosphorylated p38 MAP kinase and RelA, indicated that enhanced protein expression has no impact on activation of MAP kinase and NF-κB.

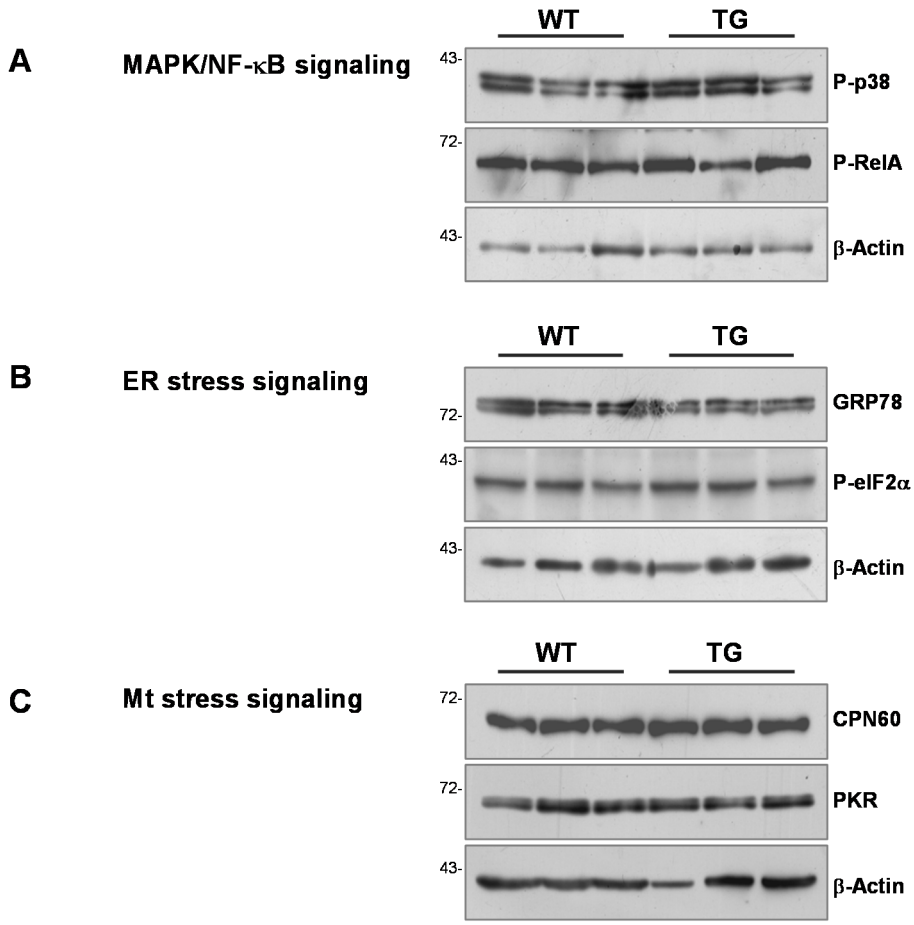

Figure 22. Protein overload upon transgene overexpression does not cause activation of NF-κB, MAP kinase, ER stress signaling, and mitochondrial stress signaling.

Protein overload-driven activation of stress-related signaling was examined by Western blotting using colonic IEC isolates. (A) Activation of NF-κB signaling was analyzed by using anti-P-RelA antibody. MAP kinase activation was determined applying anti-P-p38 antibody. (B) ER stress signaling was examined by using antibodies against GRP78 and P-eIF2α. (C) Induction of mitochondrial stress was analyzed by using anti-CPN60 and anti-PKR antibodies. Shown data represent 3 independent experiments.

Furthermore, ER stress signaling (GRP78, p-eIF2α) as well as mitochondrial stress signaling (CPN60, PKR) remained unaffected by transgene overexpression. Taken together, elevated CHOP expression does not influence protein homeostasis in an unspecific manner.

4.2 Microarray analysis identifies CHOP-dependent changes in the inflammatory gene expression program

4.2.1 Enhanced CHOP protein expression sensitizes mice to stress-responsive gene regulation

To elucidate CHOP-driven transcriptional changes, gene expression profiling of disease-free *Chop*$^{IEC\ Tg/Tg}$ mice and wild-type controls (n = 8) was performed by whole genome microarray analysis using IEC isolates from colonic tissue. 530 genes were identified as significantly regulated (*P* < *.05*) in transgenic mice compared to wild-type controls (Figure 23). 318 genes revealed an expression up to approximately 2-fold increase, whereas fold changes of most down-regulated genes appeared to be 2- to 5-fold decreased.

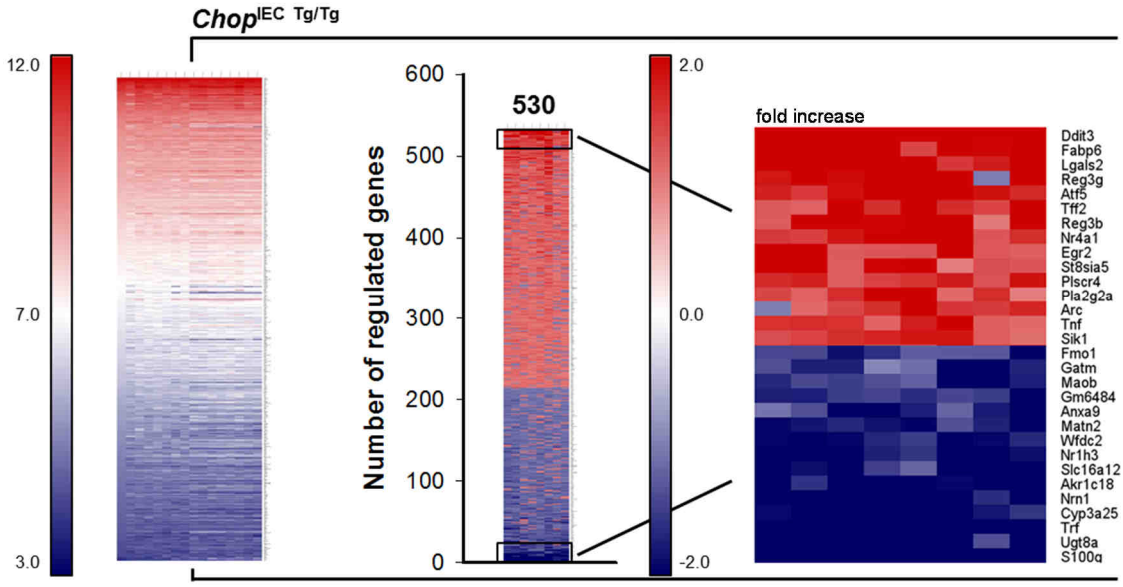

Figure 23. Gene expression profiling of *Chop*$^{IEC\ Tg/Tg}$ mice indicates changes in the inflammatory gene program.

Microarrays were performed by using freshly isolated total colonic IECs from female transgenic mice and wild-type controls with an age of 12 weeks (n = 8). Log2-based signal intensity ranged from 3 to 12. Expression data of 530 significantly regulated genes (*P* < *.05*) are presented as fold-change over wild-type controls. Next, top 15 up- and down-regulated genes were illustrated.

Top 10 up- and down-regulated genes are shown in Table 7. As expected, Ddit3 appears highest induced in *Chop*$^{IEC\ Tg/Tg}$ mice, while C/EBP signaling pathway was identified as one of the most significantly regulated pathways (Table 8).

Table 7. Most highly regulated genes in *Chop*$^{IEC\ Tg/Tg}$ mice are shown as TOP 10 up-regulated and TOP 10 down-regulated genes, respectively.

Chop$^{IEC\ Tg/Tg}$ mice versus *Chop*$^{flox/flox}$ mice							
TOP 10 up-regulated				TOP 10 down-regulated			
gene ID	gene name	description	fold change	gene ID	gene name	description	fold change
13198	Ddit3	DNA-damage inducible transcript 3	3,27	12309	S100g	S100 calcium binding protein G	-5,54
16204	Fabp6	fatty acid binding protein 6	2,40	22239	Ugt8a	UDP galactosyltransferase 8A	-3,41
107753	Lgals2	lectin, galactose-binding, soluble 2	2,05	22041	Trf	transferrin	-3,37
19695	Reg3g	regenerating islet-derived 3 gamma	1,99	56388	Cyp3a25	cytochrome P450, family 3	-2,58
107503	Atf5	activating transcription factor 5	1,88	105349	Akr1c18	aldo-keto reductase family 1	-2,39
21785	Tff2	trefoil factor 2	1,86	68404	Nrn1	neuritin 1	-2,39
18489	Reg3b	regenerating islet-derived 3 beta	1,85	240638	Slc16a12	solute carrier family 16	-2,10
15370	Nr4a1	nuclear receptor subfamily 4	1,81	22259	Nr1h3	nuclear receptor subfamily 1	-2,00
13654	Egr2	early growth response 2	1,78	67701	Wfdc2	WAP four-disulfide core domain 2	-1,96
225742	St8sia5	ST8 alpha-N-acetyl-neuraminide alpha-2,8-sialyltransferase 5	1,77	17181	Matn2	matrilin 2	-1,82

Table 8. Significantly regulated signal transduction pathways in *Chop*$^{IEC\ Tg/Tg}$ mice. Analysis was performed by using the GeneRanker tool in the Genomatix Genome Analyzer.

pathway	pathway ID	genes observed	genes expected	P-value
FBJ MURINE OSTEOSARCOMA VIRAL ONCOGENE HOMOLOG B	PW_FOSB_MUS_MUSCULUS	6	0	2,77E-07
CAMP RESPONSIVE ELEMENT BINDING PROTEIN 1	PW_CREB1_MUS_MUSCULUS	18	7	9,10E-05
CCAAT/ENHANCER BINDING PROTEIN (C/EBP), BETA	PW_CEBPB_MUS_MUSCULUS	8	2	3,82E-04
CHEMOKINE (C C MOTIF) LIGAND 2	PW_CCL2_MUS_MUSCULUS	9	3	8,56E-04
HEPATOCYTE GROWTH FACTOR RECEPTOR	PW_HGF_MUS_MUSCULUS	8	3	4,16E-03
MATRIX METALLOPROTEINASE	PW_MMP_MUS_MUSCULUS	13	6	6,94E-03
P90 RIBOSOMAL PROTEIN S6 KINASE	PW_P90RSK_MUS_MUSCULUS	8	3	8,76E-03
PEROXISOME PROLIFERATOR ACTIVATED RECEPTOR GAMMA	PW_PPARG_MUS_MUSCULUS	9	4	9,96E-03

GO analysis reflecting short distance biological process child terms showed most significant gene enrichment affected by up-regulated genes, while changes in both metabolic process and localization additionally result from down-regulated gene sets (Table 9).

Table 9. Significantly regulated child terms of the GO term biological process. The shown child terms with significant enrichment of total regulated genes as well as up- and down-regulated genes, respectively, display main biological processes with a distance of 1 regarding the process tree. Analysis was performed by using the GeneRanker tool in the Genomatix Genome Analyzer.

GO-term	ID	total gene regulation			up-regulated	down-regulated
		genes observed	genes expected	P-value	P-value	P-value
metabolic process	GO:0008152	295	197	3,20E-19	2,30E-13	2,30E-07
cellular process	GO:0009987	344	277	5,02E-10	1,40E-11	--
localization	GO:0051179	130	82	2,50E-08	3,00E-05	1,70E-04
immune system process	GO:0002376	51	26	5,99E-06	6,40E-07	--
locomotion	GO:0040011	42	20	3,76E-06	6,60E-05	--
developmental process	GO:0032502	120	80	2,17E-06	5,50E-08	--
response to stimulus	GO:0050896	177	143	4,90E-04	8,90E-06	--
multi-organism process	GO:0051704	27	13	4,27E-04	6,90E-03	--
biological regulation	GO:0065007	229	189	1,57E-04	7,70E-12	--

The four most enriched categories were further processed as followed. First, the biological process child terms cellular process, metabolic process, biological regulation, and response to stimulus were analyzed for shared gene sets (Figure 24A). Second, numbers of shared genes were calculated as percentage to total numbers of annotated genes (Figure 24B). As shown in Figure 24B, high enrichment of overlapping genes could be evaluated for the GO term response to stimulus (115 out of 177). Even though it remains unsolved whether CHOP directly impacts on the expression levels of these genes, it is worth to note that top regulated genes in the GO term response to stimulus reflected most of the highest enhanced/decreased genes in *Chop*$^{IEC\ Tg/Tg}$ mice (Table 10). With respect to GO terms annotated downstream of response to stimulus, highly significant changes in gene expression could be observed associated with inflammatory responses including the defense response and response to wounding (Table 11).

Taken together, these findings suggested that *Chop*$^{IEC\ Tg/Tg}$ mice exhibit changes in the gene expression program highly associated with IEC-driven microbial defense and response to wounding, but under normal conditions develop no spontaneous inflammation.

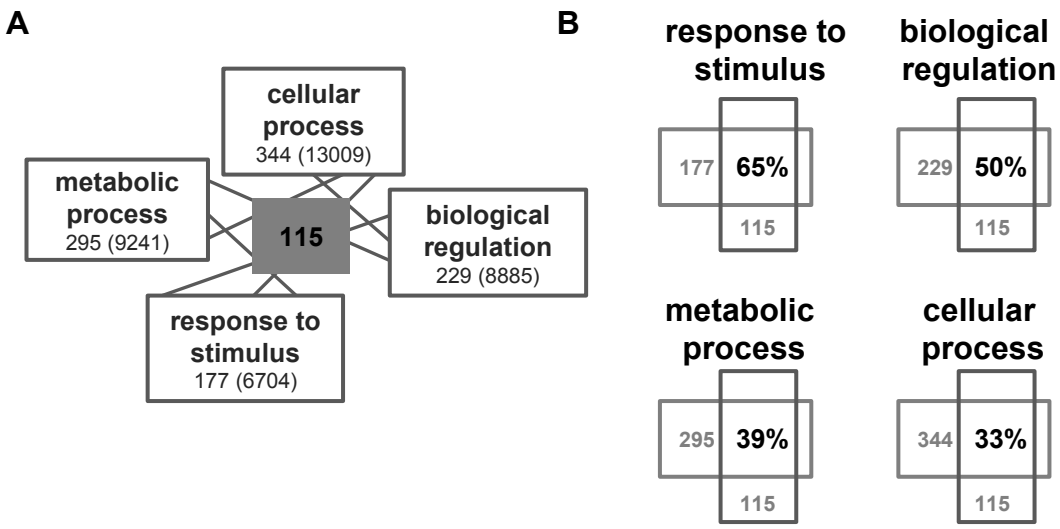

Figure 24. GO analysis regarding short distance biological process child terms revealed changes in the expression program associated with response to stimulus, death, and cell cycle.

Short distance biological process child terms indicating most enriched gene accumulation were analyzed for overlapping gene sets. (B) Total number of 115 overlapping genes was analyzed for significantly regulated biological process child terms. Herein, 10 most regulated overlapping genes associated with most significantly enriched categories were shown aside.

Table 10. Most highly regulated genes in *Chop*$^{IEC\ Tg/Tg}$ mice regarding GO term *response to stimulus* are shown as TOP 10 up-regulated and TOP 10 down-regulated genes, respectively.

response to stimulus							
TOP 10 up-regulated				**TOP 10 down-regulated**			
gene ID	**gene name**	**description**	**fold change**	**gene ID**	**gene name**	**description**	**fold change**
13198	Ddit3	DNA-damage inducible transcript 3	3,27	22041	Trf	transferrin	-3,37
19695	Reg3g	regenerating islet-derived 3 gamma	1,99	105349	Akr1c18	aldo-keto reductase family 1	-2,39
21785	Tff2	trefoil factor 2	1,86	22259	Nr1h3	nuclear receptor subfamily 1	-2,00
18489	Reg3b	regenerating islet-derived 3 beta	1,85	17181	Matn2	matrilin 2	-1,82
15370	Nr4a1	nuclear receptor subfamily 4	1,81	71790	Anxa9	annexin A9	-1,71
13654	Egr2	early growth response 2	1,78	67092	Gatm	glycine amidinotransferase	-1,59
21926	Tnf	tumor necrosis factor	1,54	57444	Isg20	interferon-stimulated protein	-1,52
17691	Sik1	salt inducible kinase 1	1,53	56615	Mgst1	microsomal glutathione S-transferase 1	-1,40
16007	Cyr61	cysteine rich protein 61	1,52	19662	Rbp4	retinol binding protein 4, plasma	-1,39
14283	Fosl1	fos-like antigen 1	1,48	237038	Nox1	NADPH oxidase 1	-1,37

Table 11. Significantly regulated child terms defense response and response to wounding of the biological process term response to stimulus. Analysis was performed regarding total regulated genes as well as up- and down-regulated genes by using the GeneRanker tool in the Genomatix Genome Analyzer.

Distance to	GO-term	ID	total gene regulation			up-regulated	down-regulated
biological process			genes observed	genes expected	P-value	P-value	P-value
1	response to stimulus	GO:0050896	177	143	4,90E-04	8,92E-06	--
2	response to stress	GO:0006950	70	41	6,52E-06	4,92E-07	--
3	defense response	GO:0006952	31	15	2,08E-04	4,73E-04	--
3	response to wounding	GO:0009611	29	12	1,64E-05	5,14E-06	--
4	inflammatory response	GO:0006954	20	8	8,95E-05	2,25E-04	--

4.2.2 Validation of gene expression profiles by analyzing Reg3β expression

With regard to microarray data, highly significant changes in the expression of gene sets, such as enhanced expression of regenerating gene 3 (Reg3) family members *Reg3*α (+1.2-fold), *Reg3*β (+1.9-fold), and *Reg3*γ (+2-fold) could be observed in the colonic epithelium of disease-free *Chop*$^{IEC\ Tg/Tg}$ mice indicating a modulation of the gene expression program associated with microbial defense and response to wounding. Microarray-based up-regulation of Reg3β in colonic IECs has been validated by Western blotting and qPCR, while Reg3β expression is not affected in distal ileum of transgenic mice (Figure 25).

Notably, different mRNA expression levels of Reg3β could be observed in proximal and distal colonic epithelial cells (*proximal colon:* ΔCT ~ -4.7, $\Delta\Delta$CT ~ 1.4*; distal colon:* ΔCT ~ -15.4, $\Delta\Delta$CT ~ 4.3), which could be confirmed at the protein expression level regarding IF for Reg3β on tissue sections of proximal and distal colon (Figure 26).

In conclusion, these findings validated microarray-based up-regulation of Reg3β in IECs of *Chop*$^{IEC\ Tg/Tg}$ mice at the level of mRNA and protein expression. Notably, the expression of Reg3β is specifically up-regulated in colonic tissue, but not in epithelial cells of the small intestine.

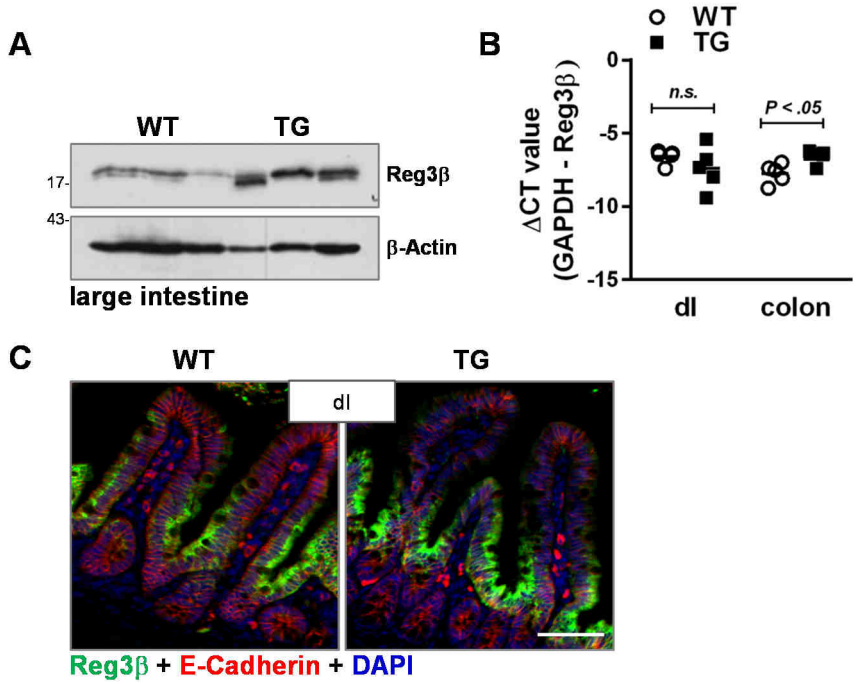

Figure 25. Reg3β expression in IECs of colon and distal ileum.

(A) Reg3β expression was analyzed by Western blotting using colonic epithelial cell isolates from transgenic mice and wild-type controls (n = 3). (B) mRNA expression of Reg3β in IECs isolates of distal ileum and colon from TG and WT mice (n = 3). Statistical significance was assessed by Student's t-test. *P < .05* was considered statistically significant. (C) Reg3β expression in IECs of distal ileum from TG and WT mice, respectively. Scale bar represents 50 µm.

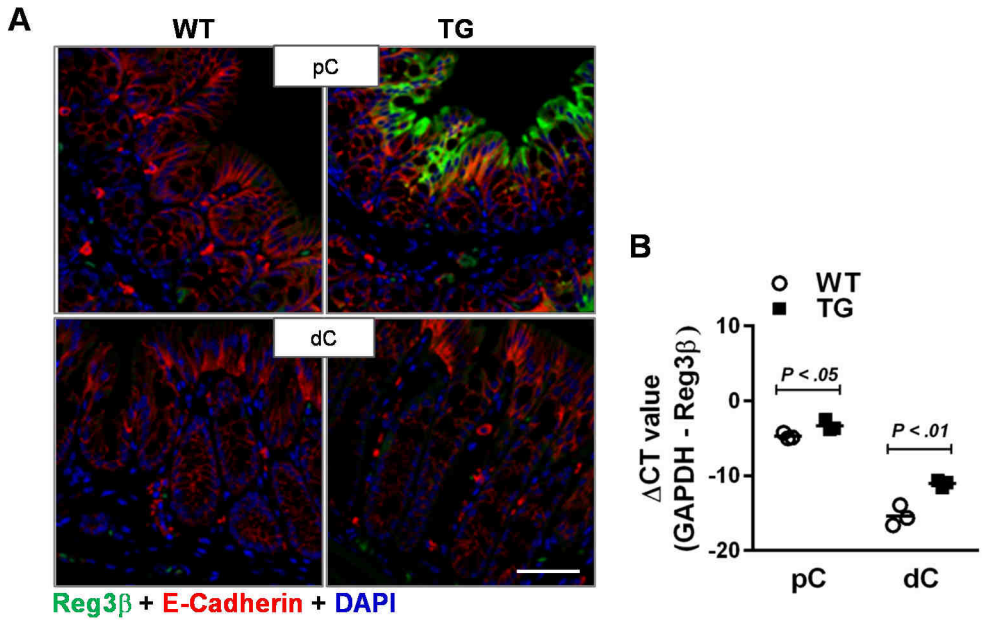

Figure 26. Validation of microarray data through the analysis of Reg3β expression.

(A) IF for Reg3β was performed on 5 µm tissue sections of proximal and distal colon from transgenic mice and wild-type controls, respectively. Scale bar represents 50 µm. (B) Reg3β expression was analyzed by qPCR using IECs derived from proximal and distal colon of *Chop*$^{IEC\ Tg/Tg}$ mice and wild-type controls (n = 3). Statistical significance was assessed by Student's t-test. *P < .05* was considered statistically significant.

4.3 IEC-specific CHOP overexpression does not affect infection with *Citrobacter rodentium*, but exacerbates DSS-induced colitis

4.3.1 Enhanced CHOP protein expression does not affect colonization and clearance of *Citrobacter rodentium*

Infection of mice with the gram-negative, mouse-specific, enteric pathogen *C. rodentium* triggers colonic inflammation associated with Goblet cell loss and epithelial hyperplasia that serves as a study model for human enteric infection with the pathogens enteropathogenic *Escherichia coli* (*E. coli*) and enterohaemorrhagic *E. coli* [210-212]. Recently published data clearly demonstrated that changes in Reg3β expression affected the outcome of colitis mediated by the gram-negative pathogen *Salmonella enteritidis* [213]. Thus, *C. rodentium*-mediated colitis is considered as an adequate study model to investigate the effects of CHOP-driven changes in the microbial defense program associated with enhanced Reg3β expression. Based on the course of infection and body weight development, *C.rodentium*-induced colitis in *Chop*$^{IEC\ Tg/Tg}$ mice proceeded comparably to infected wild-type controls (Figure 27).

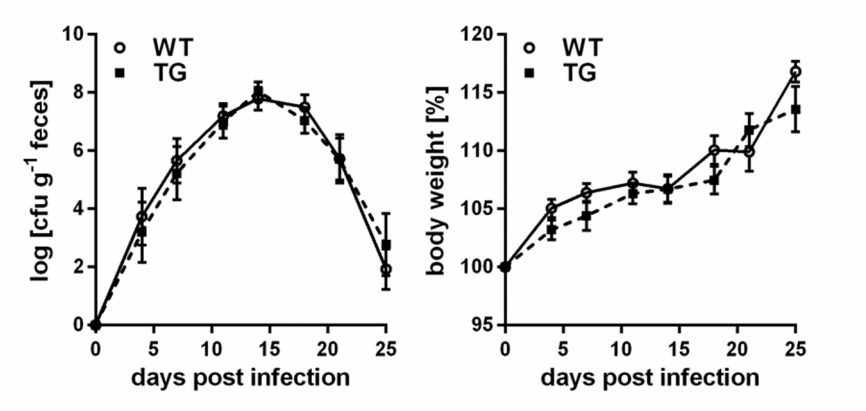

Figure 27. *C. rodentium* infection of 8 weeks old *Chop*$^{IEC\ Tg/Tg}$ mice and wild-type controls.

Female transgenic mice (n = 8) and wild-type controls (n = 10) were orally infected with approximately 2x 10^9 CFU of *C. rodentium* ICC169. Fecal pellets were collected every 2-3 days and the course of infection was assessed by determining the bacterial load of *C. rodentium* in fecal pellets. *C. rodentium* counts are plotted as mean ± SEM log10 CFU per gram of feces. Body weight changes were determined every 2-3 days. Data are presented as mean ± SEM.

Consistent with these data, similar progression of *C. rodentium* infection in transgenic mice and wild-type controls could be observed regarding colonic weight/length ratio as well as disease activity parameters, such as distal colonic crypt depth and mucus area (Figure 28).

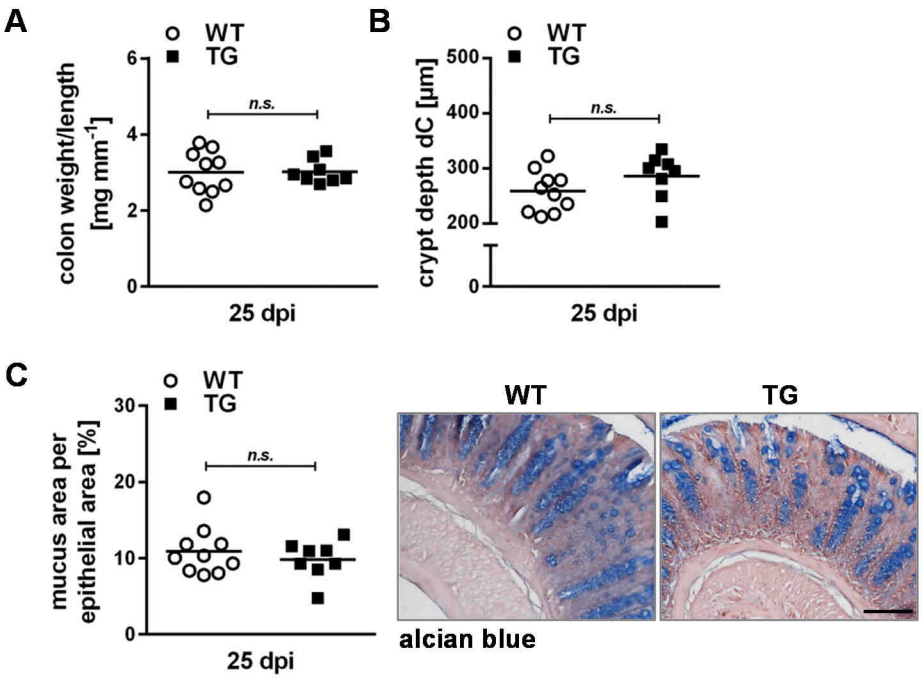

Figure 28. Disease parameter in *C. rodentium* infection.

(A) The macroscopic disease activity parameter colonic weight/length ratio in mg/mm was calculated for each mouse 25 days post infection (dpi). (B, C) 5 µm tissue sections of paraffin-embedded colonic tissue were stained with alcian blue. Crypt length, total epithelial area, and mucus area was assessed in distal colon of each mouse. Mucus area is plotted as percentage of total epithelial area. Representative tissue sections of distal colon are shown, scale bar represents 200 µm. Statistical significance was assessed by non-parametric rank-sum test, $P < .05$ was considered statistically significant.

It is known that *C. rodentium* spreads to the distal colon shortly after cecal colonization [214, 215]. Since neither colonization nor clearance of *C. rodentium* was affected in transgenic mice, we addressed Reg3β expression in first, cecal tissue of disease-free *Chop*$^{IEC\ Tg/Tg}$ mice, second colonic tissue of infected mice. Interestingly, disease-free transgenic mice showed unchanged expression of Reg3β when IEC-specific protein levels were compared to wild-type controls (Figure 29), while infected mice (WT and TG) clearly revealed elevated Reg3β expression during clearance of *C. rodentium* (Figure 30).

Taken together, these findings suggest that elevated Reg3β expression in colon of disease-free *Chop*$^{IEC\ Tg/Tg}$ mice does not play an important role in colonization and clearance of *C. rodentium*.

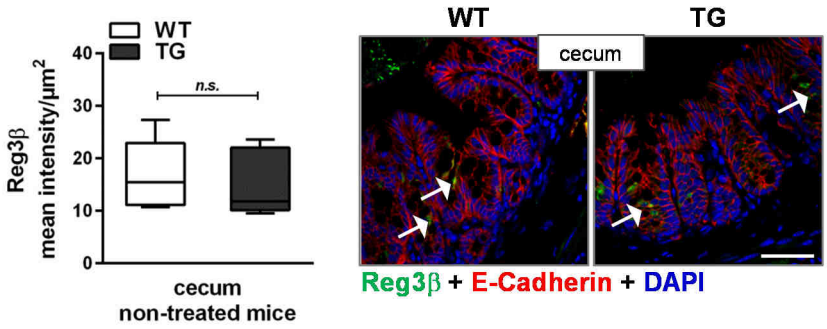

Figure 29. Reg3β expression in cecal tissue of *Chop*$^{IEC\ Tg/Tg}$ mice and wild-type controls.

Immunofluorescence was performed on 5 µm cecal tissue sections of disease-free transgenic mice and wild-type controls (n = 5 per group) by using primary antibody against Reg3β. IECs were detected applying anti-E-Cadherin antibody, DAPI was used for nuclear staining. Scale bar represents 50 µm. Reg3β-positive staining in IECs was quantified and mean intensity per µm^2 of epithelium is presented ±SD. Statistical significance was assessed by Student's t-test, $P < .05$ was considered statistically significant.

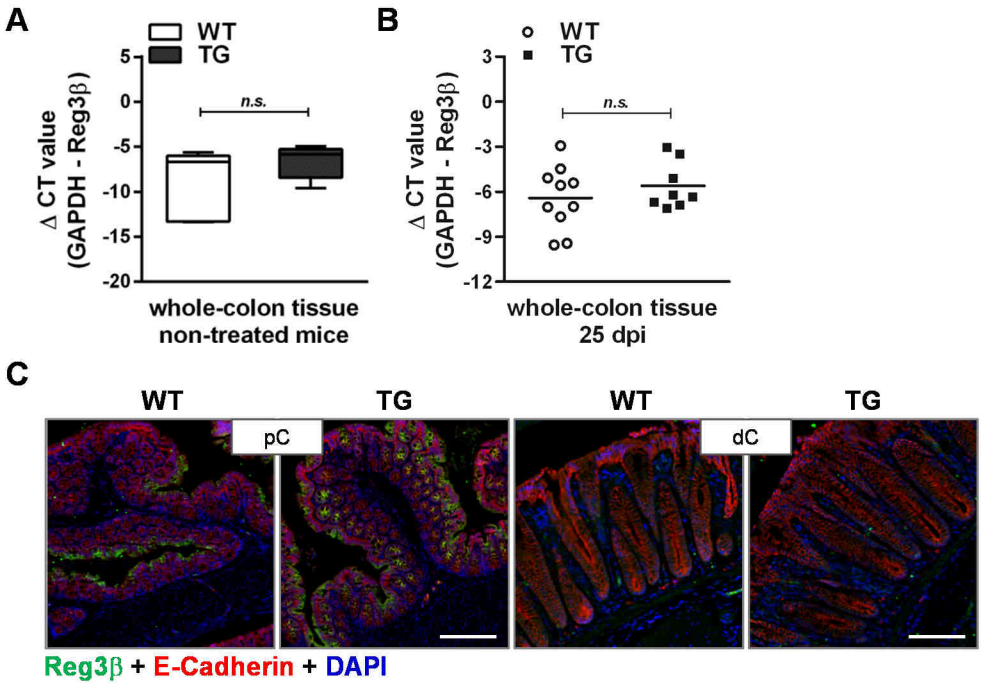

Figure 30. Analysis of Reg3β expression in mice 25 days after *C. rodentium* infection.

(A) Basal levels of Reg3β mRNA expression in whole-colon tissue were analyzed using pathogen-free female mice (n = 5 per group). Data are plotted as ΔCT ±SD. (B) Reg3β mRNA levels of *C. rodentium*-infected mice were analyzed by using total RNA isolates of whole-colon tissue that was dissected 25 dpi. Data are presented as ΔCT ±SD. (C) IF for Reg3β was performed using 5 µm-thick tissue sections from both proximal and distal colon of *Chop*$^{IEC\ Tg/Tg}$ mice and wild-type controls (25 dpi). Epithelial cells were stained using anti-E-Cadherin antibody. DAPI was used for nuclear staining. Scale bars represent 200 µm (pC) for pC and 100 µm (dC). Statistical significance for all data sets was assessed by Student's t-test, $P < .05$ was considered statistically significant.

4.3.2 High CHOP protein expression aggravates susceptibility to DSS-induced colitis associated with delayed recovery

DSS-induced colitis is characterized by severe changes of the intestinal architecture and epithelial damage, such as hyperproliferation, goblet cell loss, crypt loss, and ulcer formation, as well as infiltration of inflammatory cells [216, 217]. Although the specific effects of DSS on intestinal tissue are still unclear, the DSS-induced colitis model is widely used to elucidate the impact of distinct genes of interest on inflammatory processes. To investigate whether an IEC-specific CHOP overexpression has an effect on the inflammatory phenotype in experimental colitis, 2% DSS was orally given with drinking water for 3 and 7 days, respectively. *Chop*$^{IEC\ Tg/Tg}$ mice showed significantly enhanced severity in DSS-induced colitis regarding body weight loss and changes in DAI after 7 days of DSS administration (Figure 31).

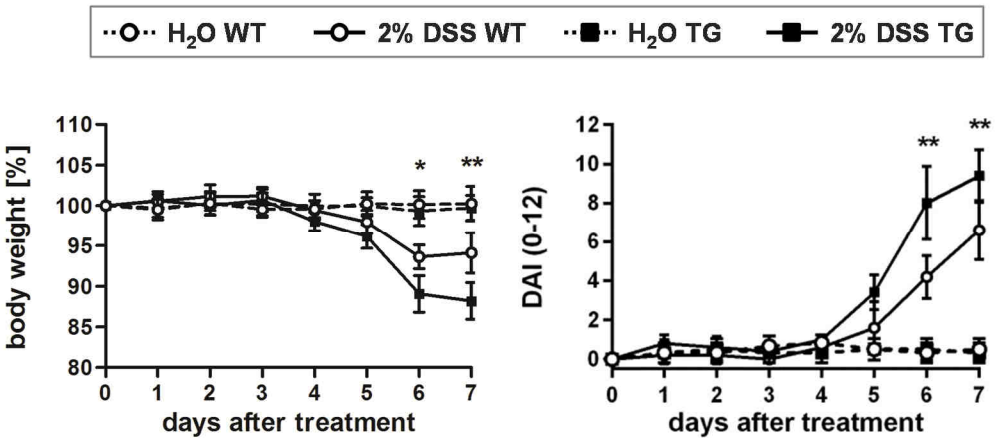

Figure 31. *Chop*$^{IEC\ Tg/Tg}$ mice are more susceptible to DSS-induced colitis.
Mice were given 2% of DSS for 7 days (n = 5), water was applied as negative control (n = 6). Body weight changes and DAI were monitored daily and percentage to initial body weight was assessed. Data sets were analyzed by TWA with genotype and DSS treatment as main factors followed by by Holm-Sidak test, $P < .05$ (*) and $P < .01$ (**) was considered statistically significant. Data were presented as means ±SD.

These data correlated with increased mucosal tissue damage in 3 and 7 days DSS-treated transgenic mice compared to wild-type controls (Figure 32A, Supplementary table 1). Similar effects were shown regarding the colonic weight/length ratio as well as the spleen/body weight ratio (Figure 32B).

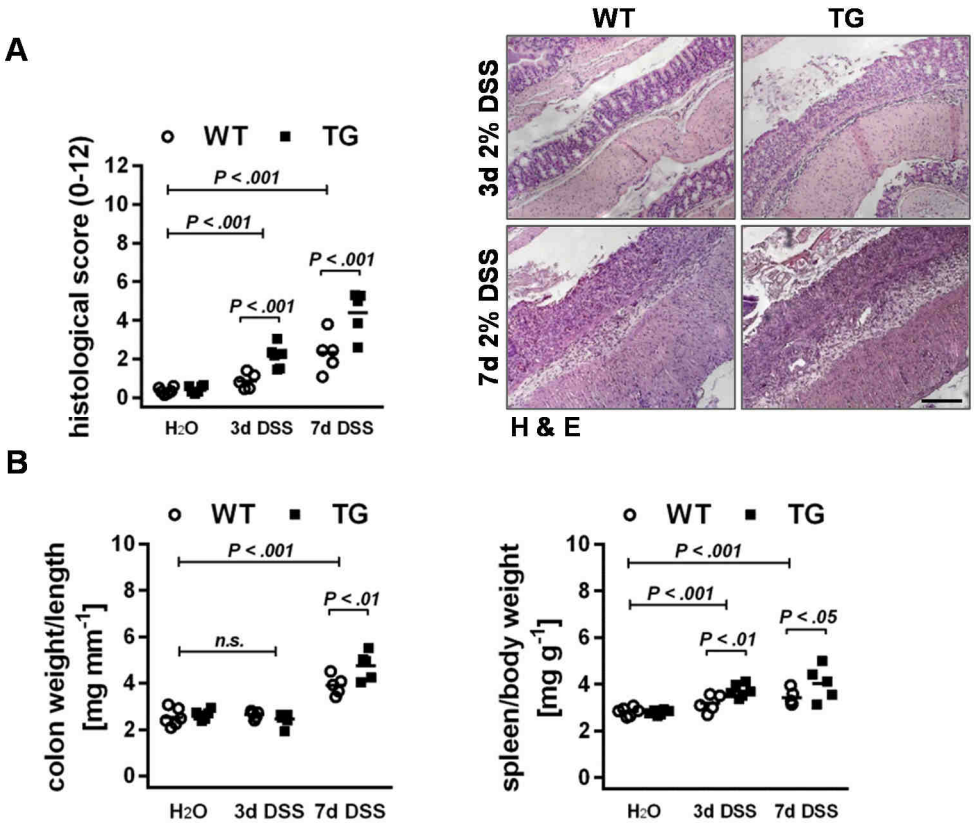

Figure 32. DSS-treated *Chop*$^{IEC\ Tg/Tg}$ mice reveal enhanced tissue pathology.

(A) Histological scores of colonic tissue sections are presented from both 3 days (*Chop*$^{IEC\ Tg/Tg}$ mice n = 6, wild-type controls n = 5) and 7 days DSS-treated mice (n = 5) as well as water-treated controls (n = 6). Representative H&E stained colonic tissue sections of DSS-treated mice are shown. Scale bar represents 200 µm. Colonic weight/length ratio in mg/ml and spleen/body weight ratio in mg/g are shown in (B). All data sets were analyzed by TWA with genotype and DSS treatment as main factors followed by Holm-Sidak test, *P < .05* was considered statistically significant. Significant differences are illustrated considering both genotype and treatment as well as genotype-dependent differences in one treatment group.

With regard to early inflammation, colonic tissue sections of 3 days DSS-treated mice were analyzed for immune cell infiltration. As shown in Figure 33, numbers of mucosa-infiltrating immune cells, including macrophages, are enhanced in *Chop*$^{IEC\ Tg/Tg}$ mice, while numbers of T cells (CD3), B cells (CD220, CD19), and neutrophils (Ly6g) remained unchanged when compared to wild-type controls.

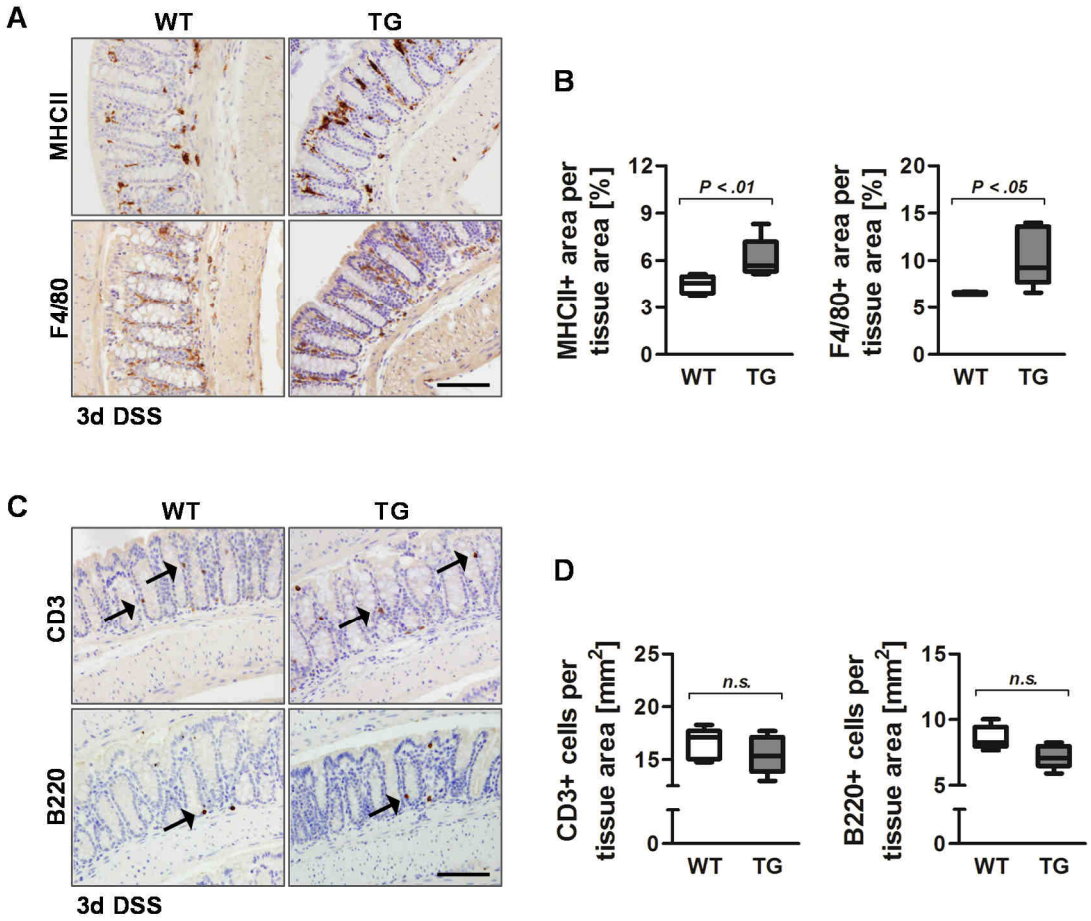

Figure 33. Analysis of mucosa-inflitrating immune cells in 3 days DSS-treated mice.
Colonic tissue sections of 3 days DSS-treated mice (n = 5-6) were analyzed for immune cell infiltration performing IHC for MHCII and F4/80 (A, B) as well as CD3 and B220 (C, D). MHCII+ and F4/80+ area, respectively, was quantified and calculated as percentage to total tissue area. CD3+ and B220+ cells were counted in total tissue and assessed as numbers of CD3+ and B220+ cells, respectively, per mm^2 of total tissue area. Statistical significance was assessed by non-parametric rank-sum test, *P < .05* was considered statistically significant.

To examine the early mechanisms of disease progression, colonic IEC were isolated from 3 days DSS-treated mice and water-treated controls, and analyzed for the expression of CHOP, GRP78 and CHOP target genes *Gadd34, Ero1α*, *Atf3*, *BIM*, *Trb3*, and *Bcl-2*. The expression of *Chop* mRNA was not significantly regulated upon DSS treatment using intron-spanning primer pair detecting both endogenous and transgenic *Chop*. Further analysis of Chop expression using primers specifically binding to the 5'-untranslated region of Chop revealed endogenous Chop mRNA expression 2.5- to 9-fold enhanced in DSS-treated mice compared to water-treated controls (Figure 34A). In contrast, endogenous CHOP protein expression was decreased, while GRP78 expression was induced in 3 days DSS-treated wild-type mice. Transgenic CHOP protein expression remained comparably regulated in DSS-and water-treated $Chop^{IEC\ Tg/Tg}$ mice (Figure 34B). Consistent with earlier observations,

CHOP-HA bands differed in molecular weight from ~26 to ~30 kDa with CHOP-HA ~26 kDa slightly more pronounced in DSS-treated mice.

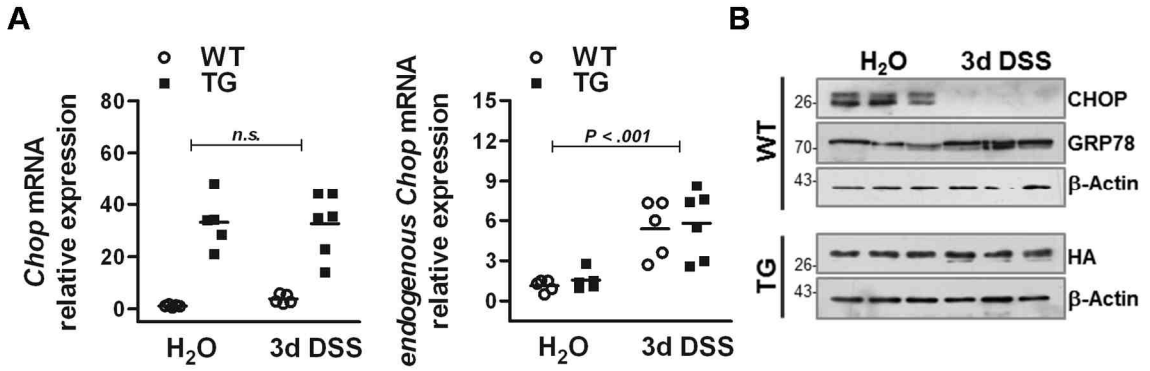

Figure 34. Analysis of CHOP and transgene expression in 3 days DSS-treated mice.
IECs were isolated from water-treated and 3d DSS-treated mice. (A) Expression of transgenic and endogenous Chop mRNA was detected by using intron-spanning primers, while endogenous Chop expression was specifically detected using primers binding to the 5'-untranslated region of Chop. Data were analyzed by TWA with genotype and DSS treatment as main factors followed by Holm-Sidak test, $P < .05$ was considered statistically significant. (B) Protein expression of CHOP, transgenic CHOP, and GRP78 (n = 3) was analyzed by Western blotting. β-Actin was used as loading control.

The analysis of CHOP target gene expression revealed significantly increased mRNA expression levels for *Gadd34*, *Ero1α* and *Atf3* in DSS-treated mice with significant higher induction of both *Gadd34* and *Ero1α* in DSS-treated transgenic mice (Figure 35). *Trb3* and *Bcl-2* could not be detected by qPCR.

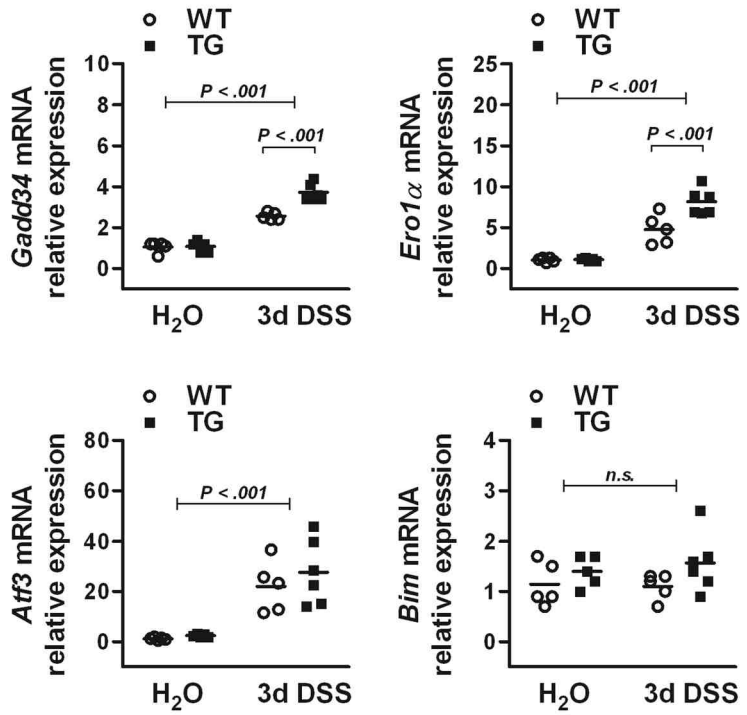

Figure 35. CHOP target gene expression in 3d DSS-treated mice.

The expression of CHOP target genes Gadd34, Ero1α, Atf3, and BIM was analyzed by qPCR using IEC isolates of 3d DSS-treated mice and water-treated controls (n = 5-6). All data sets were analyzed by TWA with genotype and DSS treatment as main factors followed by Holm-Sidak test, *P < .05* was considered statistically significant. Significant differences are illustrated considering both genotype and treatment as well as genotype-dependent differences in one treatment group.

However, significantly enhanced pro-apoptotic signaling could be achieved for 3 days DSS-treated mice regarding the cleavage of Caspase 3, which was further increased in transgenic mice (Figure 36).

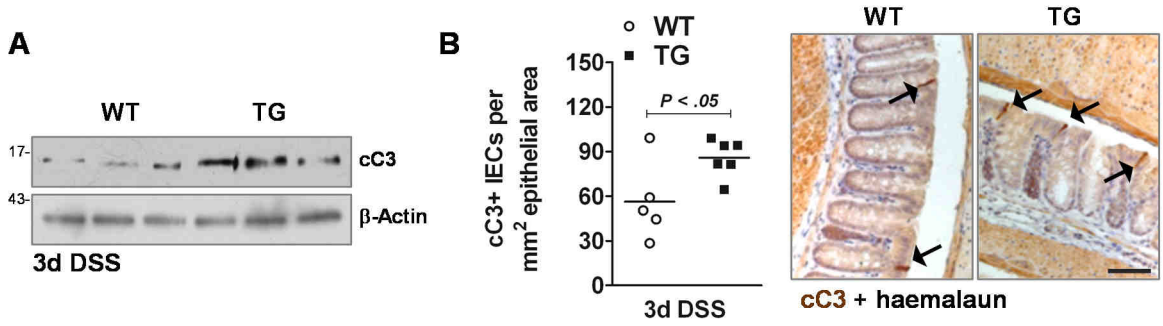

Figure 36. DSS-treated transgenic mice show an increase of cleaved caspase 3.

(A) Proapoptotic signaling was analyzed by performing Western blotting applying anti-cC3 antibody and anti-β-Actin antibody as loading control. (B) IHC was performed on 5 µm-thick colonic tissue sections of 3 days DSS-treated mice by using primary antibody against cC3. Numbers of cC3-positive IECs were assessed in a total epithelial area of 1 mm^2. Statistical significance was assessed by non-parametric rank-sum test, *P < .05* was considered statistically significant. Arrows in representative tissue sections indicate cC3-positive cells in WT and TG, scale bar represents 200 µm.

In summary, these data demonstrate that high CHOP protein expression in IECs exacerbates acute inflammation in experimental colitis in transgenic mice associated with enhanced immune cell infiltration, induced expression of CHOP target genes *Gadd34* and *Ero1*α, respectively, and increased numbers of cC3-positive epithelial cells.

Most studies dealing with CHOP and CHOP-mediated signaling have been related to pro-apoptotic signaling. Meanwhile, a growing number of studies accumulated suggesting that CHOP protein might be mechanistically involved in the regulation of proliferation as well as cell differentiation [168, 194]. To investigate whether IEC-specific CHOP protein is implicated in epithelial regeneration, mucosal healing was evaluated upon DSS-induced tissue damage. Therefore, 2% DSS was given for 5 days followed by a recovery period of 5 days. Transgenic mice were significantly retarded in their capacity to recover from DSS-induced colitis regarding the changes in body weight and DAI (Figure 37). This observation was further supported by significantly increased colonic weight/length ratio and spleen/body weight ratio, respectively (Figure 38A). In the context of epithelial regeneration, histological evaluation of affected tissue clearly indicated that disease severity was significantly associated with delayed mucosal repair in *Chop*$^{IEC\ Tg/Tg}$ mice (Figure 38B, Supplementary table 1).

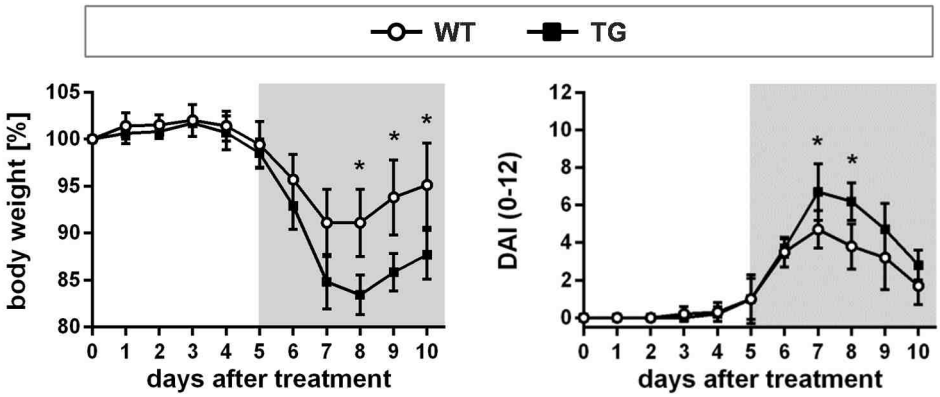

Figure 37. *Chop*$^{IEC\ Tg/Tg}$ mice reveal delayed recovery from DSS-induced colits.
Transgenic mice and wild-type controls (n = 6) were orally administered 2% DSS for 5 days followed by a period of 5 days for recovery (DSS+H_2O). Body weight changes and DAI were monitored daily and data are presented as means ±SD. Statistical significance was assessed by Student's t-test, *P < .05 (*)* was considered statistically significant.

In the recovery phase, both mRNA and protein expression of endogenous and transgenic CHOP remained unchanged comparing water-treated controls to DSS-treated mice, while GRP78 protein expression was strongly reduced in DSS-treated wild-type controls (Figure 39).

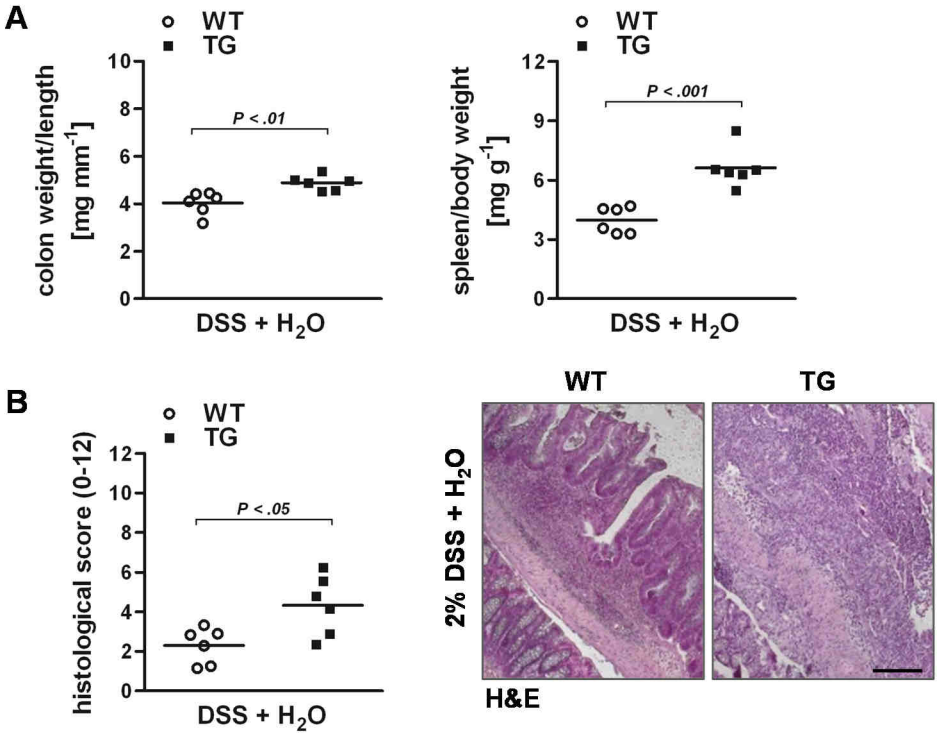

Figure 38. Delayed recovery of transgenic mice associated with enhanced tissue pathology.

(A) Colonic weight/length ratio was calculated in mg/ml, spleen/body weight ratio in mg/g. (B) Histological scores (0-12) were blindly evaluated regarding colonic tissue damage and immune cell infiltration. Representative H&E stained colonic tissue sections are shown, scale bar represents 200 µm. Statistical significance was assessed by Student's t-test, *P < .05* was considered statistically significant.

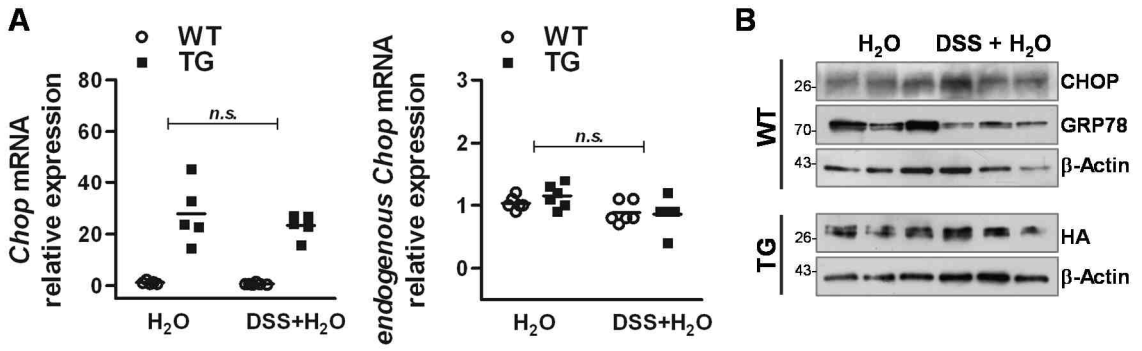

Figure 39. Expression of endogenous and transgenic CHOP is not regulated upon recovery from DSS-induced colitis.

Large IECs were isolated from water-treated and H_2O+DSS-treated mice (n = 5-6). (A) The mRNA expression of *Chop* was analyzed by using intron-spanning primer pair and primers specifically binding to the 5'-untranslated region of endogenous *Chop*. Data sets were analyzed by TWA with genotype and DSS treatment as main factors followed by Holm-Sidak test, *P < .05* was considered statistically significant. (B) Western blotting (n = 3) was performed using antibodies against CHOP, HA-tag, and β-Actin as loading control.

Regarding the mRNA expression of CHOP target genes, IEC-expressed Gadd34 appeared significantly decreased in response to DSS treatment. Ero1α, Atf3, and BIM, respectively, remained at basal expression levels, even though Atf3 has been shown to be significantly induced in water-treated *Chop*$^{IEC\ Tg/Tg}$ mice when compared to wild-type controls (Figure 40).

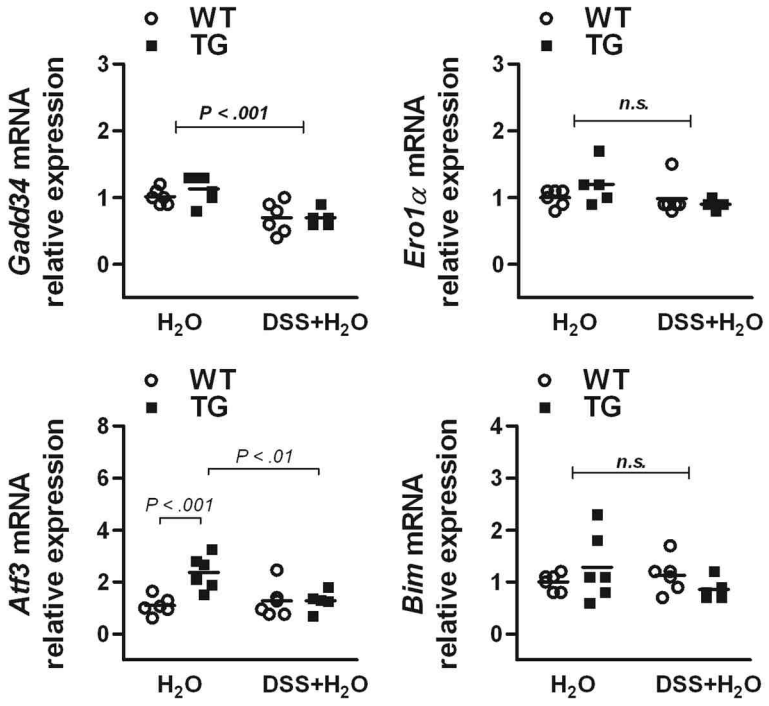

Figure 40. CHOP target gene expression in the recovery phase of DSS-induced colitis.

The expression of CHOP target genes *Gadd34*, *Ero1α*, *Atf3*, and *BIM* was analyzed by qPCR using total RNA from isolated large IECs of DSS+H_2O-treated mice and water-treated controls (n = 5-6). All data sets were analyzed by TWA with genotype and DSS treatment as main factors followed by Holm-Sidak test, $P < .05$ was considered statistically significant. Significant differences are illustrated considering both genotype and treatment as well as genotype-dependent differences in treatment groups and treatment-dependent differences within one genotype.

Taken together these data suggested that enhanced CHOP protein levels impair mucosal tissue recovery in response to DSS-induced colitis. Even though disease pathology of *Chop*$^{IEC\ Tg/Tg}$ mice might result from the more severe inflammation observed in acute experimental colitis, CHOP-mediated pro-apoptotic signaling could not be confirmed at the level of CHOP target gene expression. Thus, sustained disease severity is highly assumed to be associated with deregulated epithelial regeneration.

4.3.3 Disease severity in DSS-treated mice is independent of CHOP-driven apoptosis

Gene expression profiles of 3 days DSS-treated mice and mice in recovery were analyzed for regulation patterns leading to the more severe colitis phenotype in transgenic mice. Comparison of gene sets from water-treated and DSS-treated transgenic mice as well as wild-type controls, respectively, let assume that approximately 7865 genes might be regulated upon DSS treatment. However, in early inflammation 1235 genes were significantly regulated in *Chop*$^{IEC\ Tg/Tg}$ mice when 3d DSS-treated transgenic mice were compared to 3d DSS-treated wild-type controls, while 1469 genes have been shown to be differently expressed in the recovery phase (Figure 41).

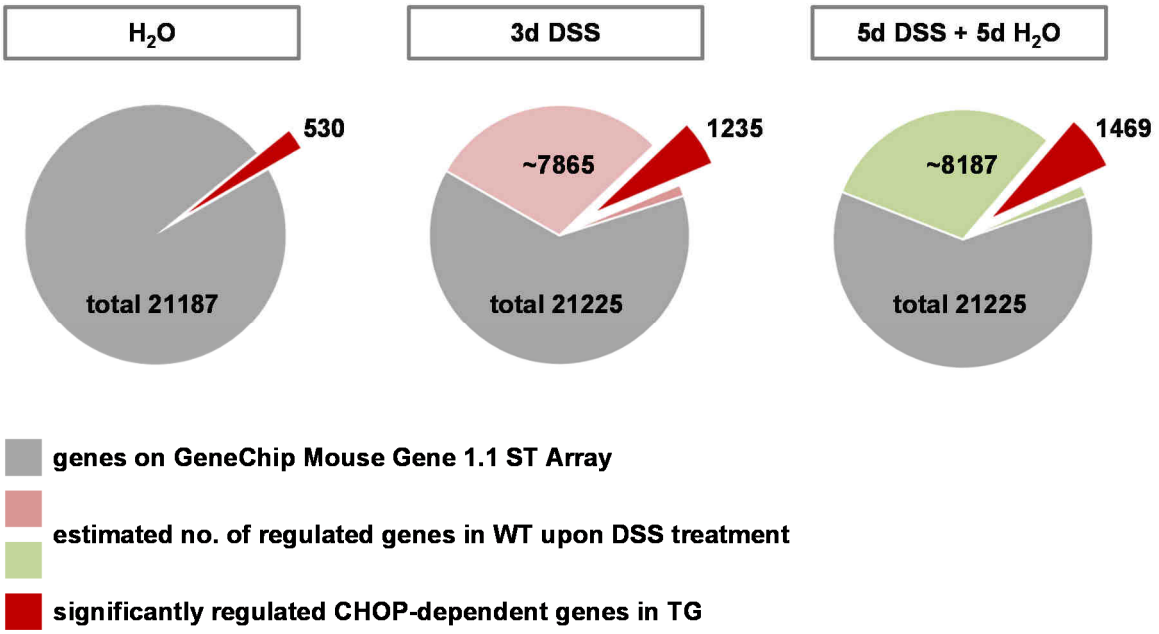

Figure 41. Overview of CHOP-dependent gene expression upon DSS treatment.
Gene expression profiles were evaluated comparing WT and TG mice in healthy and unhealthy conditions upon DSS treatment. Numbers of significantly regulated genes in TG mice are presented as CHOP-dependent genes (red). Total gene numbers (grey) referred to the number of genes on Affymetrix GeneChip®. DSS-dependent gene regulation in WT has been estimated because of different batches of microarray experiments (rose/green).

Hierarchical cluster analysis based on log2-fold change revealed that gene expression profiles of mice in early inflammation might be rather attributed to DSS treatment than to the genotype of mice (Figure 42A). With regard to CHOP-dependent gene enrichment in DSS-treated mice, 149 genes have been shown to be significantly regulated in both early inflammation and in recovery (Figure 42B).

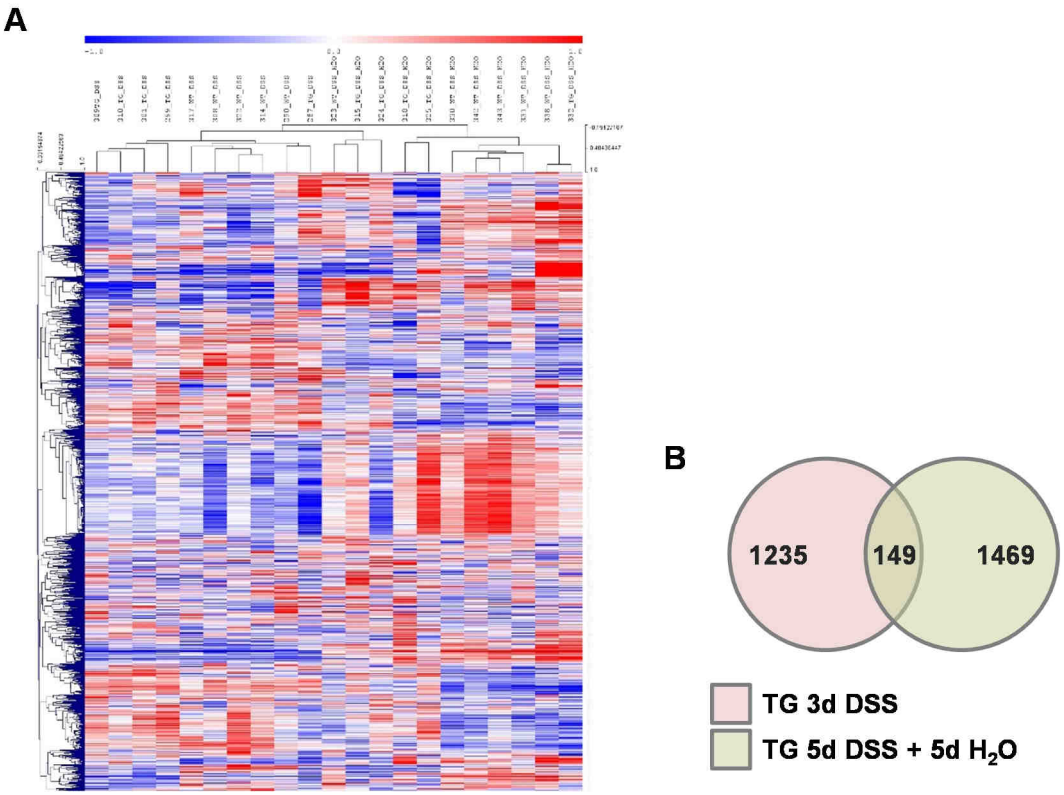

Figure 42. Hierarchical cluster analysis of DSS-treated mice.
Gene expression profiles of 3 days DSS-treated transgenic mice and *Chop*$^{IEC\ Tg/Tg}$ mice in recovery (5d DSS + 5d H_2O) were assessed by calculating fold changes to adequate DSS-treated wild-type controls. (A) Cluster analysis was performed based on log2-fold changes of 3d DSS-treated wild-type and transgenic mice, respectively, and mice in the recovery phase (5d DSS + 5d H_2O). (B) Significantly regulated genes of 3d DSS- and 5d DSS + 5d H_2O-treated transgenic mice were further analyzed for overlapping genes.

Top 10 of significantly regulated genes in 3d DSS-treated *Chop*$^{IEC\ Tg/Tg}$ mice are shown in Table 12. In this regard, genes, including *Atf5*, *Trf*, *S100g*, and *Ugt8a*, appeared comparably regulated to water-treated controls (Table 7) as well as *Chop*$^{IEC\ Tg/Tg}$ mice in recovery (Table 13). In contrast, none of the pathways significantly regulated in response to DSS treatment (Table 14) could be observed in water-treated transgenic mice.

In early inflammation, GO term analysis regarding biological process terms (Table 15) revealed reduced numbers of annotated short distance child terms when compared to analysis performed for disease-free transgenic mice (Table 9) and mice in recovery, respectively (Table 16).

In this regard, evaluation of biological process terms has been further performed by using WEB-based GEne SeT AnaLysis Toolkit [202]. Child terms within the first level in the GO biological process hierarchy have been analyzed regarding gene sets resulting from the overlap analysis (Figure 43).

Table 12. Most highly regulated genes in 3 days DSS-treated *Chop*$^{IEC\ Tg/Tg}$ mice are shown as TOP 10 up- and down-regulated genes, respectively. Gene enrichment has been evaluated by comparing transgenic mice and wild-type controls upon DSS treatment.

3d DSS *Chop*$^{IEC\ Tg/Tg}$ mice versus wild-type controls							
TOP 10 up-regulated				TOP 10 down-regulated			
gene ID	gene name	description	fold change	gene ID	gene name	description	fold change
13198	Ddit3	DNA-damage inducible transcript 3	3,32	17181	S100g	S100 calcium binding protein G	-4,00
74460	Gsdmcl-ps	gasdermin C-like, pseudogene	1,88	67701	Iigp1	interferon inducible GTPase 1	-2,61
238447	Igha	immunoglobulin heavy constant alpha	1,88	15505	Ugt8a	UDP galactosyltransferase 8A	-2,49
18784	Pla2g5	phospholipase A2, group V	1,86	66373	BC023105	cDNA sequence BC023105	-2,48
432798	Gm5453	predicted gene 5453	1,78	22041	Mir700	microRNA 700	-2,18
21333	Tac1	tachykinin 1	1,74	735285	Trf	transferrin	-2,04
17898	Myl7	myosin, light polypeptide 7, regulatory	1,68	667597	Lsm5	LSM5 homolog, U6 small nuclear RNA associated	-1,97
627860	Cyp2d37-ps	cytochrome P450, family 2, subfamily d, polypeptide 37	1,66	22239	Hsph1	heat shock 105kDa/110kDa protein 1	-1,91
268902	Robo2	roundabout homolog 2 (Drosophila)	1,64	60440	Wfdc2	WAP four-disulfide core domain 2	-1,89
107503	Atf5	activating transcription factor 5	1,64	12309	Matn2	matrilin 2	-1,83

Table 13. Most highly regulated genes in *Chop*$^{IEC\ Tg/Tg}$ mice upon recovery are shown as TOP 10 up- and down-regulated genes, respectively. Gene enrichment has been evaluated by comparing DSS-treated transgenic mice and wild-type controls in the recovery phase.

5d DSS + 5d H_2O *Chop*$^{IEC\ Tg/Tg}$ mice versus wild-type controls							
TOP 10 up-regulated				TOP 10 down-regulated			
gene ID	gene name	description	fold change	gene ID	gene name	description	fold change
13198	Ddit3	DNA-damage inducible transcript 3	3,51	76905	Lrg1	leucine-rich alpha-2-glycoprotein 1	-5,00
238447	Igha	immunoglobulin heavy constant alpha	2,58	22041	Trf	transferrin	-4,47
232889	Pla2g4c	phospholipase A2, group IVC	2,33	12309	S100g	S100 calcium binding protein G	-3,56
1,01E+08	Gm17434	predicted gene, 17434	1,97	67701	Wfdc2	WAP four-disulfide core domain 2	-2,98
107503	Atf5	activating transcription factor 5	1,95	64177	Trpv6	transient receptor potential cation channel, subfamily V, member 6	-2,03
107753	Lgals2	lectin, galactose-binding, soluble 2	1,90	69923	Agk	acylglycerol kinase	-1,95
242443	Grin3a	glutamate receptor ionotropic, NMDA3A	1,88	22259	Nr1h3	nuclear receptor subfamily 1, group H, member 3	-1,92
19692	Reg1	regenerating islet-derived 1	1,77	19933	Rpl21	ribosomal protein L21	-1,92
12895	Cpt1b	carnitine palmitoyltransferase 1b, muscle	1,76	22239	Ugt8a	UDP galactosyltransferase 8A	-1,91
432910	Trav13-3	T cell receptor alpha variable 13-3	1,76	67092	Gatm	glycine amidinotransferase	-1,82

Table 14 Significantly regulated signal transduction pathways in DSS-treated *Chop*$^{IEC\ Tg/Tg}$ mice. Analysis was performed by using the GeneRanker tool in the Genomatix Genome Analyzer.

3d DSS - pathway	**pathway ID**	**genes observed**	**genes expected**	**P-value**
PEROXISOME PROLIFERATIVE ACTIVATED RECEPTOR ALPHA	PW_PPARA_MUS_MUSCULUS	10	4	3,28E-03
GUANYLATE CYCLASE	PW_GUCY_MUS_MUSCULUS	5	1	9,61E-03
5d DSS + 5d H_2O - pathway	**pathway ID**	**genes observed**	**genes expected**	**P-value**
LOW DENSITY LIPOPROTEIN RECEPTOR RELATED PROTEIN	PW_LRP_MUS_MUSCULUS	20	9	4,43E-04
NUCLEAR RECEPTOR SUBFAMILY 1, GROUP H, MEMBER 3	PW_NR1H3_MUS_MUSCULUS	5	1	4,23E-03
ATP BINDING CASSETTE, SUB FAMILY A (ABC1)	PW_ABC1_MUS_MUSCULUS	9	3	6,58E-03
DOUBLE STRANDED RNA DEPENDENT PROTEIN KINASE/EUKARYOTIC INITIATION FACTOR 2ALPHA	PW_PKR_MUS_MUSCULUS	10	4	8,57E-03

Table 15. Analysis of biological process terms in 3d DSS treatment. The shown child terms with significant enrichment of total regulated genes as well as up- and down-regulated genes, respectively, display main biological processes with a distance of 1 regarding the process tree. Analysis was performed by using the GeneRanker tool in the Genomatix Genome Analyzer.

GO-term	**ID**	**total gene regulation**			**up-regulated**	**down-regulated**
		genes observed	genes expected	P-value	P-value	P-value
cellular process	GO:0009987	692	612	3,29E-07	3,22E-04	2,36E-04
metabolic process	GO:0008152	499	435	3,12E-05	2,24E-05	
response to stimulus	GO:0050896	379	315	1,10E-05	--	1,74E-04
multicellular organismal process	GO:0032501	307	262	7,02E-04	--	5,24E-04
signaling	GO:0023052	266	231	4,69E-03	--	1,17E-03
immune system process	GO:0002376	80	58	2,63E-03	2,96E-03	--

Table 16. Analysis of biological process terms in DSS recovery phase. The shown child terms with significant enrichment of total regulated genes as well as up- and down-regulated genes, respectively, display main biological processes with a distance of 1 regarding the process tree. Analysis was performed by using the GeneRanker tool in the Genomatix Genome Analyzer.

GO-term	ID	total gene regulation			up-regulated	down-regulated
		genes observed	genes expected	P-value	P-value	P-value
metabolic process	GO:0008152	686	536	1,68E-17	--	6,71E-24
cellular process	GO:0009987	939	755	5,72E-26	3,34E-12	3,76E-15
establishment of localization	GO:0051234	254	185	3,86E-08	2,25E-03	1,39E-06
immune system process	GO:0002376	95	72	3,42E-03	--	--
localization	GO:0051179	292	223	3,35E-07	2,73E-03	1,48E-05
developmental process	GO:0032502	267	218	1,72E-04	1,36E-05	--
response to stimulus	GO:0050896	464	389	2,96E-06	8,56E-09	--
cellular component organization or biogenesis	GO:0071840	227	192	3,64E-03	--	5,17E-04
biological regulation	GO:0065007	632	516	2,10E-11	3,33E-15	--
multicellular organismal process	GO:0032501	384	323	4,72E-05	7,27E-11	--
signaling	GO:0023052	346	285	2,20E-05	2,07E-12	--

As shown in Figure 43A, GO analysis considering overlapping gene sets revealed similar distribution patterns of biological process child terms when compared to annotations of individually regulated genes in 3d DSS-treated mice and mice in recovery, respectively. Of note, cell death-associated genes appeared not regulated in a CHOP-dependent manner. 82 genes have been annotated to biological process child term death in early inflammation, while 108 genes seem to be regulatory involved in mechanisms underlying cell death in the recovery phase. In this regard, only 12 genes have been shared, even though both DSS treatments resulted in more severe colitis in transgenic mice when compared to wild-type controls. With regard to total numbers of shared genes, comparison of fold-change values demonstrated that various gene sets were inversely regulated upon DSS treatments (Figure 43B). 70 overlapping genes have been found in total overlap analysis including expression profiles of disease-free *Chop*$^{IEC\ Tg/Tg}$ mice (4.2.1). Herein, comparison of fold-change values revealed similar expression patterns in all three conditions (Figure 43C, Supplementary table 2). Top 10 up- and down-regulated genes of total overlap analysis are presented in Table 17.

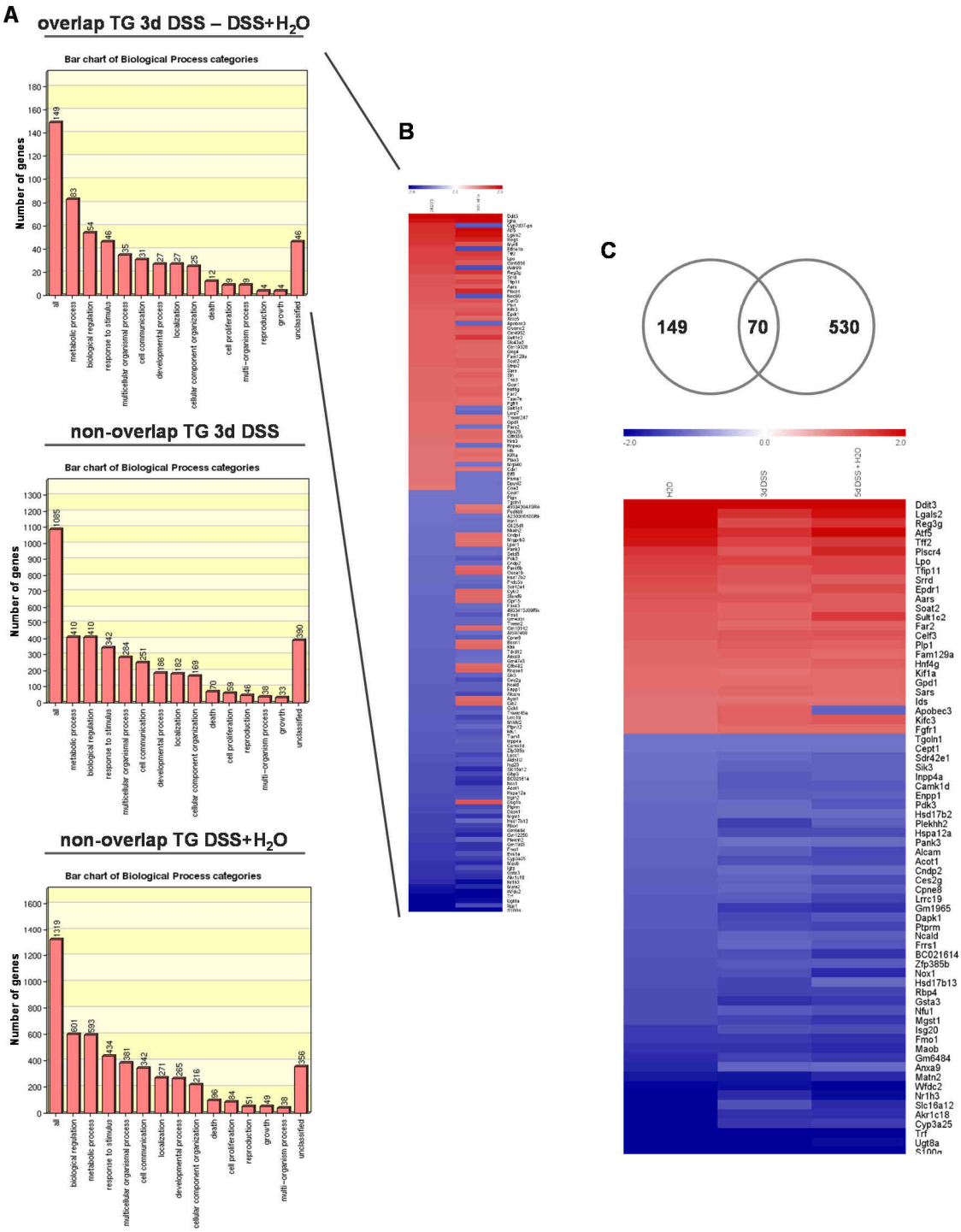

Figure 43. GO analysis of biological process terms regarding gene sets individually and commonly regulated upon DSS treatments.

Significantly regulated genes in transgenic mice were assessed with regard to gene expression in adequate wild-type controls. (A) Expression profiles of DSS-treated transgenic mice were studied by GO analysis regarding first levels in hierarchy of biological process child terms. Annotations are shown for shared and individually regulated gene sets. (B) Fold-change values of shared genes upon DSS treatment were illustrated in a range of -2 to 2. (C) Total overlap analysis was performed considering significantly regulated genes in disease-free, 3d DSS-treated, and 5d DSS + 5d H2O-treated *Chop*$^{IEC\ Tg/Tg}$ mice. Fold-change values of totally shared genes that were regulated in a CHOP-dependent manner were illustrated in a range of -2 to 2.

Table 17. TOP 10 up- and down-regulated genes resulting from overlap analysis of gene sets significantly regulated in disease-free, 3d DSS-, and 5d DSS + 5d H_2O-treated transgenic mice when compared to adequate wild-type controls.

overlapping genes in TG upon H_2O / 3d DSS / 5d DSS + 5d H_2O					
TOP 10 up-regulated			TOP 10 down-regulated		
gene name	description	log2	gene name	description	log2
Ddit3	DNA-damage inducible transcript 3	3.27 / 3.32 / 3.51	S100g	S100 calcium binding protein G	-5.54 / -4.00 / -3.56
Lgals2	lectin, galactose-binding, soluble 2	2.05 / 1.62 / 1.90	Ugt8a	UDP galactosyltransferase 8A	-3.41 / -2.49 / -1.91
Reg3g	regenerating islet-derived 3 gamma	1.99 / 1.42 / 1.61	Trf	transferrin	-3.37 / -2.03 / -4.47
Atf5	activating transcription factor 5	1.88 / 1.64 / 1.95	Cyp3a25	cytochrome P450, family 3, subfamily a, polypeptide 25	-2.58 / -1.55 / -1.51
Tff2	trefoil factor 2	1.86 / 1.48 / 1.54	Akr1c18	aldo-keto reductase family 1, member C18	- 2.39 / -1.61 / -1.63
Plscr4	phospholipid scramblase 4	1.59 / 1.31 / 1.71	Slc16a12	solute carrier family 16, member 12	-2.09 / -1.36 / -1.65
Lpo	lactoperoxidase	1.50 / 1.48 / 1.47	Nr1h3	nuclear receptor subfamily 1, group H, member 3	-2.00 / -1.65 / -1.92
Tfip11	tuftelin interacting protein 11	1.47 / 1.33 / 1.48	Wfdc2	WAP four-disulfide core domain 2	-1.96 / -1.89 / -2.98
Srrd	SRR1 domain containing	1.42 / 1.33 / 1.26	Matn2	matrilin 2	-1.82 / -1.83 / -1.66
Epdr1	ependymin related protein 1	1.39 / 1.25 / 1.41	Anxa9	annexin A9	-1.71 / -1.22 / -1.17

Regarding to gene sets in total overlap, changes in gene expression could be observed modulating epithelial cell proliferation as well as cell migration, such as *Tff2* and *Atf5* [218, 219]

In order to gain a better understanding of gene regulation in the recovery phase, gene expression profiles of transgenic mice and wild-type controls, respectively, were compared between 3 days DSS treatment and recovery. 4512 and 2889 genes were significantly regulated in wild-type and transgenic mice, respectively, when gene expression profiles of 3 days DSS-treated mice were compared to gene regulations in recovery (Figure 44A). In this regard, overlap analysis revealed 1353 shared genes (Figure 44B).

GO analysis for biological process terms showed that 324 and 173 genes were annotated to child terms cell proliferation and growth in wild-type mice, respectively, while 180 and 86 significantly regulated genes were annotated to corresponding child terms in *Chop*$^{IEC\ Tg/Tg}$ mice (Figure 45). Herein, 95 (cell proliferation) and 45 genes (growth), respectively, have been shared by *Chop*$^{IEC\ Tg/Tg}$ mice and wild-type controls indicating that transgenic mice progressed towards, but were delayed in the recovery phase. However, top 10 up- and down-regulated genes considering overlapping and non-overlapping gene sets are shown in Tables 18-21.

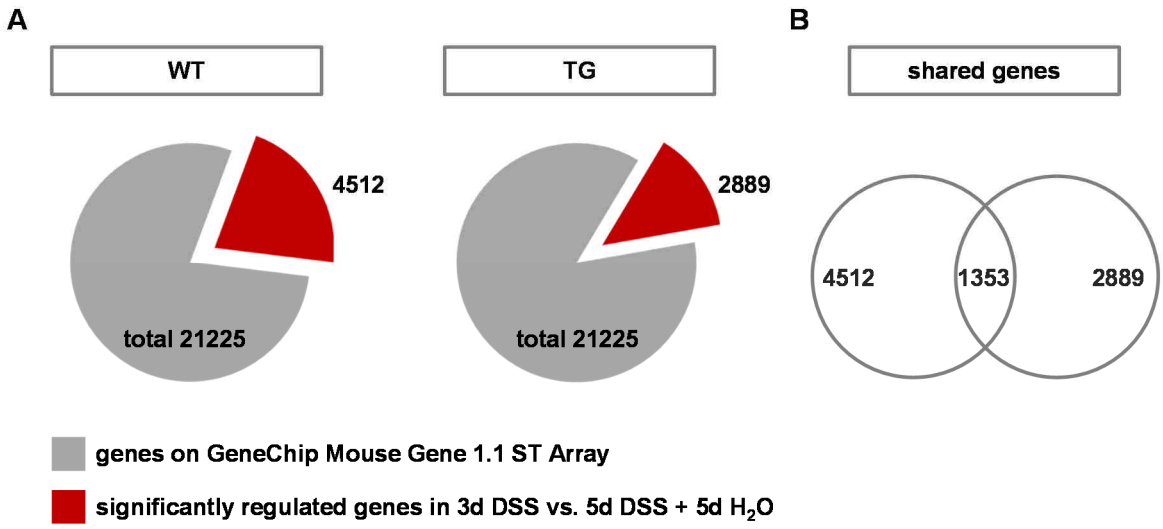

Figure 44. Gene expression profiles of WT and TG comparing 3d DSS and 5d DSS + 5d H_2O treatment.

(A) Significantly regulated genes were assessed in wild-type controls and transgenic mice comparing gene expression profiles of 3d DSS treatment versus 5d DSS + 5d H_2O. (B) Overlap analysis of genes that are significantly regulated comparing 3d DSS versus 5d DSS + 5d H_2O showed 1353 shared genes between WT and TG.

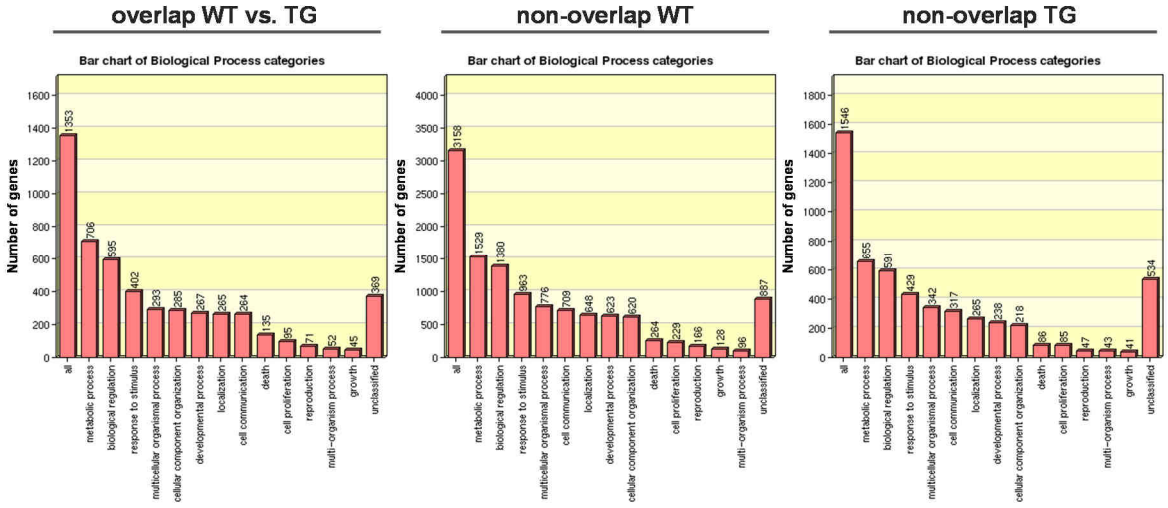

Figure 45. GO analysis of biological process terms regarding gene sets individually and commonly regulated in *Chop*$^{IEC\ Tg/Tg}$ mice and wild-type controls, respectively.

Gene expression profiles were assessed for WT and TG, respectively, comparing 3d DSS and 5d DSS + H2O. Gene sets of WT and TG mice were further analyzed for overlapping and non-overlapping genes (Figure 44). The resulting expression profiles of transgenic mice and wild-type controls were studied by GO analysis regarding first levels in hierarchy of biological process child terms. Annotations are shown for shared and individually regulated gene sets.

Table 18. Most highly regulated individual genes in wild-type mice comparing gene expression profiles of 3d DSS-treated mice and mice in recovery are shown as TOP 10 up- and down-regulated genes.

WT 3d DSS versus 5d DSS + 5d H_2O - individual genes							
TOP 10 up-regulated				TOP 10 down-regulated			
gene ID	gene name	description	fold change	gene ID	gene name	description	fold change
20201	S100a8	S100 calcium binding protein A8	3,89	667597	BC023105	cDNA sequence BC023105	-2,85
20568	Slpi	secretory leukocyte peptidase inhibitor	3,48	13615	Edn2	endothelin 2	-2,08
16176	Il1b	interleukin 1 beta	3,34	60440	Igp1	interferon inducible GTPase 1	-1,99
245195	Retnlg	resistin like gamma	3,26	224093	Fam43a	family with sequence similarity 43, member A	-1,96
105892	9030619P08Rik	RIKEN cDNA 9030619P08 gene	2,82	384061	Fndc5	fibronectin type III domain containing 5	-1,94
18126	Nos2	nitric oxide synthase 2, inducible	2,64	23886	Gdf15	growth differentiation factor 15	-1,89
20202	S100a9	S100 calcium binding protein A9	2,62	71785	Pdgfd	platelet-derived growth factor, D polypeptide	-1,85
68713	Ifitm1	interferon induced transmembrane protein 10	2,45	27057	Ncoa4	nuclear receptor coactivator 4	-1,84
17110	Lyz1	lysozyme 1	2,44	394436	Ugt1a1	UDP glucuronosyltransferase 1 family, polypeptide A1	-1,80
12365	Casp14	caspase 14	2,43	242443	Grin3a	glutamate receptor ionotropic	-1,79

Table 19. Most highly regulated individual genes in *Chop*$^{IEC\ Tg/Tg}$ mice comparing gene expression profiles of 3d DSS-treated mice and mice in recovery are shown as TOP 10 up- and down-regulated genes.

TG 3d DSS versus 5d DSS + 5d H_2O - individual genes							
TOP 10 up-regulated				TOP 10 down-regulated			
gene ID	gene name	description	fold change	gene ID	gene name	description	fold change
100303740	Snora75	small nucleolar RNA, H/ACA box 75	3,37	66289	Mptx1	mucosal pentraxin 1	-4,99
100039904	Gm20819	predicted gene, 20819	2,51	19933	Rpl21	ribosomal protein L21	-2,19
70935	Speer4f	spermatogenesis associated glutamate (E)-rich protein 4f	2,17	67701	Wfdc2	WAP four-disulfide core domain 2	-2,18
735268	Mir680-1	microRNA 680-1	2,14	433247	Cyp2c68	cytochrome P450, family 2, subfamily c, polypeptide 68	-2,06
100043123	Gm11710	predicted gene 11710	2,13	16803	Lbp	lipopolysaccharide binding protein	-1,95
104307	Rnu12	RNA U12, small nuclear	2,11	15129	Hbb-b1	Hbb-b1	-1,94
20531	Slc34a2	solute carrier family 34 (sodium phosphate), member 2	2,06	619597	Gm6086	predicted gene 6086	-1,74
664608	Rhox4g	reproductive homeobox 4G	1,99	100040244	Gm14698	serine/threonine/tyrosine interaction protein pseudogene	-1,66
243420	Igkv1-135	immunoglobulin kappa variable 1-135	1,90	269378	Ahcy	S-adenosylhomocysteine hydrolase-like 1	-1,63
104369	Snora69	small nucleolar RNA, H/ACA box 69	1,77	668178	Mettl7a3	methyltransferase like 7A3	-1,62

Table 20. Most highly regulated overlapping genes in wild-type mice comparing gene expression profiles of 3d DSS-treated mice and mice in recovery are shown as TOP 10 up- and down-regulated genes.

WT 3d DSS versus 5d DSS + 5d H_2O - shared genes							
TOP 10 up-regulated				TOP 10 down-regulated			
gene ID	gene name	description	fold change	gene ID	gene name	description	fold change
76905	Lrg1	leucine-rich alpha-2-glycoprotein 1	8,45	193740	Hspa1a	heat shock protein 1A	-9,60
18780	Pla2g2a	phospholipase A2, group IIA	7,43	15505	Hsph1	heat shock 105kDa/110kDa protein 1	-4,44
17225	Mcpt2	mast cell protease 2	6,43	69983	Sis	sucrase isomaltase (alpha-glucosidase)	-2,85
21941	Tnfrsf8	tumor necrosis factor receptor superfamily, member 8	5,95	74646	Spsb1	splA/ryanodine receptor domain and SOCS box containing 1	-2,79
368204	Khdc1a	KH domain containing 1A	5,73	13170	Dbp	protein kinase C, delta binding protein	-2,73
17224	Mcpt1	mast cell protease 1	4,75	18627	Per2	period circadian clock 2	-2,57
100529074	Snora33	small nucleolar RNA, H/ACA box 33	4,14	12837	Col8a1	collagen, type VIII, alpha 1	-2,45
19871	Rnu73b	U73B small nuclear RNA	3,91	15370	Nr4a1	nuclear receptor subfamily 4, group A, member 1	-2,30
20730	Spink3	serine peptidase inhibitor, Kazal type 3	3,87	26878	B3galt2	GlcNAc beta 1,3-galactosyltransferase	-2,27
16819	Lcn2	lipocalin 2	3,85	53325	Banp	BTG3 associated nuclear protein	-2,26

Table 21. Most highly regulated overlapping genes in *Chop*$^{IEC\ Tg/Tg}$ mice comparing gene expression profiles of 3d DSS-treated mice and mice in recovery are shown as TOP 10 up- and down-regulated genes.

TG 3d DSS versus 5d DSS + 5d H_2O - shared genes							
TOP 10 up-regulated				TOP 10 down-regulated			
gene ID	gene name	description	fold change	gene ID	gene name	description	fold change
17225	Mcpt2	mast cell protease 2	5,39	193740	Hspa1a	heat shock protein 1A	-3,76
368204	Khdc1a	KH domain containing 1A	5,32	15505	Hsph1	heat shock 105kDa/110kDa protein 1	-2,73
100529074	Snora33	small nucleolar RNA, H/ACA box 33	4,53	13170	Dbp	protein kinase C, delta binding protein	-2,41
19850	Rnu3a	U3A small nuclear RNA	4,36	11572	Crisp3	cysteine-rich secretory protein 3	-2,24
16819	Lcn2	lipocalin 2	4,19	246709	Rgs13	regulator of G-protein signaling 13	-2,23
17224	Mcpt1	mast cell protease 1	3,88	229599	Gm129	predicted gene 12942	-2,15
18780	Pla2g2a	phospholipase A2, group IIA	3,86	18828	Plscr2	phospholipid scramblase 2	-2,07
21941	Tnfrsf8	tumor necrosis factor receptor superfamily, member 8	3,63	16425	Itih2	inter-alpha trypsin inhibitor, heavy chain 2	-2,03
27211	Snord35a	small nucleolar RNA, C/D box 35A	3,37	18627	Per2	period circadian clock 2	-2,03
100217428	Snord57	small nucleolar RNA, C/D box 57	3,37	353320	Defb37	defensin beta 37	-1,99

In conclusion, these data indicated that DSS-induced colitis in transgenic mice is independent of CHOP-mediated apoptosis. In this regard, susceptibility to DSS-driven colonic inflammation might be rather affected by mechanisms underlying defective epithelial proliferation, consequently leading to decreased regenerative capacity in early inflammation and recovery, respectively.

Based on animal experimentation, we further addressed the effects of CHOP on cell proliferation by performing *in vitro* studies in the colonic epithelial cell line ptk6.

4.4 High CHOP protein expression delays cell cycle progression in colonic epithelial ptk6 cells

Enhanced CHOP protein expression has been reported to impact on cell cycle progression *in vitro* by inducing G1 arrest in NIH-3T3 cells [160]. However, recent studies demonstrated that the inhibitory effect of CHOP protein on cell proliferation seemed to be dependent on its subcellular localization, which in turn is strongly dependent on its transcriptional activation. Thus, we addressed two main questions by *in vitro* experimentation [156, 168]. First, we investigated the regulatory mechanisms that might occur in IECs affecting the transcriptional activity of CHOP, and second, we studied CHOP-driven effects on the proliferative capacity of IECs.

4.4.1 Transgenic CHOP-HA protein is degraded by the proteasome and post-translationally modified by phosphorylation

According to previous reports, proteasomal degradation of CHOP-HA protein has been investigated to evaluate the correlation between transgene mRNA expression and CHOP-HA protein levels [152, 153]. Therefore, colonic epithelial ptk6 cells were transfected with pcDNA3.1(-)-CHOP-HA for 24 hours and subsequently treated with the proteasome inhibitor Lactacystine. As indicated in Figure 46, CHOP-HA protein expression is increased in response to Lactacystine treatment.

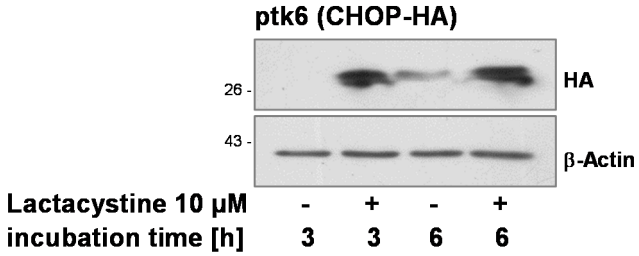

Figure 46. CHOP-HA undergoes proteasomal degradation in transiently transfected ptk6 cells.

Colonic epithelial ptk6 cells were transfected with pcDNA3.1(-)-CHOP-HA for 24h followed by incubation with proteasome inhibitor Lactacyctine (10 µM) for 3h and 6h, respectively. Whole protein extracts were analyzed by Western blotting using anti-HA antibody and anti-β-Actin antibody as loading control.

With regard to protein band pattern detected by Western blotting using IEC isolates from transgenic mice, the molecular weight of CHOP-HA differs from ~26 kDa to ~30 kDa. Notably, CHOP-HA protein exhibited similar expression pattern *in vitro* and *in vivo* (Figure 47A).

Since transcriptional activity of CHOP protein is regulated by phosphorylation, CHOP protein band pattern was further analyzed upon dephosphorylation [150, 151]. Treatment of native protein lysates from transfected ptk6 cells with AP yielded into a shift towards lower molecular masses clearly suggesting post-translational modification of CHOP-HA by phosphorylation (Figure 47B).

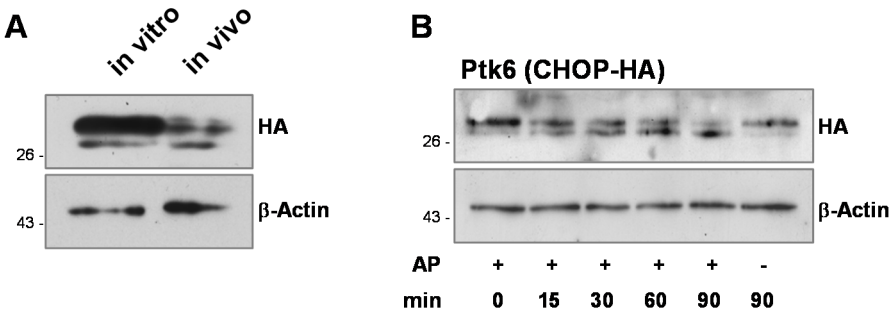

Figure 47. *In vitro* data indicate post-translational modification of CHOP-HA protein by phosphorylation.

(A) Protein lysates of CHOP-HA-transfected ptk6 cells and colonic IECs from *Chop*$^{IEC\ Tg/Tg}$ mice were analyzed by Western blotting using anti-HA antibody and anti-β-Actin antibody as loading control. (B) Native protein lysates of CHOP-HA transfected ptk6 cells were treated with AP for 0, 15, 30, and 60 min, as well as for 90 min with and without AP. SDS-15% Page was performed followed by Western blot analysis using anti-HA antibody. Shown Western blot data represent 3 independent experiments.

In fact, CHOP protein was found to be phosphorylated by p38 MAP kinase at serine residues 78/81 as well as by casein kinase II at adjacent serine residues 14/15 and 30/31 regulating its transcriptional activation [150, 151]. Consequently, specific serine residues have been replaced by alanine generating plasmid constructs containing CHOP-HA [S14/15A], CHOP-HA [S30/31A], CHOP-HA [S14/15A, S30/31A], CHOP-HA [S78/81A], and CHOP-HA [S14/15A, S30/31A, S78/81A] (Figure 48A).

Transfection of ptk6 cells with mutated plasmid constructs and subsequent treatment of corresponding native protein lysates with AP showed that CHOP-HA protein is post-translationally modified by phosphorylation at p38 MAP kinase-specific phosphorylation sites, serine residues 78/81 (Figure 48B). Accordingly, CHOP-HA [S78/81A] could be detected as a single protein band that indicated a molecular weight comparably to AP-treated protein lysates. Representative Western blot analysis using protein lysates of transfected ptk6 cells with CHOP-HA and CHOP-HA [S78/81A] further confirmed changes in molecular weight due the inhibition of phosphorylation at p38 MAP kinase-specific phosphorylation sites (Figure 48C).

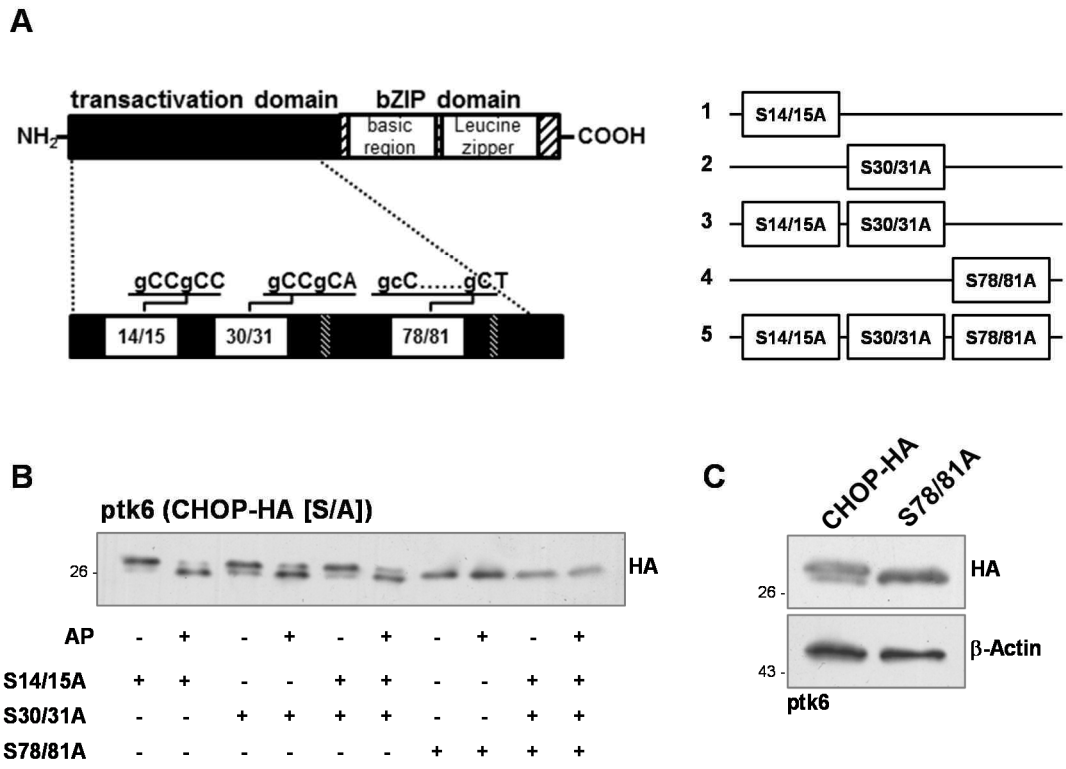

Figure 48. CHOP-HA is post-translationally modified at p38 MAP kinase-specific phosphorylation sites

(A) Overview of phosphorylation sites regulating the transcriptional activation of CHOP protein according to Wang et al. (1996) and Ubeda et al. (2003). CHOP mutant constructs were generated replacing specific serine residues by alanine. (B) Non-differentiated ptk6 cells were transfected with mutated CHOP-HA constructs [14/15A], [30/31A], [S14/15A, S30/31A], [S78/81A], and [S14/15A, S30/31A, S78/81A] for 40h. Native protein lysates were incubated with and without AP for 90 min. SDS-15% Page was performed followed by Western blotting using anti-HA antibody. (C) Western blot analysis of protein lysates derived from ptk6 cells expressing CHOP-HA and CHOP-HA [S78/81A] was performed by using anti-HA antibody and anti-β-Actin antibody as loading control.

Taken together, these findings suggested that CHOP-HA undergoes post-translational modifications at p38 MAP kinase-specific phosphorylation sites, which is highly associated with the transcriptional activation of CHOP. In contrast, CHOP-HA mRNA-protein correlation is strongly affected by proteasomal degradation, thus reducing the total amount of transgenic protein.

4.4.2 CHOP protein promotes cell cycle delay in colonic epithelial ptk6 cells associated with impaired scratch closure

Transcriptional activation of CHOP is strongly associated with cell death [86]. Since CHOP-activating p38 MAP kinase appeared regulatory involved in the post-translational modification of CHOP-HA *in vitro*, p38 MAPK activation was further analyzed upon 3 days DSS treatment and recovery from DSS-induced colitis. As indicated in Figure 22, phosphorylation of p38 MAPK in IECs of *Chop*$^{IEC\ Tg/Tg}$ mice was comparable to wild-type controls. The analysis of IECs derived from DSS-treated mice indicated changes in the phosphorylation status of p38 MAPK similarly regulated in both transgenic and wild-type mice. 3 days DSS-treated mice displayed enhanced activation of p38 MAPK in IECs, while decreased levels of P-p38 MAPK were detected upon recovery from DSS-induced colitis (Figure 49). Notably, Western blot analysis was performed in time with those of Figure 34 and Figure 39 using similar sample volumes. Since P-p38 and β-Actin reveal similar molecular masses (~40 kDa), loading control is indicated by β-Actin of corresponding Western blots. Histon 3 (~19 kDa) was not available as adequate protein loading control.

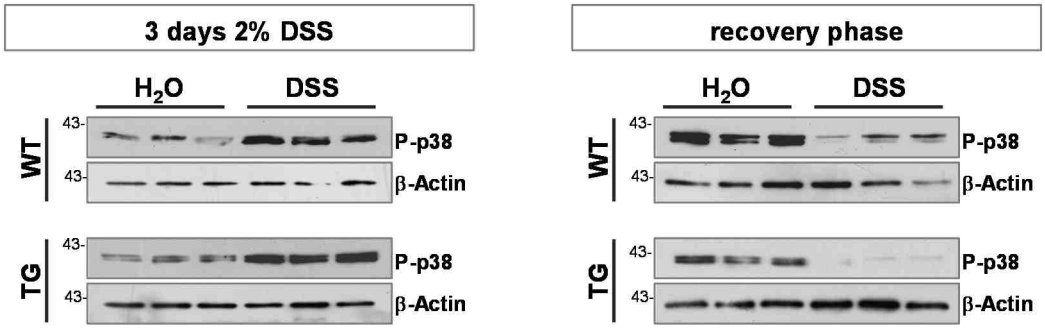

Figure 49. Phosphorylation status of p38 MAPK upon 3 days 2% DSS and recovery from DSS-induced colitis.

Protein lysates of IECs derived from water-treated mice as well as 3 days DSS-treated mice and mice in recovery from DSS-induced colitis (n = 3) were analyzed by Western blotting using anti-P-p38 antibody. Protein load is indicated by applying β-Actin on parallel performed Western blots using similar sample volumes.

With regard to functional consequences that may be driven in dependence on the phosphorylation status of CHOP protein, we generated stable ptk6 cell lines expressing CHOP-HA and CHOP-HA [S78/81A], respectively (Figure 50A).

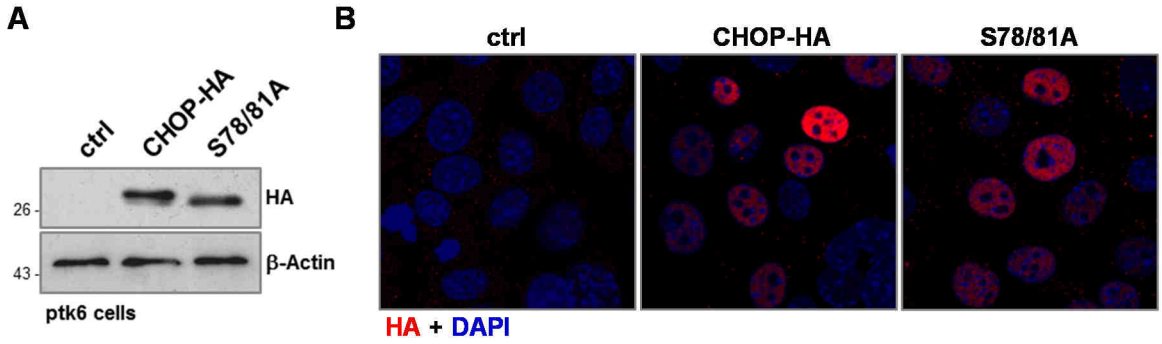

Figure 50. Stably transfected ptk6 cell lines comparably express CHOP-HA and CHOP-HA [S78/81A].

(A) Western blot analysis was performed using protein lysates derived from stably transfected ptk6 cells. Transgene expression was demonstrated by applying anti-HA antibody and anti-β-Actin antibody as loading control. Nuclear localization of CHOP-HA and CHOP-HA [S78/81A] is shown in (B).

First, we could show that both CHOP-HA and CHOP-HA [S78/81A] protein is mainly located in nuclei of ptk6 cell lines (Figure 50B). Second, we examined the effects of high CHOP-HA and CHOP-HA [S78/81A] expression on barrier function by measuring TEER, showing that neither CHOP-HA nor CHOP-HA [S78/81A] affected the epithelial integrity of ptk6 monolayers (Figure 51A).

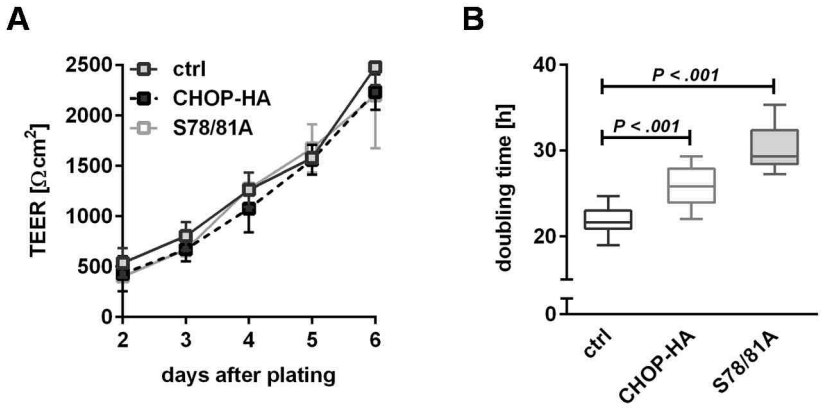

Figure 51. CHOP-HA does not impact on epithelial integrity, but impairs epithelial cell proliferation.

(A) Epithelial integrity was examined for stable cell lines ptk6:ctrl, ptk6:CHOP-HA, and ptk6:CHOP-HA [S78/81A] (technical replicates n = 4). TEER measurement was performed for 5 days, starting 2 days after plating cells into transwell inserts. Data in Ohm.cm^2 are plotted as means ± SD. (B) Cell proliferation (technical replicates n = 10) was observed for 5 days and evaluated using cell proliferation ELISA. Doubling time was assessed and statistical significance was calculated by non-parametric rank-sum test. *P < .05* was considered statistically significant.

Interestingly, high CHOP protein expression diminished the proliferation of ptk6 cells, which was most decreased in cells expressing CHOP-HA [S78/81A] (Figure 51B). This effect was highly associated with an impaired cell migration evaluated by an *in vitro* scratch wound healing assay (Figure 52).

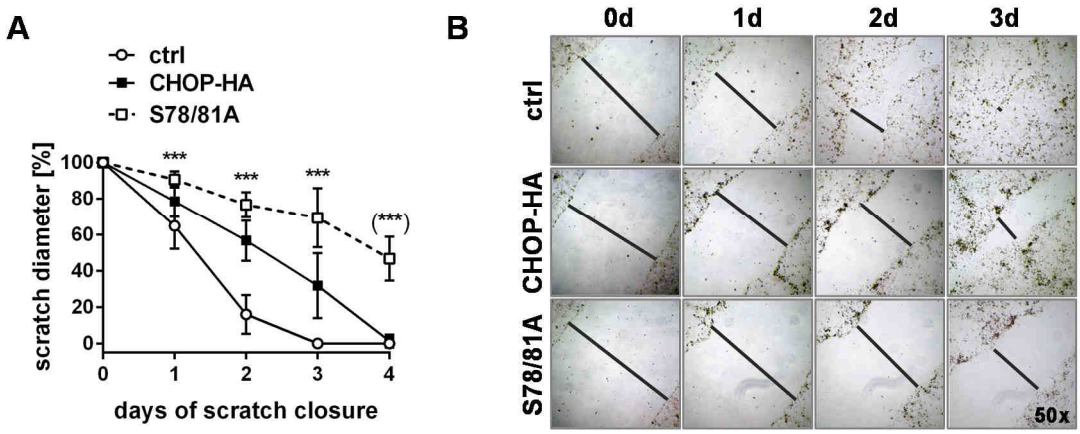

Figure 52. CHOP-HA overexpression leads to impaired scratch closure in ptk6 cells.
(A) Stable ptk6 cell lines ptk6:ctrl, ptk6:CHOP-HA, and ptk6:CHOP-HA [S78/81A] were scratched 4 days after reaching confluency (n = 20). Scratch closure was daily monitored and scratch diameter was calculated as percentage of initial scratch size. In non-parametric rank-sum test. $P < .001$ (***) was considered statistically significant. Statistical significance on day 4 refers to differences between ptk6:ctrl and ptk6:CHOP-HA. Scratch closure is shown in (B). Shown data represent 3 independent experiments.

The limit of the proliferative capacity of CHOP overexpressing ptk6 cells seemed to be independent of CHOP-driven cell death induction as both numbers of necrotic and apoptotic cells remained unchanged (Figure 53).

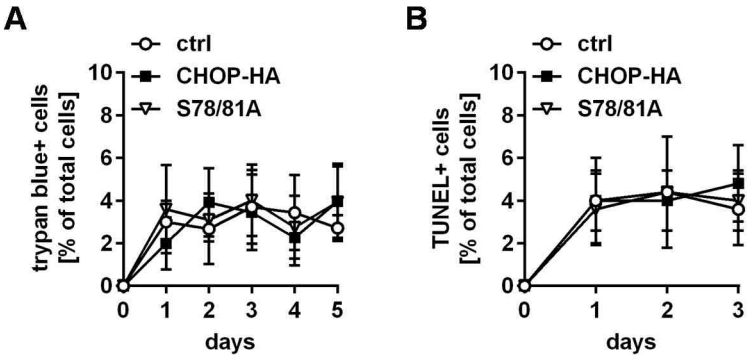

Figure 53. High CHOP protein expression does not induce cell death in ptk6 cells
Markers of cell death were monitored in stable cell lines ptk6:ctrl, ptk6:CHOP-HA, and ptk6:CHOP-HA [S78/81A]. (A) 20.000 cells/ml were seeded into 24-well plates and numbers of necrotic cells were analyzed by trypan blue staining for 5 days (technical replicates n = 8). (B) 100.000 cells/ml were seeded into 24-well plates and numbers of apoptotic cells were assessed by performing TUNEL assay. Numbers of apoptotic cells were calculated as percentage of total cells (technical replicates n = 4). All data are plotted as means ± SD.

The effect of CHOP-HA and CHOP-HA [S78/81A] overexpression, respectively, on cell proliferation was further evaluated by flow cytometry using propidium iodide DNA staining. As shown in Figure 54, overexpression of CHOP-HA caused cell accumulation in G0/G1 associated with decreased number of cells in G2/M. In contrast, overexpression of CHOP-HA [S78/81A] resulted in increased accumulation of cells in G2/M associated with reduced number of cells in G0/G1. Notably, the S phase of the mitotic cell cycle was not affected by transgene overexpression.

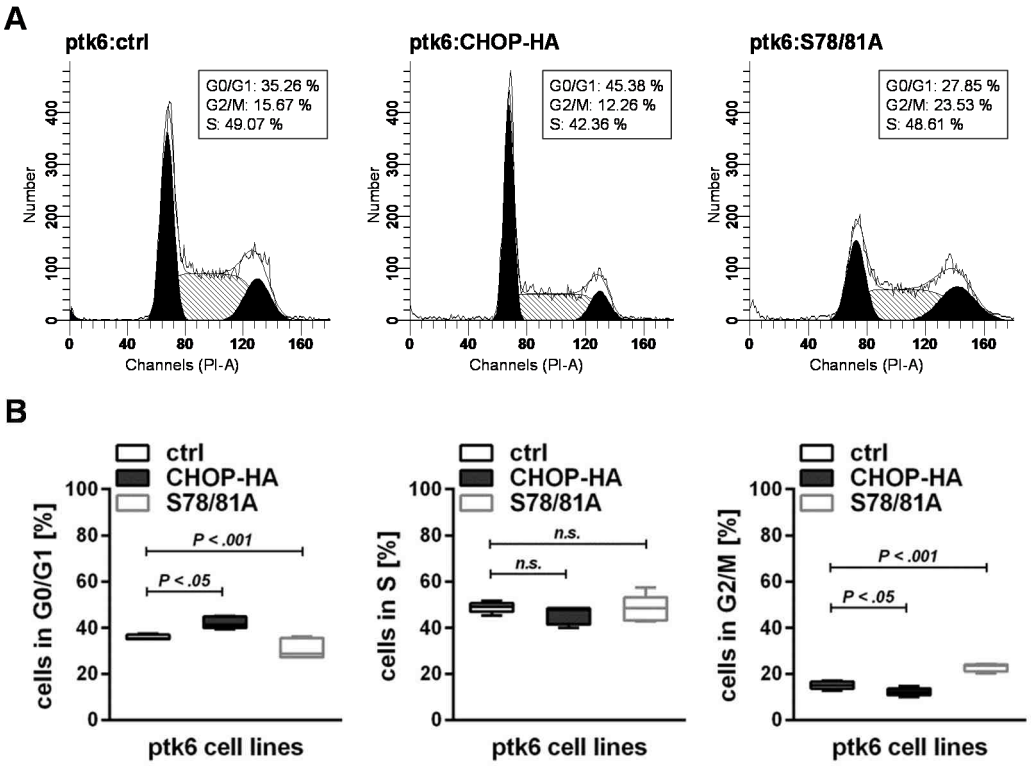

Figure 54. Enhanced CHOP-HA and CHOP-HA [S78/81A] expression alters cell cycle progression in ptk6 cells.

(A) Cell cycle of stable ptk6 cell lines ptk6:ctrl, ptk6:CHOP-HA, and ptk6:CHOP-HA [S78/81A], respectively, was analyzed by flow cytometry using propidium iodide DNA staining. (B) Number of cells in G1, S, and G2 phase of the mitotic cell cycle was given as percentage of total cell number. Data are presented as means ±SD. Statistical significance was assessed by non-parametric rank-sum test. *P < .05* was considered statistically significant. Shown data represent 5 independent experiments.

In the context of proliferation, CHOP has been reported to implicate in Wnt signaling at the level of TCF binding [194]. With regard to these data, c-Myc and Cyclin D1 mRNA expression has been examined in stable ptk6 cell lines and colonic IEC isolates of *Chop*$^{IEC\ Tg/Tg}$ mice and wild-type controls. As indicated in Figure 55, both Wnt target genes remained unaffected by CHOP *in vitro* and *in vivo*.

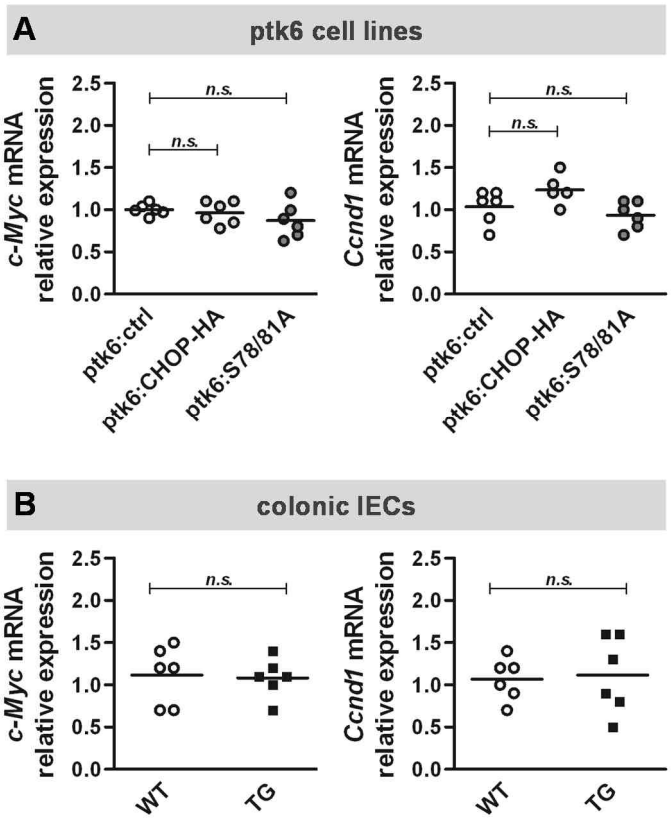

Figure 55. High CHOP protein expression does not affect Wnt signaling.

Ptk6 cell lines ptk6:ctrl, ptk6:CHOP-HA, ptk6:CHOP-HA [S78/81A] (A) and colonic IECs of transgenic and wild-type mice (n =6) (B) were analyzed for mRNA expression of Wnt target genes *c-Myc* and *Cyclin D1* by qPCR. Non-confluent cells were harvested at 6 different time points. All data sets were analyzed by non-parametric rank-sum test. $P < .05$ was considered statistically significant.

In conclusion, these data indicated that CHOP impairs the proliferative capacity of colonic epithelial ptk6 cells independent of CHOP-driven cell death. Both, CHOP-HA and CHOP-HA [S78/81A] affected cell cycle progression associated with decreased cell migration suggesting that enhanced CHOP protein expression implicates in epithelial cell regeneration of *Chop*$^{IEC\ Tg/Tg}$ mice.

Based on these results, proliferation and cell migration of IECs were investigated in *Chop*$^{IEC\ Tg/Tg}$ mice by performing *in vivo* BrdU labeling.

4.5 CHOP overexpression decreases numbers of proliferative cells in transgenic mice associated with impaired mucosal tissue repair

To investigate whether high CHOP-HA expression has an effect on epithelial cell proliferation, disease-free *Chop*$^{IEC\ Tg/Tg}$ mice and wild-type controls were injected with BrdU for *in vivo* labeling of proliferative cells. Mice were sacrificed on days 1 and 3 post BrdU injection and tissue sections of jejunum, ileum, and distal colon were analyzed for BrdU-positive cells. Numbers of BrdU-positive cells were calculated as percentage of cells along the villus/crypt axis and migration rate of BrdU-positive cells was presented as percentage of distance to villus/crypt tip. As shown in Figure 56, CHOP-HA overexpression did not affect IEC proliferation in jejunum and distal ileum, respectively.

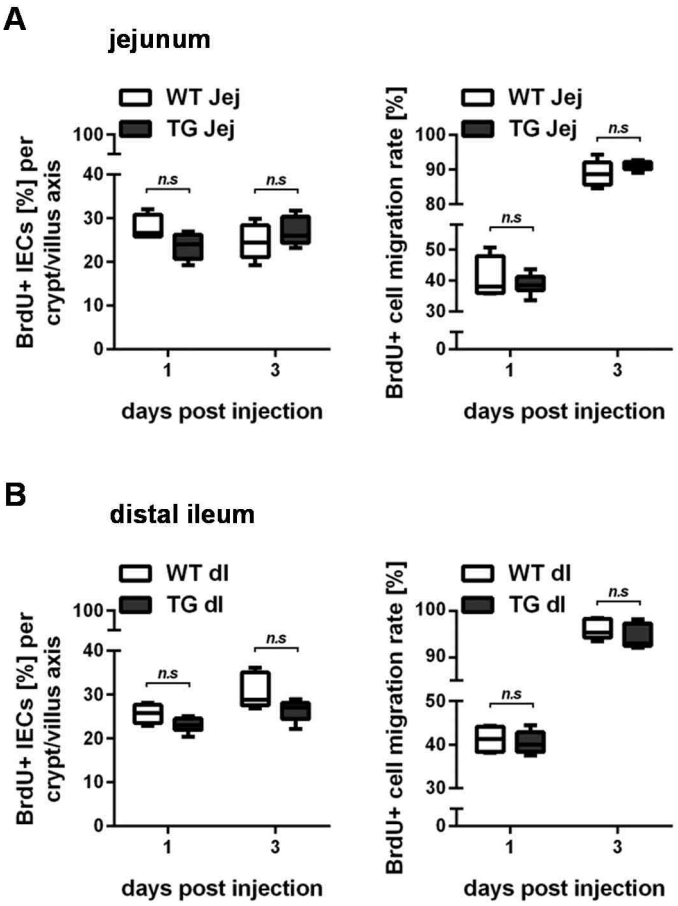

Figure 56. CHOP-HA overexpression has no effect on epithelial cell proliferation in jejunum and distal ileum of *Chop*$^{IEC\ Tg/Tg}$ mice.

Transgenic mice and wild-type controls were injected with BrdU for *in vivo* labeling of proliferative cells and sacrificed on days 1 and 3 post injection. 5 µm tissue sections of jejunum (A) and distal ileum (B) were analyzed for BrdU-positive cells by IHC. Number of BrdU-positive cells was calculated as percentage of total cell number along the villus/crypt axis. Migration rate of BrdU-positive cells was assessed as percentage relative to villus/crypt height. All data sets were analyzed by non-parametric rank-sum test. $P < .05$ was considered statistically significant.

In contrast, proliferation of IECs was found to be significantly decreased in distal colon of *Chop*$^{IEC\ Tg/Tg}$ mice when compared to wild-type controls (Figure 57). With regard to the proliferation markers used in this experiment, BrdU-positive cells specifically represented IECs in the S-phase, while Ki-67-positive cells referred to cells in all phases of the cell cycle except G0 (Figure 57A).

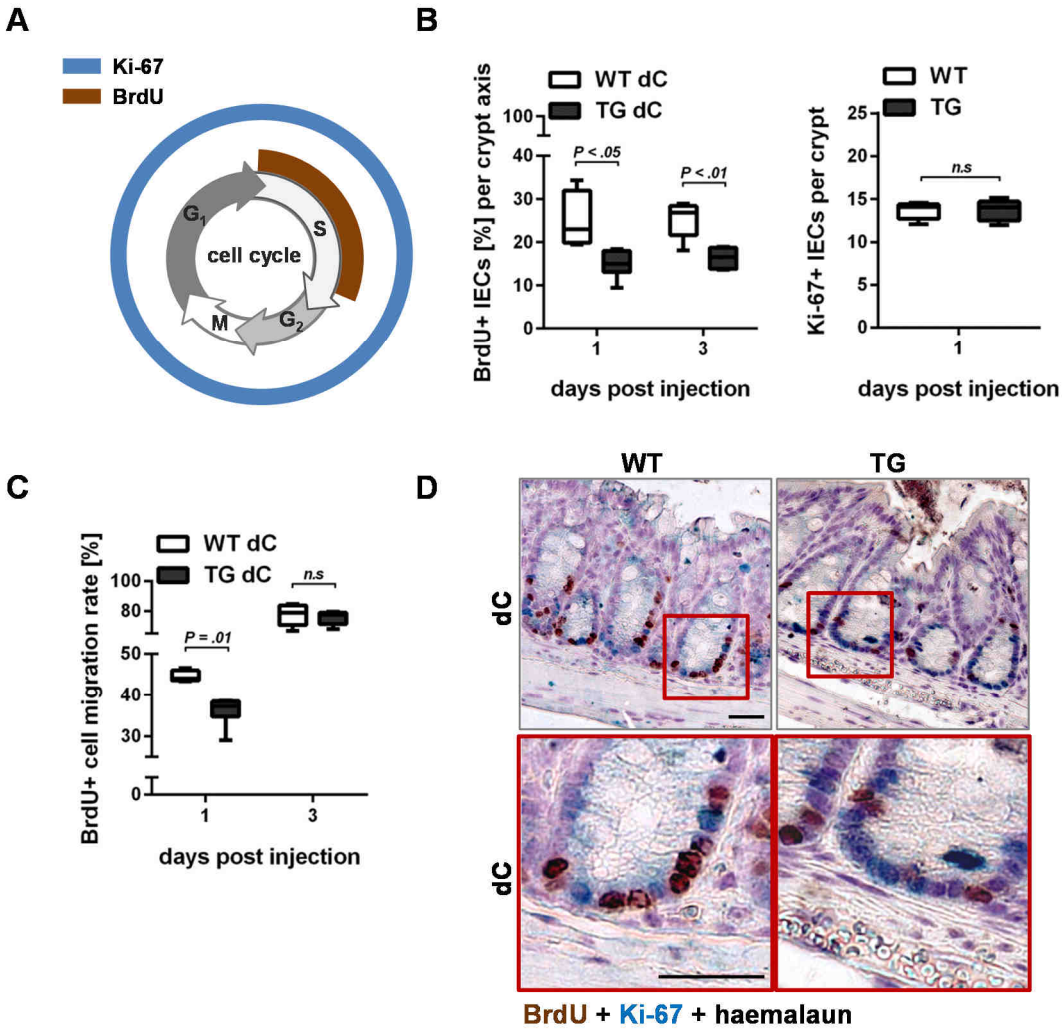

Figure 57. CHOP-HA overexpression in distal colon leads to reduced numbers of proliferative cells associated with decreased migration.

Colonic tissue sections of transgenic mice and wild-type controls sacrificed on days 1 and 3 post BrdU injection (n = 5), were analyzed for BrdU- and Ki-67 positive cells. Detection of proliferation markers BrdU and Ki-67 within the cell cycle is illustrated in (A). (B) Numbers of BrdU- and Ki-67-positive cells were assessed by IHC. Numbers of BrdU+ cells are given as percentage to total cell numbers along the crypt axis. Numbers of Ki-67+ cells were assessed per crypt. (C) Migration rate of BrdU-positive cells was assessed as percentage relative to crypt depth. (D) Representative colonic tissue sections from *Chop*$^{IEC\ Tg/Tg}$ mice and wild-type controls were stained for both BrdU- and Ki-67-positive epithelial cells. Haemalaun was used for nuclear counterstaining. Scale bars represent 50 µm. All data sets were analyzed by non-parametric rank-sum test, $P < .05$ was considered statistically significant.

Reduced numbers of BrdU-positive IECs were associated with a delayed migration rate of colonic epithelial cells (Figure 57B and C). However, numbers of Ki-67-positive cells remained unchanged in *Chop*$^{IEC\ Tg/Tg}$ mice compared to wild-type controls. Similar results could be assessed in BrdU-labeled mice further illustrated by representative tissue sections of distal colon that were co-stained for BrdU and Ki-67 (Figure 57C and D).

Taken together, these data clearly demonstrated that enhanced CHOP protein expression implicates in cell cycle progression of colonic IECs associated with decreased ratio of BrdU- to Ki-67-positive cells and significantly reduced cell migration.

4.6 CHOP protein impairs wound healing in disease-free transgenic mice

Based on our previous findings, we could show that disease severity in response to DSS treatment is significantly enhanced in *Chop*$^{IEC\ Tg/Tg}$ mice. Since IEC-specific CHOP overexpression further decreased the process of epithelial regeneration upon DSS-induced mucosal tissue damage, we strongly suggested that this effect might be associated with the reduced proliferation and cell migration of colonic IECs observed in disease-free transgenic mice. Following this hypothesis, we next evaluated mucosal tissue repair of mechanically induced wounds. Accordingly, mechanical wounds were induced in colonic mucosa of disease-free *Chop*$^{IEC\ Tg/Tg}$ mice and wild-type controls. Wound healing was followed by video colonoscopy on days 0, 1, 2, 3 and 5 calculating wound diameters as percentage of initial wound size. In transgenic mice, wound closure was significantly retarded when compared to wild-type controls (Figure 58).

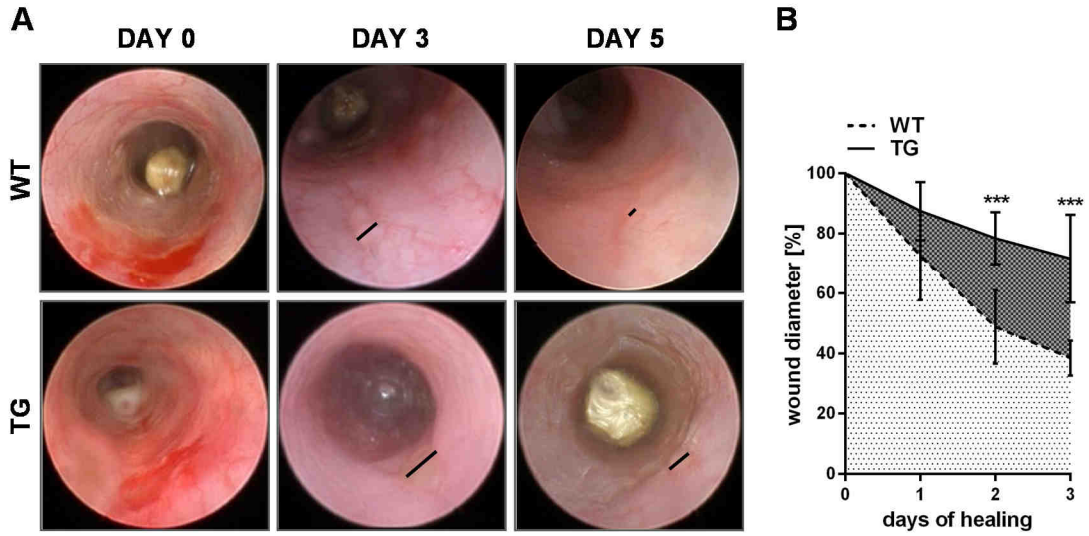

Figure 58. Wound healing is impaired in *Chop*$^{IEC\ Tg/Tg}$ mice.
(A) Colonic mucosal lesions were mechanically induced in *Chop*$^{IEC\ Tg/Tg}$ mice and wild-type controls (n = 6 per group). Wound healing was monitored by video colonoscopy on days 0, 1, 2, 3, and 5. (B) Wound diameters were assessed and calculated as percentage to initial wound size. Data for days 0, 1, 2, and 3 (n = 6) are presented as means ±SD. Statistical significance was assessed by Student's t-test, $P < .001$ (***) was considered statistically significant.

Wound closure was further evaluated at the histological level comparing H&E staining as well as IF for E-Cadherin. Therefore, mice were sacrificed on days 3 and 5 of healing (n = 3 per group and day). As shown in Figure 59, the epithelial cell layer was still disintegrated in *Chop*$^{IEC\ Tg/Tg}$ mice on days 3 and 5 of healing, while healing as sufficiently progressed to wound closure in wild-type controls. Notably, TUNEL assay did not detect apoptotic epithelial cells in wound regions of transgenic mice.

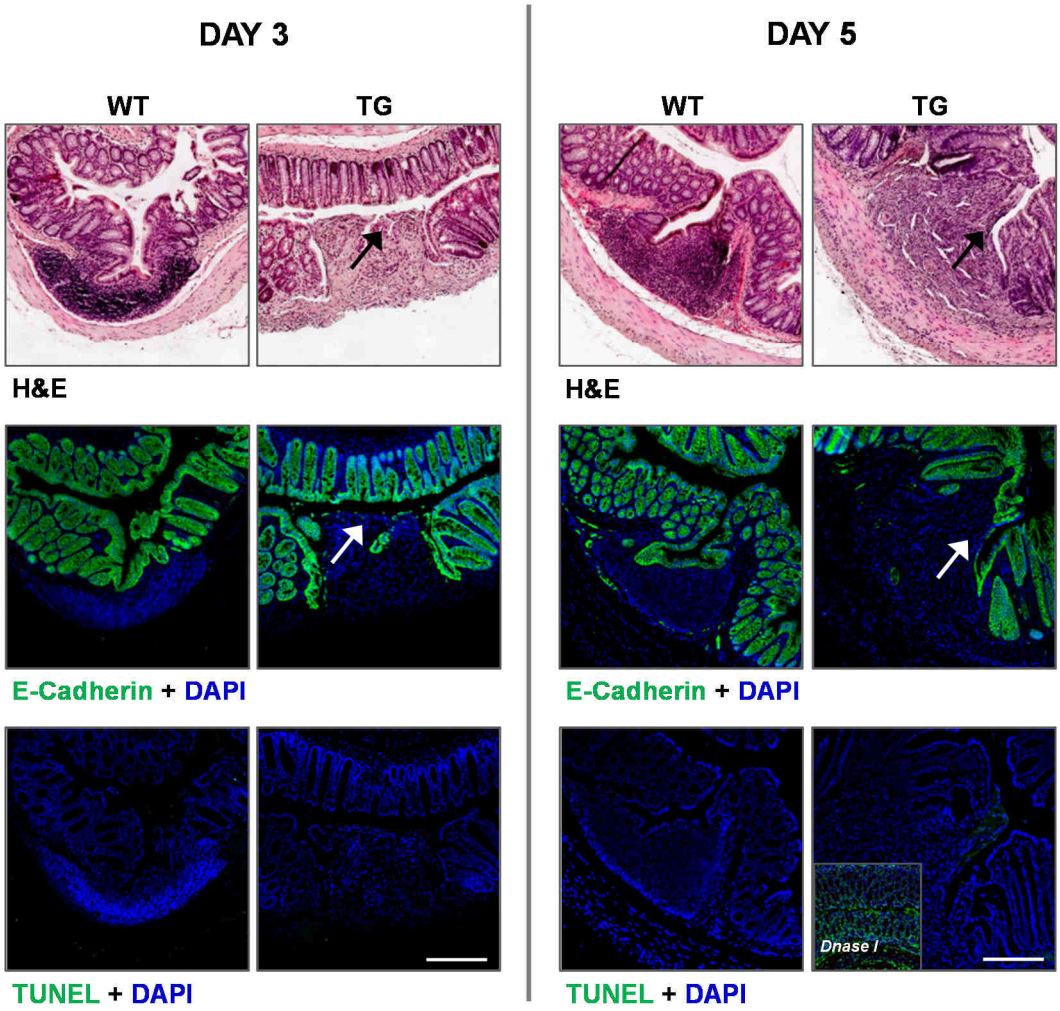

Figure 59. Transgenic mice show delays in colonic epithelial regeneration.
Mice were sacrificed by cervical dislocation at days 3 and 5 (n = 3 per group and day). 5 µm-thick colonic tissue sections of *Chop*$^{IEC\ Tg/Tg}$ mice and wild-type controls were stained with H&E. IF was performed by using primary antibody against E-Cadherin. DAPI was used for nuclear staining. TUNEL assay was performed after 3 and 5 days of mechanical injury. Positive control was treated with DNaseI. Arrows indicate disrupted epithelial cell layer. Scale bars represent 200 µm.

With regard to wound regions, wild-type mice displayed enhanced immune cell infiltration when compared to *Chop*$^{IEC\ Tg/Tg}$ mice. Analysis of immune cell stainings revealed that progressing wound closure correlated with infiltration of CD19-positive B cells, while delayed wound healing seemed to be associated with increased Vimentin production (Figure 60). In this context, we compared numbers of CD19-positive cells in disease-free and DSS-treated mice, respectively, showing that infiltration with mucosal CD19-positive B cells was specifically enhanced in the recovery phase of DSS-treated mice (Figure 61).

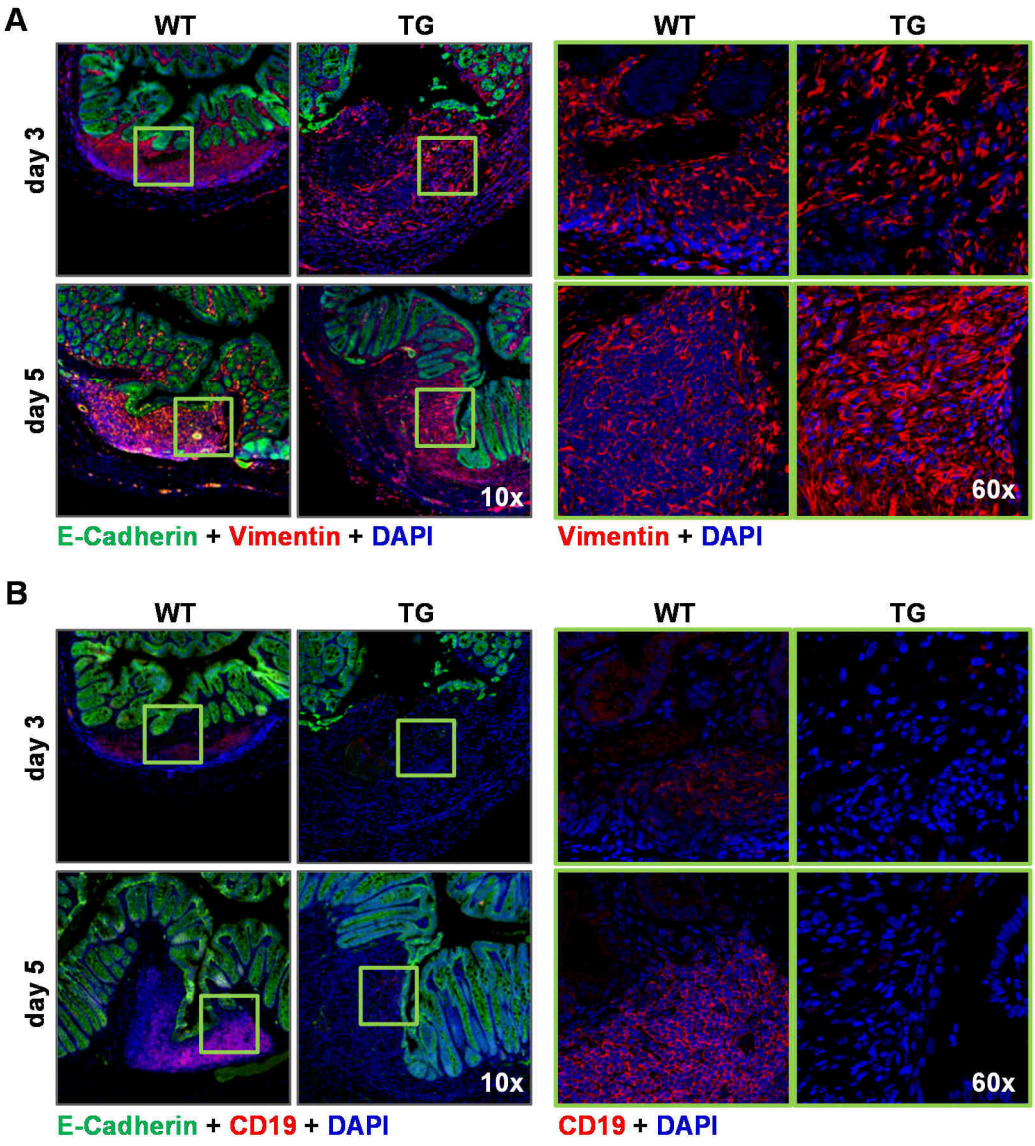

Figure 60. Delayed wound closure is associated with enhanced Vimentin production and reduced CD19+ immune cell infiltration.

Mucosal healing was analyzed on days 3 and 5 after wound induction. (A) Tissue sections containing wound regions were stained for Vimentin as a marker for fibroblasts. E-Cadherin staining was performed illustrating the epithelial cell layer. DAPI was used for nuclear counterstain. (B) Tissue sections were analyzed for B cell infiltration using anti-CD19 antibody. E-Cadherin staining was performed to illustrate the epithelial cell layer. DAPI was used for nuclear counterstain.

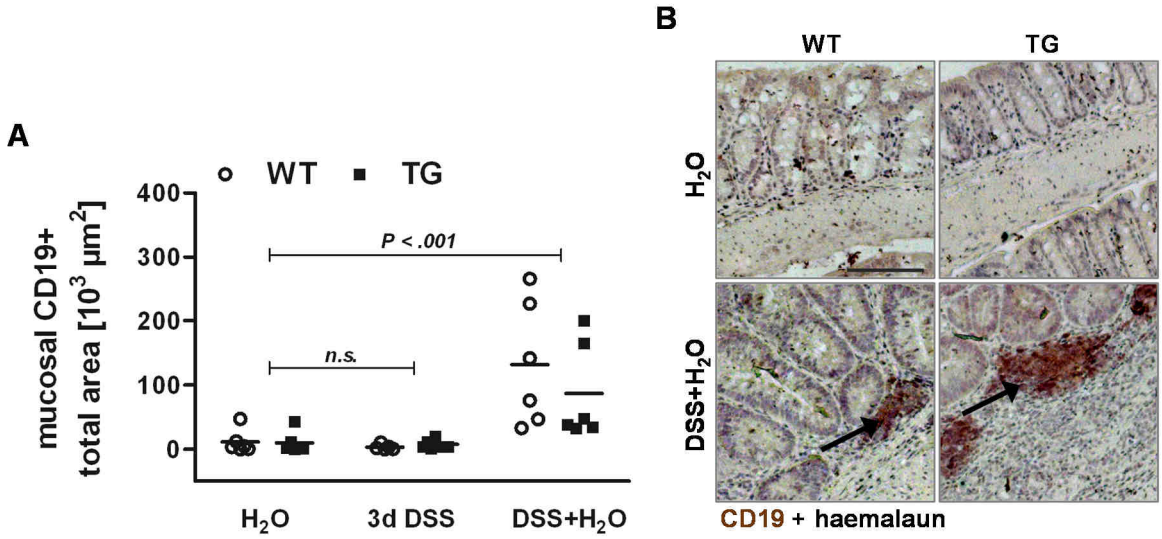

Figure 61. Mucosal CD19+ cell infiltration in response to DSS treatment.

(A) Colonic tissue sections of disease-free and DSS-treated mice were analyzed for CD19-positive cells by IHC. CD19-positive areas were measured in whole Swissroll sections. Data are presented as CD19+ area in total tissue area. Data sets were analyzed by TWA with genotype and DSS treatment as main factors followed by multiple comparison procedure by Holm-Sidak method, $P < .05$ was considered statistically significant. (B) IHC of representative tissue sections is shown for disease-free mice and mice in recovery. Arrows indicate CD19-positive B cell accumulation, scale bar represents 200 µm.

In summary, these findings suggested that enhanced CHOP protein expression does not only affect the severity of inflammation in DSS-induced colitis, but rather implicates in epithelial regeneration in response to mechanically induced mucosal wounds, thus leading to prolonged tissue damage and impaired mucosal healing.

5 Discussion

IBD are multifactorial disorders that are strongly associated with immunological dysfunction. In this regard, maintenance of epithelial integrity highly contributes to the intestinal immune homeostasis. Deregulated epithelial cell signaling has been reported to affect innate immune mechanisms, thus promoting the development of chronic inflammation [38, 220]. Epithelial integrity is strongly dependent on epithelial turnover that is tightly regulated by various mechanisms underlying cell proliferation and apoptosis [169, 186, 221]. In this context, CHOP has been shown to be involved in both apoptosis and proliferation [54, 160]. Even though direct implications of CHOP in IBD remains elusive, inflammation-related signaling leading to CHOP expression has been linked to the disease phenotype. Both, ER UPR and mtUPR were up-regulated in IBD, while CHOP expression has been observed to be significantly reduced at mRNA and protein levels in UC [28, 40, 164, 165]. With regard to previous studies, consequences of CHOP-mediated signaling has been attributed to pro-apoptotic effects rather than mechanisms involved in the regulation of cell proliferation [86]. Subsequently, CHOP down-regulation in colonic inflammation might reflect protective mechanisms; which first let assume that CHOP expression does not correlate with IBD-associated apoptosis and further raise the question of whether CHOP is regulated in an UPR-independent manner.

To address the IEC-specific function and consequences of CHOP protein expression in the context of intestinal inflammation, a genetically modified mouse model (*Chop*$^{IEC\ Tg/Tg}$) was generated conditionally overexpressing CHOP in the intestinal epithelial layer. We characterized the effects of high CHOP protein expression in disease-free mice and mice that were challenged by colitis-inducing *C. rodentium* and DSS, respectively.

Our findings demonstrate for the first time that IEC-expressed CHOP does not promote apoptotic signaling, but strongly affects the proliferative capacity of epithelial cells. Even though disease-free mice seemed to compensate reduced proliferation of colonic epithelial cells, defective proliferation impairs epithelial regeneration in response to mucosal tissue damage. In this regard, decrease in the regenerative capacity is highly suggested to cause enhanced susceptibility to early DSS-induced inflammation as well as delayed mucosal healing of DSS-induced tissue damage. Along this line, down-regulation of CHOP in UC might contribute to an increased epithelial turnover as a consequence of inflammation-driven apoptosis [164, 169]. In conclusion, our study provides important insights into IEC-specific signaling and consequences underlying environmental challenges that affect gut homeostasis in health and disease.

5.1 High CHOP protein expression leads to defective proliferation of IECs

First, we characterized *Chop*$^{IEC\ Tg/Tg}$ mice, demonstrating that high CHOP protein expression in IECs does not cause spontaneous inflammation in the intestine. IEC phenotype of transgenic mice was comparable to healthy wild-type controls considering morphological alterations as well as inflammatory pathology, including immune cell infiltration, mucus production, and changes in both apoptotic (Caspase 3 cleavage) and proliferative (Ki-67) rate. With regard to previous studies, CHOP expression is frequently described in correlation with the onset of apoptosis mediated by various ER stress-inducing agents, such as tunicamycin, breveldin A, and thapsigargin [54, 222]. In pro-apoptotic conditions, transcriptional activation of CHOP is mediated by phosphorylation through p38 MAP kinase as well as dimer formation with specific binding partners, such as C/EBPβ [151, 156]. In this context, Chiribau et al. showed that protein expression of both CHOP and binding partner C/EBPβ isoform LIP was strongly dependent on ER stress signaling [156]. We could not find elevated ER stress as well as enhanced p38 MAP kinase activation in *Chop*$^{IEC\ Tg/Tg}$ mice when compared to wild-type controls, while LIP expression remained below detectable levels (data not shown). Thus, we strongly suggested that CHOP-induced cell death might be regulated by several interrelated apoptotic mechanisms that are absent in IECs of non-stressed transgenic mice. In fact, also the expression of CHOP is tightly regulated in non-stressed cells. Various transcriptional, post-transcriptional, and post-translational regulation patterns limit the expression of CHOP under physiological conditions [147-149, 153]. Since transgenic CHOP is controlled by the CAGGS promoter, we exclusively analyzed mechanisms affecting CHOP protein expression. According to cell culture experiments performed with the colonic epithelial ptk6 cell line, we could show that transgenic CHOP protein is degraded by the proteasome. Hence, we suggested that transgene mRNA expression and CHOP protein abundance did not correlate in *Chop*$^{IEC\ Tg/Tg}$ mice. Even though protein levels might be decreased in transgenic mice, CHOP is still largely expressed when compared to wild-type controls. Interestingly, we found that transgenic CHOP is strongly accumulated in nuclei of IECs. In this regard, it has been assumed that CHOP does not possess a functional nuclear localization site, which in turn makes nuclear translocation strongly dependent on heterodimer formation [156]. Unfortunately, analysis of heterodimer formation by performing immunofluorescence double staining with antibodies against HA and C/EBPβ (LAP, LIP), ATF3, and ATF4, respectively, remained without results (data not shown). Nevertheless, nuclear translocation of CHOP protein pointed towards its transcriptional activation. We thus examined CHOP target gene expression, including ER stress-responsive genes, such as *Gadd34*, *Ero1α*, *Atf3*, *BIM*, as well as mtUPR-specific *Cpn60* expression. Herein, only Atf3 was significantly regulated (+2,7-fold) at mRNA expression level following gene expression profile

of colonic epithelial cells derived from *Chop*$^{IEC\ Tg/Tg}$ mice and wild-type controls. ATF3 has been reported to form dimers with CHOP, but it remains elusive how these proteins may interact with each other in transgenic mice [155]. However, with regard to the expression patterns of nuclear CHOP protein, we found patchy distributions along the vertical axis, which might result from proteasomal degradation [152-154]. In this context, it is worth mentioning that *vil-Cre* mice were used for the generation of *Chop*$^{IEC\ Tg/Tg}$ mice that have been reported to equally express Cre recombinase along the vertical and horizontal axis of the intestine [206]. Another indication of post-translational modification was given by Western blot analysis detecting CHOP-HA protein bands with different molecular weights (~26 kDa - ~30 kDa). According to previous findings demonstrating that CHOP became phosphorylated in order to promote or inhibit its transcriptional activity, respectively, we investigated banding patterns of several protein variants lacking specific phosphorylation sites [150, 151]. Following this approach, we found that CHOP became partly phosphorylated at p38 MAP kinase-specific phosphorylation sites *in vitro*, suggesting similar post-translational regulation patterns *in vivo*. Phosphorylation at serine-residues 79/82 (human) and 78/81 (mouse) has been strongly associated with enhanced transcriptional activity of CHOP protein in response to prolonged ER stress, which in turn favors apoptosis of unhealthy cells [151]. Contrary, we clearly showed that both transgenic CHOP protein as well as the [S78/81A] protein variant were involved in the regulation of epithelial cell proliferation, but not apoptosis/necrosis, following our cell culture experiments with colonic ptk6 cell lines. As a consequence, we hypothesized that CHOP rather implicates in IEC proliferation than cell death *in vivo*.

Little is known about the effects of CHOP on cell proliferation. In 1994, Barone et al. first described that microinjection of CHOP expression plasmids into NIH-3T3 cells led to cell-cycle G1 arrest [160]. Since then just a few studies supported a correlation between CHOP expression and proliferation. Horndasch et al. clearly demonstrated that CHOP is implicated in Wnt signaling in *Xenopus larvae*, thereby suppressing the expression of Wnt target genes, including *c-Myc* [194]. Thus, we further examined epithelial proliferation in *Chop*$^{IEC\ Tg/Tg}$ mice. Distinct markers have been applied to determine proliferative cells [223]. The antigen Ki-67 can be detected in all phases of the cell cycle except G0, while BrdU incorporation exclusively takes place during DNA replication. Since we found numbers of Ki-67-positive cells unchanged in *Chop*$^{IEC\ Tg/Tg}$ mice and wild-type controls, we analyzed BrdU incorporation in IECs. We could show that numbers of BrdU-positive IECs were significantly reduced in transgenic mice associated with decreased cell migration rate. Notably, these effects could just be observed in colon, but not jejunum and ileum of *Chop*$^{IEC\ Tg/Tg}$ mice, which might be explained by basic differences between small and large intestine considering gene expression profiles as well as responsiveness to changes in the basal expression levels [165]. In accordance to our *in vitro* studies, we strongly suggested that CHOP did not affect total

numbers of proliferative colonic IECs, but numbers of cells entering the S phase for DNA replication, which in turn resulted in an accumulation of cells in G1 (Figure 62).

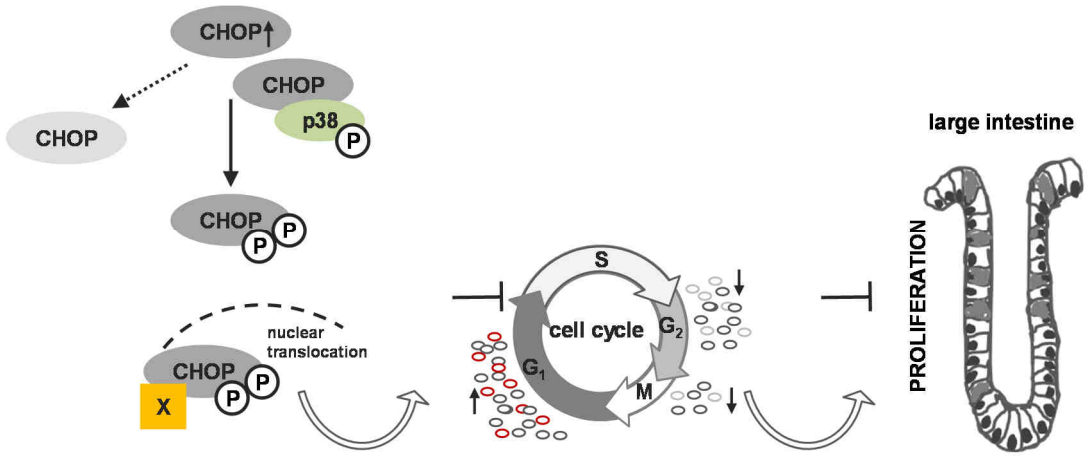

Figure 62. Hypothetic inhibitory function of CHOP on cell cycle progression in colonic IECs.
Overexpression of CHOP protein results in increased post-translational modification of CHOP at p38-specific phosphorylation sites, serine-residues 78 and 81. Since CHOP is suggested to lack a functional nuclear localization signal, nuclear translocation is mediated by heterodimer formation with CHOP binding partner X. Enhanced CHOP protein expression impacts on cell cycle progression by inducing accumulation of cells in G1, which *in vitro* is rather associated with depletion of cells in G2/M. The CHOP-mediated delay in cell cycle progression leads to impaired proliferative capacity of colonic IECs, which consequently affects the cell migration rate along the crypt axis.

Defective proliferation in *Chop*$^{IEC\ Tg/Tg}$ mice as well as adequate ptk6 cell lines was not associated with reduced mRNA expression of Wnt target genes, including *c-Myc* and *Cyclin D1*. Wnt signaling occurs most prominently in intestinal stem cells at the crypt base, but is reduced along the vertical crypt axis from stem cell populations to transit amplifying cells [224]. In this context, Heijmans et al. recently reported that the expression of stem cell-specific genes was inversely correlated with the activation of ER stress-responsive genes. Enhanced ER stress signaling appeared highly associated with IEC differentiation, while CHOP expression has been strongly suggested to be substantially involved in mechanisms underlying the loss of stem cell properties [42]. In *Chop*$^{IEC\ Tg/Tg}$ mice, the transgene was only expressed in small amounts regarding IECs at crypt base of small and large intestine, respectively. Therefore, CHOP might not have any effects on proliferation of stem cell populations. Highly decreased CHOP protein expression in intestinal stem cells could either result from proteasomal degradation or incomplete *Cre*-recombination. It is not clear to which extent *vil-Cre*-mediated recombination affected stem cell populations in *Chop*$^{IEC\ Tg/Tg}$ mice. Hence, we might assume incomplete *Cre*-recombination in Lgr5-positive stem cells, but not in TA cells. In general, this aspect could be further investigated by using *lgr5-Cre*-positive

mice. As a consequence of both, transgenic CHOP protein expression is strongly suggested to reduce proliferation of TA cells rather than Lgr5-positive stem cells. In this case, differences in Wnt target gene expression could be below detectable levels when both TA and stem cells were mixed during IEC isolation. However, increasing rates of both epithelial cell proliferation and apoptosis have been observed in UC patients, while CHOP mRNA and protein expression has been reported to be reduced in UC [164, 169, 225]. With regard to our data, these findings strongly suggested that the regulation of CHOP expression most likely underlies mechanisms controlling disease-related epithelial proliferation rather than apoptosis.

5.2 Defective proliferation of IECs aggravates mucosal tissue regeneration

Disease-free *Chop*$^{IEC\ Tg/Tg}$ mice exhibited highly significant changes in the expression of gene sets annotated to the biological process GO term response to stimulus, including the child terms defense response, and response to wounding. In this context, we observed alterations in the gene expression program strongly associated with proliferation and cell migration. To investigate whether CHOP-mediated defects in IEC proliferation implicates in epithelial integrity, we determined barrier-forming ability of CHOP overexpressing ptk6 cell lines by measuring TEER. We could show that transgenic CHOP as well as CHOP-HA[S78/81A] did not affect barrier function, thus strongly suggesting that CHOP did not impact on the epithelial barrier in transgenic mice. However, according to further *in vitro* studies, we observed that defective proliferation was strongly associated with impaired cell migration following delayed scratch closure in differentiated ptk6 cell monolayers. Along this line, we examined wound closure of mechanically induced colonic injuries, demonstrating that transgenic mice were significantly retarded in mucosal tissue healing independent of enhanced apoptosis. In fact, intestinal wound healing comprises three cellular events considering re-epithelialization, including epithelial restitution, proliferation, and differentiation [226]. In this context, Wnt5a has been shown to play an important role in colonic crypt regeneration [227]. Wnt5a describes a non-canonical Wnt ligand that has been reported to inhibit proliferation of canonical Wnt-active IECs. In regenerative conditions, mesenchymal cell-derived Wnt5a has been associated with mucosal invaginations upon colonic crypt formation [227]. Disease-free *Chop*$^{IEC\ Tg/Tg}$ mice revealed enhanced expression of Wnt5a (+1.5-fold) following gene expression profiles of colonic epithelial cells. Since IEC-derived Wnt5a did not promote wound healing in *Chop*$^{IEC\ Tg/Tg}$ mice, we strongly suggested that up-regulation of Wnt5a contributed to intrinsic mechanisms underlying the differentiation process of IECs, which in turn caused impaired epithelial proliferation [228]. To further address the correlation between CHOP and Wnt5a upon IEC differentiation, corresponding expression levels could be analyzed in sorted cell populations. However, impaired mucosal tissue regeneration was further associated with deficiency of mucosal infiltrating CD19-positive lymphocytes that have been recently reported to contribute to wound healing in skin tissue [229]. Since we found CD19-positive cells in transgenic mice that recovered from DSS treatment, we assumed that infiltration of cells was just delayed, but not absent in mechanically injured *Chop*$^{IEC\ Tg/Tg}$ mice.

Conclusively, we demonstrated that CHOP-induced defects in IEC proliferation consequently diminished the regenerative ability of the epithelial lining, even though epithelial integrity could be maintained in non-challenged conditions. Thus, we strongly suggested

that down-regulation of CHOP in UC promotes epithelial cell proliferation in order to enhance healing of inflammation-driven mucosal tissue damage (Figure 63).

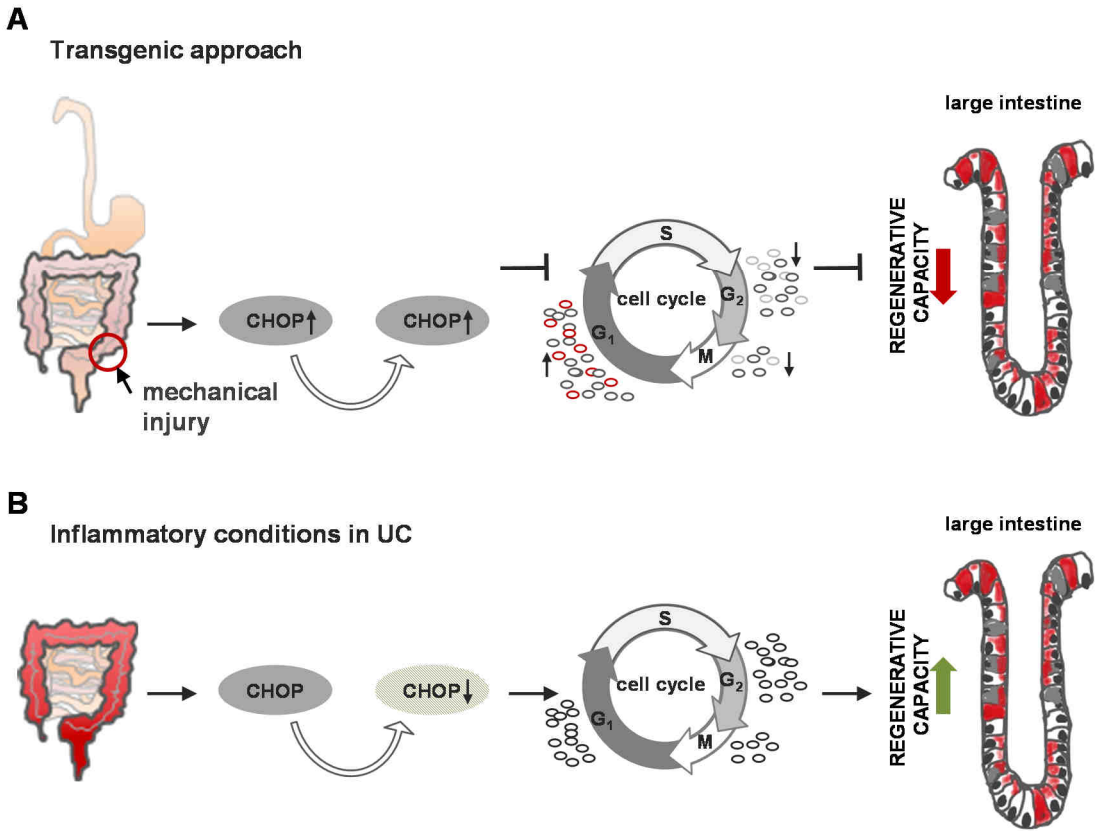

Figure 63. Possible consequences of CHOP down-regulation under chronic inflammatory conditions.

(A) High CHOP protein expression impairs cell cycle progression of colonic IECs. CHOP is suggested to lack a functional nuclear localization sequence. Thus, nuclear translocation is mediated by dimer formation with CHOP binding partner X. As a consequence, cells accumulate in G1, which *in vitro* is rather associated with depletion of cells in G2/M. CHOP-induced delay in cell cycle progression is highly associated with reduced proliferation and cell migration that in total decreases the regenerative ability of the epithelial lining in response to mechanical injury. (B) Proposed consequences of CHOP down-regulation in chronic intestinal inflammation. Down-regulation of CHOP mRNA and protein expression is suggested to contribute to the regenerative capacity of the epithelial lining and in healing of inflammation-driven mucosal tissue damage.

5.3 Epithelial barrier function is maintained upon *C. rodentium* infection

Alteration of epithelial turnover has been described in the context of host adaptation to gut microbiota, including commensals and pathogens. In this regard, Savage et al. showed that IEC turnover rates were accelerated in conventional mice when compared to mice that have been raised under germ-free conditions [230]. In turn, defective IEC turnover rates seemed to drive changes in the gene expression profile of *Chop*$^{IEC\ Tg/Tg}$ mice highly associated with the bacterial defense program. Thus, we suggested that defects in IEC proliferation were compensated with enhanced expression of anti-microbial peptides, such as Reg3 family members (+2-fold), lactoperoxidase (+1.5-fold), and lysozyme 1 (+1.3-fold). However, it has been demonstrated that defective proliferation was strongly associated with impaired bacterial clearance in response to *C. rodentium* infection [231]. With regard to our data, we could show that clearance of *C. rodentium* remained unchanged upon sustained CHOP expression, suggesting that defective proliferation did not further affect epithelial barrier function in *Chop*$^{IEC\ Tg/Tg}$ mice. Even more, we demonstrated that up-regulation of anti-microbial peptides had no effect on the onset of *C. rodentium* colonization. Even though Reg3β seemed to be involved in host response to *C. rodentium* infection considering colonic tissue staining of infected transgenic mice and wild-type controls, CHOP-driven up-regulation of Reg3β did not confer an advantage in a preconditioning fashion. Since we exclusively analyzed mice on day 25 dpi, it is difficult to interpret tissue pathology of *C. rodentium*-driven colitis. Even though there seemed to be no differences in morphological changes between transgenic mice and wild-type controls, further studies on the infection course considering more time points might give more information. However, Sellin et al. reported that *C. rodentium* stimulated β-catenin signaling, thereby inducing colonic crypt hyperplasia [232]. Thus, *C. rodentium*-induced signaling might reverse the negative effects of CHOP on epithelial proliferation. It has been shown that disease severity is strongly dependent on the genetic background of mice. Inbred mouse strains, including C3H/HeJ and FVB/N are highly susceptible to *C. rodentium* infection associated with extensive tissue damage and increased lethality, while NIH:Swiss as well as C57BL/6J mice have been characterized to be more resistant. Therefore, we might suggest that *C. rodentium*-induced colitis in mice on C57BL/6N background was not an appropriate challenge to study consequences of CHOP under inflammatory conditions.

5.4 Decrease in IEC regeneration is associated with enhanced inflammation

We could show that *Chop*$^{IEC\ Tg/Tg}$ mice were more susceptibility to DSS-induced colitis associated with impaired re-epithelialization in the recovery phase. Regarding the nature of DSS-induced colitis, patchy distribution patterns of lesions made it impossible to evaluate whether mice were delayed in recovery due to defective proliferation instead of simply enlarged wounds. Enhanced inflammation has been observed in transgenic mice in response to short-term DSS treatment and in the recovery phase. Herein, increased inflammation seemed to be independent of CHOP-mediated pro-apoptotic signaling following gene expression profiles of colonic epithelial cells derived from 3 days DSS-treated mice and mice in the recovery phase. Even though a subset of genes were similarly regulated in *Chop*$^{IEC\ Tg/Tg}$ mice upon different DSS treatments, a correlation between CHOP overexpression and impaired IEC proliferation could not be determined. Nevertheless, we found differences in p38 MAP kinase activation in early inflammation (high) and recovery (low). Although we demonstrated that the effects of CHOP protein on both cell proliferation and migration were strongly dependent on its phosphorylation status, we could not find differences in banding patterns of CHOP protein in DSS-treated transgenic mice when compared to water-treated controls. However, upon short-term DSS treatment, wild-type mice displayed strongly decreased CHOP protein expression. Thereby, down-regulation of CHOP was dissociated from ER stress induction, increased expression of CHOP target genes *Gadd34* and *Ero1*α as well as DSS-induced IEC apoptosis. We thus suggested that CHOP protein was reduced in order to enhance IEC proliferation in an early response to DSS-mediated IEC apoptosis. In this context, Araki et al. demonstrated that the onset of DSS-induced colitis was promoted by reduced epithelial turnover rates associated with enhanced apoptosis of IECs [201]. Along this line, we assumed that CHOP-mediated defects in IEC proliferation further enhanced the susceptibility to DSS-induced colitis in *Chop*$^{IEC\ Tg/Tg}$ mice. As a consequence, epithelial turnover is suggested to be further affected, consequently resulting in enhanced IEC apoptosis, elevated oxidative stress (Ero1α, Gadd34), and increased macrophage infiltration (Figure 64).

The effects of CHOP protein expression have been conversely described in disease-conditioning. Thereby, most insights into the functional role of CHOP were gained from studies on complete CHOP knockout mice [167, 233]. With regard to intestinal inflammation, *Chop*$^{-/-}$ mice exhibited less severe inflammation in response to DSS-induced colitis. Protection from colitis has been attributed to reduced numbers of mucosa infiltrating macrophages and decreased ROS production, which rather seemed to be in accordance to our data, but tissue-specific resolution remained elusive [166].

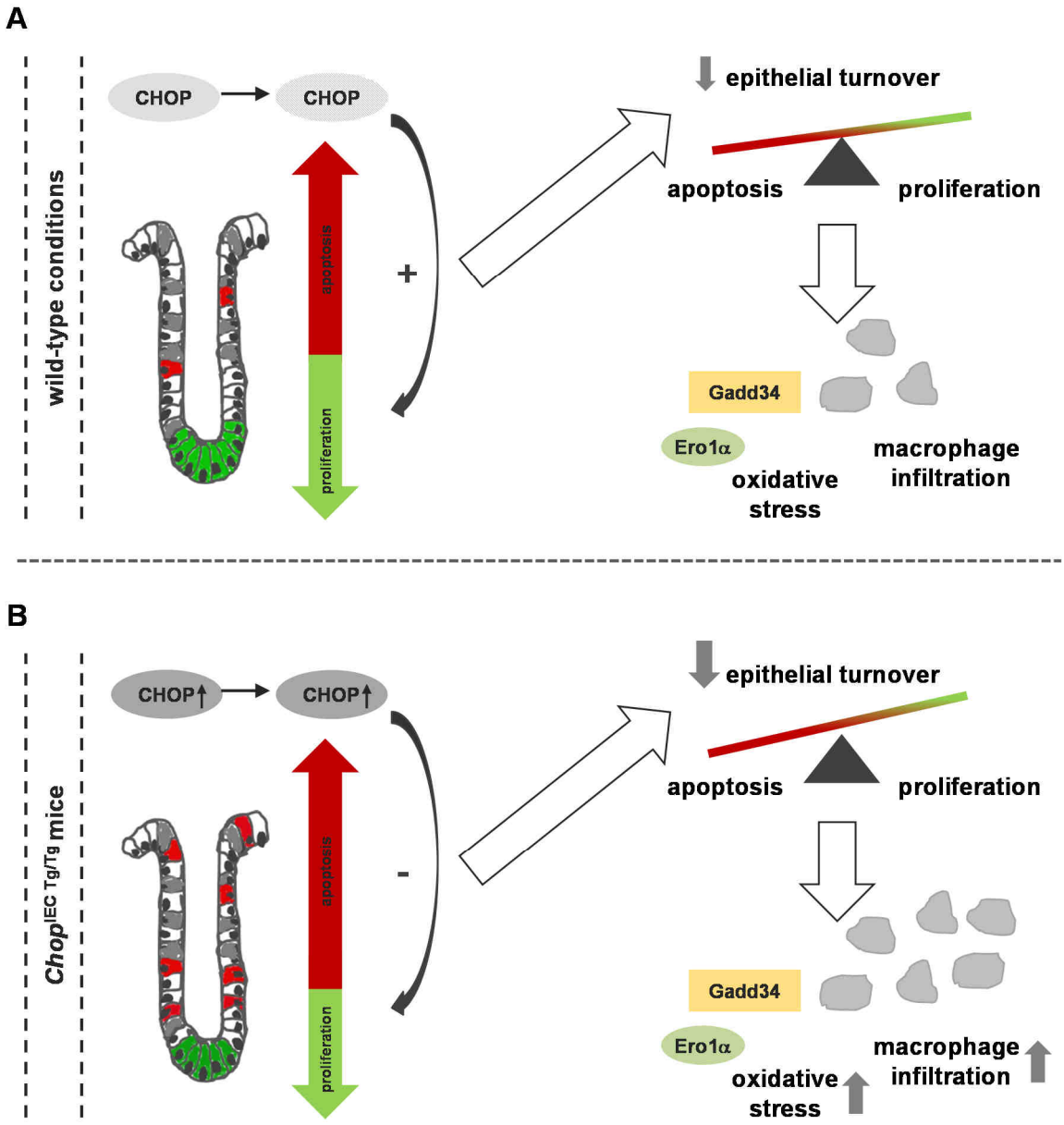

Figure 64. Proposed mechanisms underlying the increased susceptibility to DSS-induced colitis of *Chop*$^{IEC\ Tg/Tg}$ mice.

(A) Short-term DSS treatment leads to the induction of IEC apoptosis, thus affecting epithelial turnover. Increased apoptosis is characterized by elevated oxidative stress indicated by up-regulation of Ero1α and Gadd34 as well as macrophage infiltration into mucosal tissue. In early inflammation, CHOP protein is reduced in order to promote IEC proliferation. (B) Sustained CHOP protein expression results in decreased proliferation of IECs and impairs compensatory mechanisms to DSS-induced injury. As a consequence, epithelial turnover is further affected that in turn leads to enhanced IEC apoptosis associated with more elevated oxidative stress and enhanced numbers of mucosa-infiltrating macrophages.

Conclusively, we showed that CHOP-driven defects in IEC proliferation aggravated intestinal inflammation associated with changes in immune response. In this context, we demonstrated that decreased proliferation did not only delay epithelial regeneration, but resulted in impaired capacity to adapt to environmental changes.

5.5 Conclusion and perspectives

In conclusion, we showed that high CHOP protein expression in IECs could promote the development of IBD by affecting the epithelial proliferation. According to our data, we proposed that down-regulation of CHOP in UC reflected protective mechanisms underlying the regulation of epithelial proliferation in chronically inflamed tissue. Hence, it is questionable whether targeting the expression of CHOP is therapeutically significant in IBD. Since consequences of high CHOP protein expression in mice only became apparent in the onset of inflammation associated with mucosal tissue damage, CHOP might rather serve as an epithelial marker in estimating the risk of IBD.

Notably, prolonged IBD is highly associated with steadily rising risk for developing colorectal cancer [234]. Colorectal cancer is driven by cellular transformation that promotes persistent cell growth, which subsequently leads to tumor formation and gives rise to cancer cell development [235, 236]. Among others, it has been shown that CHOP down-regulation seems to be involved in the regulation of cellular transformation *in vitro*, while patients data strongly suggested that genetic alterations of CHOP contributes to the development of gastric cancer [237-239]. In this regard, recent studies demonstrated that induction of CHOP expression in human cancer cells led to cytotoxicity [240-242]. In accordance to our data, we strongly proposed that targeting CHOP protein expression is a potent therapeutic approach for the treatment of colorectal cancer. Taken together, our findings may suggest that therapeutic approaches could be considered for IBD patients in remission in order to inhibit uncontrolled epithelial proliferation and tumor risk.

6 Appendix

Standard diet V1124-300

ssniff® M-Z autoklavierbar

Alleinfuttermittel für die Zucht von Mäusen

Beschreibung

Dieses Futtermittel wurde für die Zucht von Mäusen entwickelt; der Proteingehalt und die Proteinqualität (Aminosäurenzusammensetzung) sowie die Energiedichte wurden entsprechend der hohen Leistung und des erhöhten Nährstoffbedarfs während dieser Phase angehoben.

Rohnährstoffe	[%]
Trockensubstanz	87,9
Rohprotein (N x 6,25)	22,0
Rohfett	4,5
Rohfaser	3,9
Rohasche	6,8
N-freie Extraktstoffe	50,8
Stärke	34,0
Zucker	5,0

Energie	[MJ/kg]
Bruttoenergie (GE)	16,7
Umsetzbare Energie (ME) *	13,6

Mineralstoffe	[%]
Calcium	1,00
Phosphor	0,70
Natrium	0,24
Magnesium	0,21
Kalium	1,02

Fettsäuren	[%]
C 14:0	0,01
C 16:0	0,56
C 16:1	0,03
C 18:0	0,14
C 18:1	0,99
C 18:2	2,41
C 18:3	0,29
C 20:0	0,02
C 20:1	0,01
C 20:5	---
C 22:6	---

Aminosäuren	[%]
Lysin	1,59
Methionin	0,46
Met+Cys	0,83
Threonin	0,80
Tryptophan	0,28
Arginin	1,33
Histidin	0,51
Valin	1,00
Isoleucin	0,90
Leucin	1,53
Phenylalanin	0,98
Phe+Tyr	1,67
Glycin	0,88
Glutaminsäure	4,19
Asparaginsäure	1,98
Prolin	1,33
Alanin	0,90
Serin	1,03

Vitamine	per kg
Vitamin A	25.000 IE
Vitamin D_3	1.000 IE
Vitamin E	135 mg
Vitamin K (als Menadion)	20 mg
Thiamin (B_1)	86 mg
Riboflavin (B_2)	32 mg
Pyridoxin (B_6)	31 mg
Cobalamin (B_{12})	150 µg
Nicotinsäure	145 mg
Pantothensäure	60 mg
Folsäure	10 mg
Biotin	700 µg
Cholin-Cl	3.130 mg
Inositol	100 mg

Spurenelemente	per kg
Eisen	185 mg
Mangan	65 mg
Zink	91 mg
Kupfer	17 mg
Iod	2,2 mg
Selen	0,3 mg
Cobalt	2,1 mg

Futterzusammensetzung

absteigende Reihenfolge der Gruppen (FMV)

Getreide und Getreidenebenprodukte, Ölsaatprodukte, Mineralstoffe, Bierhefe, pflanzliche Öle, Vitamine, Spurenelemente.

** ME berechnet nach der Schätzformel für Schweine, Anlage 4 der Futtermittelverordnung*

Energiedichte [MJ ME/kg] und Protein-/Energie-Verhältnis [g XP/MJ ME]

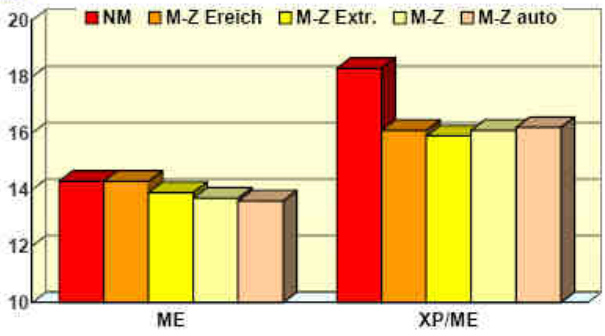

Hauptprodukte

V1124-3 10 mm Pellets
V1125-3 15 mm Pellets

Produktion und Vertrieb
ssniff Spezialdiäten GmbH
Phone: +49-(0)2921-9658-0
Fax: +49-(0)2921-9658-40
E-Mail mail@ssniff.de
www.ssniff.de

Status: 06/2005

Overview of histological scores derived from DSS experiments

Supplementary table 1. Overview of histological scores derived from DSS experiments 3d 2% DSS, 7d 2% DSS, and 5d 2% DSS + 5d H_2O. Data sets H_2O, 3d 2% DSS, and 7d 2% DSS were analyzed by TWA with genotype and DSS treatment as main factors followed by multiple comparison procedure by Holm-Sidak method, $P < .05$ (*), $P < .01$ (**), and $P < .001$ (***) was considered statistically significant. Statistical significance of 5d 2% DSS + 5d H_2O was assessed by Student's t-test, $P < .05$ (*), $P < .01$ (**), and $P < .001$ (***) was considered statistically significant.

treatment	**group**	**Changes in intestinal architecture and epithelial damage (0-6)**	**genotype**	within H2O	within DSS	**treatment**	within WT	within TG
H_2O	WT	0,275 ± 0,175	*data sets H_2O, 3d 2% DSS, and 7d 2% DSS were analyzed by TWA with genotype and DSS treatment as main factors*					
	TG	0,283 ± 0,157						
3d 2% DSS	WT	0,510 ± 0,224	***	n.s.	***	***	n.s.	***
	TG	1,331 ± 0,357						
7d 2% DSS	WT	1,375 ± 0,587	**	n.s.	***	***	**	***
	TG	2,824 ± 0,774						
5d 2% DSS + 5d H_2O	WT	1,092 ± 0,403	*data of 5d 2% DSS + 5d H_2O were analyzed by Student's t-test*					
	TG	2,450 ± 0,913	--	--	--	**	--	--

treatment	**group**	**Infiltration with inflammatory cells (0-6)**	**genotype**	within H2O	within DSS	**treatment**	within WT	within TG
H_2O	WT	0,075 ± 0,063	*data sets H_2O, 3d 2% DSS, and 7d 2% DSS were analyzed by TWA with genotype and DSS treatment as main factors*					
	TG	0,150 ± 0,063						
3d 2% DSS	WT	0,385 ± 0,234	**	n.s.	**	***	*	***
	TG	0,788 ± 0,264						
7d 2% DSS	WT	0,945 ± 0,462	*	n.s.	**	***	***	***
	TG	1,580 ± 0,419						
5d 2% DSS + 5d H_2O	WT	1,202 ± 0,627	*data of 5d 2% DSS + 5d H_2O were analyzed by Student's t-test*					
	TG	1,879 ± 0,623	--	--	--	n.s.	--	--

treatment	**group**	**histological score (0-12)**	**genotype**	within H2O	within DSS	**treatment**	within WT	within TG
H_2O	WT	0,350 ± 0,170	*data sets H_2O, 3d 2% DSS, and 7d 2% DSS were analyzed by TWA with genotype and DSS treatment as main factors*					
	TG	0,433 ± 0,189						
3d 2% DSS	WT	0,895 ± 0,420	***	n.s.	***	***	*	***
	TG	2,119 ± 0,588						
7d 2% DSS	WT	2,320 ± 1,669	**	n.s.	***	***	***	***
	TG	4,404 ± 1,170						
5d 2% DSS + 5d H_2O	WT	2,294 ± 0,911	*data of 5d 2% DSS + 5d H_2O were analyzed by Student's t-test*					
	TG	4,329 ± 1,514	--	--	--	*	--	--

Overlap analysis of H_2O-, 3d DSS-, and DSS+H_2O-treated *Chop*$^{IEC\ Tg/Tg}$ mice

Supplementary table 2. Total overlap analysis of gene expression profiles of H_2O, 3d DSS, and DSS+H_2O-treated mice.

gene name	-fold change			gene name	-fold change		
	H_2O	3d DSS	recovery		H_2O	3d DSS	recovery
Ddit3	3,27	3,32	3,51	**Hspa12a**	-1,20	-1,38	-1,41
Lgals2	2,05	1,62	1,90	**Pank3**	-1,22	-1,14	-1,17
Reg3g	1,99	1,43	1,61	**Alcam**	-1,23	-1,26	-1,43
Atf5	1,88	1,64	1,95	**Acot1**	-1,23	-1,38	-1,39
Tff2	1,86	1,48	1,54	**Cndp2**	-1,25	-1,15	-1,19
Plscr4	1,59	1,31	1,71	**Ces2g**	-1,27	-1,24	-1,40
Lpo	1,50	1,48	1,47	**Cpne8**	-1,28	-1,21	-1,29
Tfip11	1,47	1,33	1,48	**Lrrc19**	-1,28	-1,27	-1,47
Srrd	1,42	1,33	1,26	**Gm1965**	-1,29	-1,54	-1,60
Epdr1	1,39	1,25	1,41	**Dapk1**	-1,30	-1,43	-1,32
Aars	1,34	1,33	1,27	**Ptprm**	-1,30	-1,41	-1,46
Soat2	1,32	1,22	1,29	**Ncald**	-1,33	-1,25	-1,26
Sult1c2	1,28	1,23	1,56	**Frrs1**	-1,33	-1,19	-1,32
Far2	1,26	1,18	1,25	**BC021614**	-1,34	-1,38	-1,60
Celf3	1,26	1,30	1,34	**Zfp385b**	-1,37	-1,31	-1,30
Plp1	1,22	1,28	1,25	**Nox1**	-1,37	-1,38	-1,67
Fam129a	1,18	1,22	1,16	**Hsd17b13**	-1,38	-1,46	-1,17
Hnf4g	1,18	1,19	1,25	**Rbp4**	-1,39	-1,47	-1,46
Kif1a	1,14	1,12	1,17	**Gsta3**	-1,39	-1,61	-1,54
Gpd1	1,14	1,16	1,16	**Nfu1**	-1,40	-1,28	-1,36
Sars	1,13	1,20	1,16	**Mgst1**	-1,40	-1,46	-1,58
Ids	1,12	1,13	1,12	**Isg20**	-1,52	-1,36	-1,39
Apobec3	1,12	1,24	-1,22	**Fmo1**	-1,54	-1,55	-1,61
Kifc3	1,11	1,25	1,30	**Maob**	-1,60	-1,60	-1,68
Fgfr1	1,10	1,17	1,15	**Gm6484**	-1,65	-1,48	-1,58
Tgoln1	-1,09	-1,09	-1,11	**Anxa9**	-1,71	-1,22	-1,17
Cept1	-1,09	-1,08	-1,09	**Matn2**	-1,82	-1,83	-1,66
Sdr42e1	-1,14	-1,17	-1,24	**Wfdc2**	-1,96	-1,89	-2,98
Sik3	-1,14	-1,23	-1,23	**Nr1h3**	-2,00	-1,65	-1,92
Inpp4a	-1,15	-1,30	-1,23	**Slc16a12**	-2,09	-1,36	-1,65
Camk1d	-1,15	-1,30	-1,29	**Akr1c18**	-2,39	-1,61	-1,63
Enpp1	-1,16	-1,25	-1,25	**Cyp3a25**	-2,58	-1,55	-1,51
Pdk3	-1,18	-1,15	-1,32	**Trf**	-3,37	-2,04	-4,47
Hsd17b2	-1,19	-1,17	-1,15	**Ugt8a**	-3,41	-2,49	-1,91
Plekhh2	-1,19	-1,50	-1,24	**S100g**	-5,54	-4,00	-3,56

Sequence data of mutated plasmid constructs CHOP-HA

CLUSTAL 2.1 multiple sequence alignment – CHOP-HA[S14/15A]

```
S14/15A_klon3           ACCATGGCAGCTGAGTCCCTGCCTTTCACCTTGGAGACGGTGGCCGCCTGGGAGCTGGAA 60
S14/15A_klon4           ACCATGGCAGCTGAGTCCCTGCCTTTCACCTTGGAGACGGTGGCCGCCTGGGAGCTGGAA 60
CHOP                    ---ATGGCAGCTGAGTCCCTGCCTTTCACCTTGGAGACGGTGTCCAGCTGGGAGCTGGAA 57
                        ************************************ **. *************

S14/15A_klon3           GCCTGGTATGAGGATCTGCAGGAGGTCCTGTCCTCAGATGAAATTGGGGGCACCTATATC 120
S14/15A_klon4           GCCTGGTATGAGGATCTGCAGGAGGTCCTGTCCTCAGATGAAATTGGGGGCACCTATATC 120
CHOP                    GCCTGGTATGAGGATCTGCAGGAGGTCCTGTCCTCAGATGAAATTGGGGGCACCTATATC 117
                        ************************************************************

S14/15A_klon3           TCATCCCCAGGAAACGAAGAGGAAGAATCAAAAACCTTCACTACTCTTGACCCTGCGTCC 180
S14/15A_klon4           TCATCCCCAGGAAACGAAGAGGAAGAATCAAAAACCTTCACTACTCTTGACCCTGCGTCC 180
CHOP                    TCATCCCCAGGAAACGAAGAGGAAGAATCAAAAACCTTCACTACTCTTGACCCTGCGTCC 177
                        ************************************************************

S14/15A_klon3           CTAGCTTGGCTGACAGAGGAGCCAGGGCCAACAGAGGTCACACGCACATCCCAAAGCCCT 240
S14/15A_klon4           CTAGCTTGGCTGACAGAGGAGCCAGGGCCAACAGAGGTCACACGCACATCCCAAAGCCCT 240
CHOP                    CTAGCTTGGCTGACAGAGGAGCCAGGGCCAACAGAGGTCACACGCACATCCCAAAGCCCT 237
                        ************************************************************

S14/15A_klon3           CGCTCTCCAGATTCCAGTCAGAGTTCTATGGCCCAGGAGGAAGAGGAGGAAGAGCAAGGA 300
S14/15A_klon4           CGCTCTCCAGATTCCAGTCAGAGTTCTATGGCCCAGGAGGAAGAGGAGGAAGAGCAAGGA 300
CHOP                    CGCTCTCCAGATTCCAGTCAGAGTTCTATGGCCCAGGAGGAAGAGGAGGAAGAGCAAGGA 297
                        ************************************************************

S14/15A_klon3           AGAACTAGGAAACGGAAACAGAGTGGTCAGTGCCCAGCCCGGCCTGGGAAGCAACGCATG 360
S14/15A_klon4           AGAACTAGGAAACGGAAACAGAGTGGTCAGTGCCCAGCCCGGCCTGGGAAGCAACGCATG 360
CHOP                    AGAACTAGGAAACGGAAACAGAGTGGTCAGTGCCCAGCCCGGCCTGGGAAGCAACGCATG 357
                        ************************************************************

S14/15A_klon3           AAGGAGAAGGAGCAGGAGAACGAGCGGAAAGTGGCACAGCTAGCTGAAGAGAACGAGCGG 420
S14/15A_klon4           AAGGAGAAGGAGCAGGAGAACGAGCGGAAAGTGGCACAGCTAGCTGAAGAGAACGAGCGG 420
CHOP                    AAGGAGAAGGAGCAGGAGAACGAGCGGAAAGTGGCACAGCTAGCTGAAGAGAACGAGCGG 417
                        ************************************************************

S14/15A_klon3           CTCAAGCAGGAAATCGAGCGCCTGACCAGGGAGGTGGAGACCACACGGCGGGCTCTGATC 480
S14/15A_klon4           CTCAAGCAGGAAATCGAGCGCCTGACCAGGGAGGTGGAGACCACACGGCGGGCTCTGATC 480
CHOP                    CTCAAGCAGGAAATCGAGCGCCTGACCAGGGAGGTGGAGACCACACGGCGGGCTCTGATC 477
                        ************************************************************

S14/15A_klon3           GACCGCATGGTCAGCCTGCACCAAGCAGCGGCCGCTTACCCATACGATGTTCCAGATTAC 540
S14/15A_klon4           GACCGCATGGTCAGCCTGCACCAAGCAGCGGCCGCTTACCCATACGATGTTCCAGATTAC 540
CHOP                    GACCGCATGGTCAGCCTGCACCAAGCA--------------------TGA---------- 507
                        ***************************                   **:
```

CLUSTAL 2.1 multiple sequence alignment – CHOP-HA[S30/31A]

```
CHOP                    -----------------------------------------ATGGCAGCTGAGTCCCTGC 19
S30/31A_klonA           CCGGGGGGGGCAGCGTTTACGGGCCCTCTAGACTCGAGACCATGGCAGCTGAGTCCCTGC 60
                                                                  ******************

CHOP                    CTTTCACCTTGGAGACGGTGTCCAGCTGGGAGCTGGAAGCCTGGTATGAGGATCTGCAGG 79
S30/31A_klonA           CTTTCACCTTGGAGACGGTGTCCAGCTGGGAGCTGGAAGCCTGGTATGAGGATCTGCAGG 120
                        ************************************************************

CHOP                    AGGTCCTGTCCTCAGATGAAATTGGGGGCACCTATATCTCATCCCCAGGAAACGAAGAGG 139
S30/31A_klonA           AGGTCCTGGCCGCAGATGAAATTGGGGGCACCTATATCTCATCCCCAGGAAACGAAGAGG 180
                        ******** ** **************************************************

CHOP                    AAGAATCAAAAACCTTCACTACTCTTGACCCTGCGTCCCTAGCTTGGCTGACAGAGGAGC 199
S30/31A_klonA           AAGAATCAAAAACCTTCACTACTCTTGACCCTGCGTCCCTAGCTTGGCTGACAGAGGAGC 240
                        ************************************************************


CHOP                    CAGGGCCAACAGAGGTCACACGCACATCCCAAAGCCCTCGCTCTCCAGATTCCAGTCAGA 259
S30/31A_klonA           CAGGGCCAACAGAGGTCACACGCACATCCCAAAGCCCTCGCTCTCCAGATTCCAGTCAGA 300
                        ************************************************************

CHOP                    GTTCTATGGCCCAGGAGGAAGAGGAGGAAGAGCAAGGAAGAACTAGGAAACGGAAACAGA 319
S30/31A_klonA           GTTCTATGGCCCAGGAGGAAGAGGAGGAAGAGCAAGGAAGAACTAGGAAACGGAAACAGA 360
                        ************************************************************
```

```
CHOP                    GTGGTCAGTGCCCAGCCCGGCCTGGGAAGCAACGCATGAAGGAGAAGGAGCAGGAGAACG 379
S30/31A_klonA           GTGGTCAGTGCCCAGCCCGGCCTGGGAAGCAACGCATGAAGGAGAAGGAGCAGGAGAACG 420
                        ************************************************************

CHOP                    AGCGGAAAGTGGCACAGCTAGCTGAAGAGAACGAGCGGCTCAAGCAGGAAATCGAGCGCC 439
S30/31A_klonA           AGCGGAAAGTGGCACAGCTAGCTGAAGAGAACGAGCGGCTCAAGCAGGAAATCGAGCGCC 480
                        ************************************************************

CHOP                    TGACCAGGGAGGTGGAGACCACACGGCGGGCTCTGATCGACCGCATGGTCAGCCTGCACC 499
S30/31A_klonA           TGACCAGGGAGGTGGAGACCACACGGCGGGCTCTGATCGACCGCATGGTCAGCCTGCACC 540
                        ************************************************************

CHOP                    AAGCA--------------------TGA--------------------------------- 507
S30/31A_klonA           AAGCAGCGGCCGCTTACCCATACGATGTTCCAGATTACGCTTAGGGATCCGAGCTCGGTA 600
                        *****                   **:
```

CLUSTAL 2.1 multiple sequence alignment – CHOP-HA[S14/15A, S30/31A]

```
CHOP                    --ATGGCAGCTGAGTCCCTGCCTTTCACCTTGGAGACGGTGTCCAGCTGGGAGCTGGAAG 58
S14/15/30/31A_klonB     CCATGGCAGCTGAGTCCCTGCCTTTCACCTTGGAGACGGTGGCCGCCTGGGAGCTGGAAG 60
                          ************************************ **. **************

CHOP                    CCTGGTATGAGGATCTGCAGGAGGTCCTGTCCTCAGATGAAATTGGGGGCACCTATATCT 118
S14/15/30/31A_klonB     CCTGGTATGAGGATCTGCAGGAGGTCCTGGCCGCAGATGAAATTGGGGGCACCTATATCT 120
                        ***************************** ** *************************

CHOP                    CATCCCCAGGAAACGAAGAGGAAGAATCAAAAACCTTCACTACTCTTGACCCTGCGTCCC 178
S14/15/30/31A_klonB     CATCCCCAGGAAACGAAGAGGAAGAATCAAAAACCTTCACTACTCTTGACCCTGCGTCCC 180
                        ************************************************************

CHOP                    TAGCTTGGCTGACAGAGGAGCCAGGGCCAACAGAGGTCACACGCACATCCCAAAGCCCTC 238
S14/15/30/31A_klonB     TAGCTTGGCTGACAGAGGAGCCAGGGCCAACAGAGGTCACACGCACATCCCAAAGCCCTC 240
                        ************************************************************

CHOP                    GCTCTCCAGATTCCAGTCAGAGTTCTATGGCCCAGGAGGAAGAGGAGGAAGAGCAAGGAA 298
S14/15/30/31A_klonB     GCTCTCCAGATTCCAGTCAGAGTTCTATGGCCCAGGAGGAAGAGGAGGAAGAGCAAGGAA 300
                        ************************************************************

CHOP                    GAACTAGGAAACGGAAACAGAGTGGTCAGTGCCCAGCCCGGCCTGGGAAGCAACGCATGA 358
S14/15/30/31A_klonB     GAACTAGGAAACGGAAACAGAGTGGTCAGTGCCCAGCCCGGCCTGGGAAGCAACGCATGA 360
                        ************************************************************

CHOP                    AGGAGAAGGAGCAGGAGAACGAGCGGAAAGTGGCACAGCTAGCTGAAGAGAACGAGCGGC 418
S14/15/30/31A_klonB     AGGAGAAGGAGCAGGAGAACGAGCGGAAAGTGGCACAGCTAGCTGAAGAGAACGAGCGGC 420
                        ************************************************************

CHOP                    TCAAGCAGGAAATCGAGCGCCTGACCAGGGAGGTGGAGACCACACGGCGGGCTCTGATCG 478
S14/15/30/31A_klonB     TCAAGCAGGAAATCGAGCGCCTGACCAGGGAGGTGGAGACCACACGGCGGGCTCTGATCG 480
                        ************************************************************

CHOP                    ACCGCATGGTCAGCCTGCACCAAGCA--------------------TGA----------- 507
S14/15/30/31A_klonB     ACCGCATGGTCAGCCTGCACCAAGCAGCGGCCGCTTACCCATACGATGTTCCAGATTACG 540
                        *************************                   **:
```

CLUSTAL 2.1 multiple sequence alignment – CHOP-HA[S78/81A]

```
CHOP-HA                 ------------------------------GTCTCGAGACCATGGCAGCTGAGTCCCTG 29
S78/81A_klon1           CCCGGGGAGTTGCGTTTTAACGGGCCCTCTAGACTCGAGACCATGGCAGCTGAGTCCCTG 60
                                                 *:**************************

CHOP-HA                 CCTTTCACCTTGGAGACGGTGTCCAGCTGGGAGCTGGAAGCCTGGTATGAGGATCTGCAG 89
S78/81A_klon1           CCTTTCACCTTGGAGACGGTGTCCAGCTGGGAGCTGGAAGCCTGGTATGAGGATCTGCAG 120
                        ************************************************************
CHOP-HA                 GAGGTCCTGTCCTCAGATGAAATTGGGGGCACCTATATCTCATCCCCAGGAAACGAAGAG 149
S78/81A_klon1           GAGGTCCTGTCCTCAGATGAAATTGGGGGCACCTATATCTCATCCCCAGGAAACGAAGAG 180
                        ************************************************************

CHOP-HA                 GAAGAATCAAAAACCTTCACTACTCTTGACCCTGCGTCCCTAGCTTGGCTGACAGAGGAG 209
S78/81A_klon1           GAAGAATCAAAAACCTTCACTACTCTTGACCCTGCGTCCCTAGCTTGGCTGACAGAGGAG 240
                        ************************************************************

CHOP-HA                 CCAGGGCCAACAGAGGTCACACGCACATCCCAAAGCCCTCGCTCTCCAGATTCCAGTCAG 269
S78/81A_klon1           CCAGGGCCAACAGAGGTCACACGCACATCCCAAGCCCCTCGCGCTCCAGATTCCAGTCAG 300
                        *********************************. ******* *****************
```

```
CHOP-HA                 AGTTCTATGGCCCAGGAGGAAGAGGAGGAAGAGCAAGGAAGAACTAGGAAACGGAAACAG 329
S78/81A_klon1           AGTTCTATGGCCCAGGAGGAAGAGGAGGAAGAGCAAGGAAGAACTAGGAAACGGAAACAG 360
                        ************************************************************

CHOP-HA                 AGTGGTCAGTGCCCAGCCCGGCCTGGGAAGCAACGCATGAAGGAGAAGGAGCAGGAGAAC 389
S78/81A_klon1           AGTGGTCAGTGCCCAGCCCGGCCTGGGAAGCAACGCATGAAGGAGAAGGAGCAGGAGAAC 420
                        ************************************************************

CHOP-HA                 GAGCGGAAAGTGGCACAGCTAGCTGAAGAGAACGAGCGGCTCAAGCAGGAAATCGAGCGC 449
S78/81A_klon1           GAGCGGAAAGTGGCACAGCTAGCTGAAGAGAACGAGCGGCTCAAGCAGGAAATCGAGCGC 480
                        ************************************************************

CHOP-HA                 CTGACCAGGGAGGTGGAGACCACACGGCGGGCTCTGATCGACCGCATGGTCAGCCTGCAC 509
S78/81A_klon1           CTGACCAGGGAGGTGGAGACCACACGGCGGGCTCTGATCGACCGCATGGTCAGCCTGCAC 540
                        ************************************************************

CHOP-HA                 CAAGCAGCGGCCGCTTACCCATACGATGTTCCAGATTACGCTTAGGGATCC--ACTAG-- 565
S78/81A_klon1           CAAGCAGCGGCCGCTTACCCATACGATGTTCCAGATTACGCTTAGGGATCCGAGCTCGGT 600
                        ************************************************  .**.*
```

CLUSTAL 2.1 multiple sequence alignment – CHOP-HA[S14/15A, S30/31A, S78/81A] (klon2)

```
CHOP-HA                 ----------------------GTCTCGAGACCATGGCAGCTGAGTCCCTGCCTTTCACC 38
S14/15/30/31/78/81A     GCGTGTGGTTTACGGGCCTCTAGACTCGAGACCATGGCAGCTGAGTCCCTGCCTTTCACC 60
                                             *:***********************************

CHOP-HA                 TTGGAGACGGTGTCCAGCTGGGAGCTGGAAGCCTGGTATGAGGATCTGCAGGAGGTCCTG 98
S14/15/30/31/78/81A     TTGGAGACGGTGGCCGCCTGGGAGCTGGAAGCCTGGTATGAGGATCTGCAGGAGGTCCTG 120
                        ************ **. ******************************************

CHOP-HA                 TCCTCAGATGAAATTGGGGGCACCTATATCTCATCCCCAGGAAACGAAGAGGAAGAATCA 158
S14/15/30/31/78/81A     GCCGCAGATGAAATTGGGGGCACCTATATCTCATCCCCAGGAAACGAAGAGGAAGAATCA 180
                         ** ************************************************************

CHOP-HA                 AAAACCTTCACTACTCTTGACCCTGCGTCCCTAGCTTGGCTGACAGAGGAGCCAGGGCCA 218
S14/15/30/31/78/81A     AAAACCTTCACTACTCTTGACCCTGCGTCCCTAGCTTGGCTGACAGAGGAGCCAGGGCCA 240
                        ************************************************************

CHOP-HA                 ACAGAGGTCACACGCACATCCCAAAGCCCTCGCTCTCCAGATTCCAGTCAGAGTTCTATG 278
S14/15/30/31/78/81A     ACAGAGGTCACACGCACATCCCAAGCCCCTCGCGCTCCAGATTCCAGTCAGAGTTCTATG 300
                        ************************. ******* *************************

CHOP-HA                 GCCCAGGAGGAAGAGGAGGAAGAGCAAGGAAGAACTAGGAAACGGAAACAGAGTGGTCAG 338
S14/15/30/31/78/81A     GCCCAGGAGGAAGAGGAGGAAGAGCAAGGAAGAACTAGGAAACGGAAACAGAGTGGTCAG 360
                        ************************************************************

CHOP-HA                 TGCCCAGCCCGGCCTGGGAAGCAACGCATGAAGGAGAAGGAGCAGGAGAACGAGCGGAAA 398
S14/15/30/31/78/81A     TGCCCAGCCCGGCCTGGGAAGCAACGCATGAAGGAGAAGGAGCAGGAGAACGAGCGGAAA 420
                        ************************************************************

CHOP-HA                 GTGGCACAGCTAGCTGAAGAGAACGAGCGGCTCAAGCAGGAAATCGAGCGCCTGACCAGG 458
S14/15/30/31/78/81A     GTGGCACAGCTAGCTGAAGAGAACGAGCGGCTCAAGCAGGAAATCGAGCGCCTGACCAGG 480
                        ************************************************************

CHOP-HA                 GAGGTGGAGACCACACGGCGGGCTCTGATCGACCGCATGGTCAGCCTGCACCAAGCAGCG 518
S14/15/30/31/78/81A     GAGGTGGAGACCACACGGCGGGCTCTGATCGACCGCATGGTCAGCCTGCACCAAGCAGCG 540
                        ************************************************************

CHOP-HA                 GCCGCTTACCCATACGATGTTCCAGATTACGCTTAGGGATCC--ACTAG----------- 565
S14/15/30/31/78/81A     GCCGCTTACCCATACGATGTTCCAGATTACGCTTAGGGATCCGAGCTCGGTACCAAGCTT 600
                        ****************************************  .**.*
```

LIST OF FIGURES

LIST OF TABLES

ABBREVIATIONS

AARE	amino-acid-regulatory element
Agr2	anterior gradient 2
AP	alkaline phosphatase
ARE	antioxidant response element
ATF	activating transcription factor
Atg16L1	autophagy-related protein 16-1
CAGGS	CMV early enhancer/chicken β-
cC3	cleaved Caspase 3
Ccnd1	Cyclin D1
CD	Crohn's disease
C/EBP	CCAAT/enhancer-binding protein
CFU	colony-forming unit
CHOP	C/EBP homologous protein
C. rodentium	*Citrobacter rodentium*
CKII	casein kinase II
CPEB4	cytoplasmic polyadenlylation element binding protein 4
CRE	cAMP response element
DAI	disease activity index
Ddit3	DNA-damage-inducible transcript
ΔIEC	intestinal epithelial cell-specific deletion
DKK	Dickkopf
DOC	downstream of CHOP
dpi	days post infection
DSS	Dextran Sodium Suphate
E. coli	*Escherichia coli*
eIF2α	eukaryotic initiation factor-2α
ER	endoplasmic reticulum
ERAD	ER-associated degradation
ERSE	ER stress element
g	gram
GADD153	growth arrest- and DNA damage-inducible gene 153
GCN2	general control noonderepressible kinase 2
GO	gene ontology
GRP	glucose-regulating peptide
GWAS	genome wide association study
HM	hypomorphic mutation
HRI	heme-regulated inhibitory kinase
HSF	heat shock factor
HSP	heat-shock protein
IBD	inflammatory bowel diseases
IEC	intestinal epithelial cell
IEC Tg/Tg	intestinal epithelial cell-specific overexpression
IF	immunofluorescence staining
IHC	immunohistochemistry
IRE	inositol requiring enzyme 1
JNK	JUN N-terminal kinase
kDa	kiladalton
LAP	liver activating protein
LAS	Leica Application Suite
Lgr5	Leucine-rich repeat-containing G-protein coupled receptor 5
LIP	liver inhibitory protein
MAP	mitogen activating protein
MAPK	MAP kinase
mg	milligram
mm	millimeter
mt	mitochondria
MUC2	Mucin 2
MW	molecular weight
ORMDL3	ORM 1-like 3
OTCΔ	truncated ornithine
PDI	protein disulfide isomerase
PERK	PKR-like ER kinase
PKR	RNA-activated protein kinase
Reg	regenerating gene
RIDD	regulated IRE1-dependent decay
RIN	RNA integrity number
ROS	reactive oxygen species
S1P	site-1 protease
S2P	site-2 protease
SERINC3	serine incorporator 3
TA	transit-amplifying
TCF	T cell factor
TEER	transepitheleal electrical
TG	transgenic mice
TLR	toll-like receptor
TNBS	2,4,6-trinitrobenzenesulfonic acid
UC	ulcerative colitis
uORF	upstream open reading frames
UPR	unfolded protein response
UPRE	UPR element
UTR	untranslated region
***vil* -Cre**	Villin promoter-driven Cre
w/v	weight/volume
WT	wild-type mice
XBP1	X-box binding protein 1
XBP1s	spliced XBP1
XBP1u	unspliced XBP1
µm	micrometer
-/-	complete knock-out

REFERENCES

1. Meisner LF, Gilbert E, Ris HW, et al. Genetic mechanisms in cancer predisposition: report of a cancer family. Cancer 1979;43:679-89.
2. Kirk RL, Theophilus J, Whitehouse S, et al. Genetic susceptibility to diabetes mellitus: the distribution of properdin factor B (Bf) and glyoxalase (GLO) phenotypes. Diabetes 1979;28:949-51.
3. Hirschhorn JN, Daly MJ. Genome-wide association studies for common diseases and complex traits. Nat Rev Genet 2005;6:95-108.
4. Venter JC, Adams MD, Myers EW, et al. The sequence of the human genome. Science 2001;291:1304-51.
5. Lander ES, Linton LM, Birren B, et al. Initial sequencing and analysis of the human genome. Nature 2001;409:860-921.
6. McLeod HL. Cancer pharmacogenomics: early promise, but concerted effort needed. Science 2013;339:1563-6.
7. McCarthy MI, Hirschhorn JN. Genome-wide association studies: potential next steps on a genetic journey. Hum Mol Genet 2008;17:R156-65.
8. Ramos RG, Olden K. Gene-environment interactions in the development of complex disease phenotypes. Int J Environ Res Public Health 2008;5:4-11.
9. Bernstein CN. Why and where to look in the environment with regard to the etiology of inflammatory bowel disease. Dig Dis 2012;30 Suppl 3:28-32.
10. Kitsios GD, Tangri N, Castaldi PJ, et al. Laboratory mouse models for the human genome-wide associations. PLoS One 2010;5:e13782.
11. Schwartz DA, Freedman JH, Linney EA. Environmental genomics: a key to understanding biology, pathophysiology and disease. Hum Mol Genet 2004;13 Spec No 2:R217-24.
12. Hossain P, Kawar B, El Nahas M. Obesity and diabetes in the developing world--a growing challenge. N Engl J Med 2007;356:213-5.
13. Sartor RB. Mechanisms of disease: pathogenesis of Crohn's disease and ulcerative colitis. Nat Clin Pract Gastroenterol Hepatol 2006;3:390-407.
14. Nugent R. Chronic diseases in developing countries: health and economic burdens. Ann N Y Acad Sci 2008;1136:70-9.
15. Rodgers A, Ezzati M, Vander Hoorn S, et al. Distribution of major health risks: findings from the Global Burden of Disease study. PLoS Med 2004;1:e27.
16. Sands BE, Grabert S. Epidemiology of inflammatory bowel disease and overview of pathogenesis. Med Health R I 2009;92:73-7.
17. Renz H, von Mutius E, Brandtzaeg P, et al. Gene-environment interactions in chronic inflammatory disease. Nat Immunol 2011;12:273-7.
18. Cho JH. The genetics and immunopathogenesis of inflammatory bowel disease. Nat Rev Immunol 2008;8:458-66.
19. Frank DN, St Amand AL, Feldman RA, et al. Molecular-phylogenetic characterization of microbial community imbalances in human inflammatory bowel diseases. Proc Natl Acad Sci U S A 2007;104:13780-5.
20. Marks DJ, Harbord MW, MacAllister R, et al. Defective acute inflammation in Crohn's disease: a clinical investigation. Lancet 2006;367:668-78.
21. Mazmanian SK, Round JL, Kasper DL. A microbial symbiosis factor prevents intestinal inflammatory disease. Nature 2008;453:620-5.
22. Cadwell K. Crohn's disease susceptibility gene interactions, a NOD to the newcomer ATG16L1. Gastroenterology 2010;139:1448-50.
23. Barrett JC, Hansoul S, Nicolae DL, et al. Genome-wide association defines more than 30 distinct susceptibility loci for Crohn's disease. Nat Genet 2008;40:955-62.
24. Consortium UIG, Barrett JC, Lee JC, et al. Genome-wide association study of ulcerative colitis identifies three new susceptibility loci, including the HNF4A region. Nat Genet 2009;41:1330-4.

25. Imielinski M, Baldassano RN, Griffiths A, et al. Common variants at five new loci associated with early-onset inflammatory bowel disease. Nat Genet 2009;41:1335-40.
26. McGovern DP, Gardet A, Torkvist L, et al. Genome-wide association identifies multiple ulcerative colitis susceptibility loci. Nat Genet 2010;42:332-7.
27. Kontoyiannis D, Boulougouris G, Manoloukos M, et al. Genetic dissection of the cellular pathways and signaling mechanisms in modeled tumor necrosis factor-induced Crohn's-like inflammatory bowel disease. J Exp Med 2002;196:1563-74.
28. Kaser A, Lee AH, Franke A, et al. XBP1 links ER stress to intestinal inflammation and confers genetic risk for human inflammatory bowel disease. Cell 2008;134:743-56.
29. Kuhn R, Lohler J, Rennick D, et al. Interleukin-10-deficient mice develop chronic enterocolitis. Cell 1993;75:263-74.
30. Maeda S, Hsu LC, Liu H, et al. Nod2 mutation in Crohn's disease potentiates NF-kappaB activity and IL-1beta processing. Science 2005;307:734-8.
31. Pickert G, Neufert C, Leppkes M, et al. STAT3 links IL-22 signaling in intestinal epithelial cells to mucosal wound healing. J Exp Med 2009;206:1465-72.
32. Muise AM, Walters TD, Glowacka WK, et al. Polymorphisms in E-cadherin (CDH1) result in a mis-localised cytoplasmic protein that is associated with Crohn's disease. Gut 2009;58:1121-7.
33. Jostins L, Ripke S, Weersma RK, et al. Host-microbe interactions have shaped the genetic architecture of inflammatory bowel disease. Nature 2012;491:119-24.
34. Cummings JR, Ahmad T, Geremia A, et al. Contribution of the novel inflammatory bowel disease gene IL23R to disease susceptibility and phenotype. Inflamm Bowel Dis 2007;13:1063-8.
35. Cella M, Fuchs A, Vermi W, et al. A human natural killer cell subset provides an innate source of IL-22 for mucosal immunity. Nature 2009;457:722-5.
36. Khor B, Gardet A, Xavier RJ. Genetics and pathogenesis of inflammatory bowel disease. Nature 2011;474:307-17.
37. Monteleone G, Fina D, Caruso R, et al. New mediators of immunity and inflammation in inflammatory bowel disease. Curr Opin Gastroenterol 2006;22:361-4.
38. Gunther C, Martini E, Wittkopf N, et al. Caspase-8 regulates TNF-alpha-induced epithelial necroptosis and terminal ileitis. Nature 2011;477:335-9.
39. Deuring JJ, Fuhler GM, Konstantinov SR, et al. Genomic ATG16L1 risk allele-restricted Paneth cell ER stress in quiescent Crohn's disease. Gut 2013.
40. Rath E, Berger E, Messlik A, et al. Induction of dsRNA-activated protein kinase links mitochondrial unfolded protein response to the pathogenesis of intestinal inflammation. Gut 2012;61:1269-78.
41. Fritz T, Niederreiter L, Adolph T, et al. Crohn's disease: NOD2, autophagy and ER stress converge. Gut 2011;60:1580-8.
42. Heijmans J, van Lidth de Jeude JF, Koo BK, et al. ER stress causes rapid loss of intestinal epithelial stemness through activation of the unfolded protein response. Cell Rep 2013;3:1128-39.
43. Clevers H. The intestinal crypt, a prototype stem cell compartment. Cell 2013;154:274-84.
44. Fulda S, Gorman AM, Hori O, et al. Cellular stress responses: cell survival and cell death. Int J Cell Biol 2010;2010:214074.
45. Hetz C. The unfolded protein response: controlling cell fate decisions under ER stress and beyond. Nat Rev Mol Cell Biol 2012;13:89-102.
46. Zdralevic M, Guaragnella N, Antonacci L, et al. Yeast as a tool to study signaling pathways in mitochondrial stress response and cytoprotection. ScientificWorldJournal 2012;2012:912147.
47. Bukau B, Weissman J, Horwich A. Molecular chaperones and protein quality control. Cell 2006;125:443-51.

48. Santoro MG. Heat shock factors and the control of the stress response. Biochem Pharmacol 2000;59:55-63.
49. Braakman I, Bulleid NJ. Protein folding and modification in the mammalian endoplasmic reticulum. Annu Rev Biochem 2011;80:71-99.
50. Hartl FU, Hayer-Hartl M. Molecular chaperones in the cytosol: from nascent chain to folded protein. Science 2002;295:1852-8.
51. Ron D, Walter P. Signal integration in the endoplasmic reticulum unfolded protein response. Nat Rev Mol Cell Biol 2007;8:519-29.
52. Schroder M, Kaufman RJ. The mammalian unfolded protein response. Annu Rev Biochem 2005;74:739-89.
53. Lee AS. Mammalian stress response: induction of the glucose-regulated protein family. Curr Opin Cell Biol 1992;4:267-73.
54. Zinszner H, Kuroda M, Wang X, et al. CHOP is implicated in programmed cell death in response to impaired function of the endoplasmic reticulum. Genes Dev 1998;12:982-95.
55. Tabas I, Ron D. Integrating the mechanisms of apoptosis induced by endoplasmic reticulum stress. Nat Cell Biol 2011;13:184-90.
56. Schulzke JD, Ploeger S, Amasheh M, et al. Epithelial tight junctions in intestinal inflammation. Ann N Y Acad Sci 2009;1165:294-300.
57. Eizirik DL, Cardozo AK, Cnop M. The role for endoplasmic reticulum stress in diabetes mellitus. Endocr Rev 2008;29:42-61.
58. Wang S, Kaufman RJ. The impact of the unfolded protein response on human disease. J Cell Biol 2012;197:857-67.
59. Bobrovnikova-Marjon E, Grigoriadou C, Pytel D, et al. PERK promotes cancer cell proliferation and tumor growth by limiting oxidative DNA damage. Oncogene 2010;29:3881-95.
60. Oyadomari S, Koizumi A, Takeda K, et al. Targeted disruption of the Chop gene delays endoplasmic reticulum stress-mediated diabetes. J Clin Invest 2002;109:525-32.
61. Ho YS, Yang X, Lau JC, et al. Endoplasmic reticulum stress induces tau pathology and forms a vicious cycle: implication in Alzheimer's disease pathogenesis. J Alzheimers Dis 2012;28:839-54.
62. Bossolasco M, Veillette F, Bertrand R, et al. Human TDE1, a TDE1/TMS family member, inhibits apoptosis in vitro and stimulates in vivo tumorigenesis. Oncogene 2006;25:4549-58.
63. Cantero-Recasens G, Fandos C, Rubio-Moscardo F, et al. The asthma-associated ORMDL3 gene product regulates endoplasmic reticulum-mediated calcium signaling and cellular stress. Hum Mol Genet 2010;19:111-21.
64. Sidrauski C, Walter P. The transmembrane kinase Ire1p is a site-specific endonuclease that initiates mRNA splicing in the unfolded protein response. Cell 1997;90:1031-9.
65. Ortiz-Zapater E, Pineda D, Martinez-Bosch N, et al. Key contribution of CPEB4-mediated translational control to cancer progression. Nat Med 2012;18:83-90.
66. Aoki S, Su Q, Li H, et al. Identification of an axotomy-induced glycosylated protein, AIGP1, possibly involved in cell death triggered by endoplasmic reticulum-Golgi stress. J Neurosci 2002;22:10751-60.
67. Goodall JC, Wu C, Zhang Y, et al. Endoplasmic reticulum stress-induced transcription factor, CHOP, is crucial for dendritic cell IL-23 expression. Proc Natl Acad Sci U S A 2010;107:17698-703.
68. Heazlewood CK, Cook MC, Eri R, et al. Aberrant mucin assembly in mice causes endoplasmic reticulum stress and spontaneous inflammation resembling ulcerative colitis. PLoS Med 2008;5:e54.
69. Zheng W, Rosenstiel P, Huse K, et al. Evaluation of AGR2 and AGR3 as candidate genes for inflammatory bowel disease. Genes Immun 2006;7:11-8.

70. Hampe J, Franke A, Rosenstiel P, et al. A genome-wide association scan of nonsynonymous SNPs identifies a susceptibility variant for Crohn disease in ATG16L1. Nat Genet 2007;39:207-11.
71. Eri RD, Adams RJ, Tran TV, et al. An intestinal epithelial defect conferring ER stress results in inflammation involving both innate and adaptive immunity. Mucosal Immunol 2011;4:354-64.
72. Hasnain SZ, Tauro S, Das I, et al. IL-10 promotes production of intestinal mucus by suppressing protein misfolding and endoplasmic reticulum stress in goblet cells. Gastroenterology 2013;144:357-368 e9.
73. Zhao F, Edwards R, Dizon D, et al. Disruption of Paneth and goblet cell homeostasis and increased endoplasmic reticulum stress in Agr2-/- mice. Dev Biol 2010;338:270-9.
74. Cadwell K, Liu JY, Brown SL, et al. A key role for autophagy and the autophagy gene Atg16l1 in mouse and human intestinal Paneth cells. Nature 2008;456:259-63.
75. Cadwell K, Patel KK, Komatsu M, et al. A common role for Atg16L1, Atg5 and Atg7 in small intestinal Paneth cells and Crohn disease. Autophagy 2009;5:250-2.
76. Haynes CM, Petrova K, Benedetti C, et al. ClpP mediates activation of a mitochondrial unfolded protein response in C. elegans. Dev Cell 2007;13:467-80.
77. Ostermann J, Horwich AL, Neupert W, et al. Protein folding in mitochondria requires complex formation with hsp60 and ATP hydrolysis. Nature 1989;341:125-30.
78. Horibe T, Hoogenraad NJ. The chop gene contains an element for the positive regulation of the mitochondrial unfolded protein response. PLoS One 2007;2:e835.
79. Aldridge JE, Horibe T, Hoogenraad NJ. Discovery of genes activated by the mitochondrial unfolded protein response (mtUPR) and cognate promoter elements. PLoS One 2007;2:e874.
80. Marciniak SJ, Yun CY, Oyadomari S, et al. CHOP induces death by promoting protein synthesis and oxidation in the stressed endoplasmic reticulum. Genes Dev 2004;18:3066-77.
81. Ron D, Habener JF. CHOP, a novel developmentally regulated nuclear protein that dimerizes with transcription factors C/EBP and LAP and functions as a dominant-negative inhibitor of gene transcription. Genes Dev 1992;6:439-53.
82. Price BD, Calderwood SK. Gadd45 and Gadd153 messenger RNA levels are increased during hypoxia and after exposure of cells to agents which elevate the levels of the glucose-regulated proteins. Cancer Res 1992;52:3814-7.
83. Carlson SG, Fawcett TW, Bartlett JD, et al. Regulation of the C/EBP-related gene gadd153 by glucose deprivation. Mol Cell Biol 1993;13:4736-44.
84. Bruhat A, Jousse C, Wang XZ, et al. Amino acid limitation induces expression of CHOP, a CCAAT/enhancer binding protein-related gene, at both transcriptional and post-transcriptional levels. J Biol Chem 1997;272:17588-93.
85. Wang XZ, Lawson B, Brewer JW, et al. Signals from the stressed endoplasmic reticulum induce C/EBP-homologous protein (CHOP/GADD153). Mol Cell Biol 1996;16:4273-80.
86. Oyadomari S, Mori M. Roles of CHOP/GADD153 in endoplasmic reticulum stress. Cell Death Differ 2004;11:381-9.
87. Hubbard SC, Ivatt RJ. Synthesis and processing of asparagine-linked oligosaccharides. Annu Rev Biochem 1981;50:555-83.
88. Kornfeld R, Kornfeld S. Assembly of asparagine-linked oligosaccharides. Annu Rev Biochem 1985;54:631-64.
89. Trombetta ES, Parodi AJ. Quality control and protein folding in the secretory pathway. Annu Rev Cell Dev Biol 2003;19:649-76.
90. Calfon M, Zeng H, Urano F, et al. IRE1 couples endoplasmic reticulum load to secretory capacity by processing the XBP-1 mRNA. Nature 2002;415:92-6.
91. Reimold AM, Iwakoshi NN, Manis J, et al. Plasma cell differentiation requires the transcription factor XBP-1. Nature 2001;412:300-7.

92. Dimcheff DE, Askovic S, Baker AH, et al. Endoplasmic reticulum stress is a determinant of retrovirus-induced spongiform neurodegeneration. J Virol 2003;77:12617-29.
93. Jelitto-Van Dooren EP, Vidal S, Denecke J. Anticipating endoplasmic reticulum stress. A novel early response before pathogenesis-related gene induction. Plant Cell 1999;11:1935-44.
94. Han D, Lerner AG, Vande Walle L, et al. IRE1alpha kinase activation modes control alternate endoribonuclease outputs to determine divergent cell fates. Cell 2009;138:562-75.
95. Harding HP, Zhang Y, Ron D. Protein translation and folding are coupled by an endoplasmic-reticulum-resident kinase. Nature 1999;397:271-4.
96. Harding HP, Zhang Y, Bertolotti A, et al. Perk is essential for translational regulation and cell survival during the unfolded protein response. Mol Cell 2000;5:897-904.
97. Haze K, Yoshida H, Yanagi H, et al. Mammalian transcription factor ATF6 is synthesized as a transmembrane protein and activated by proteolysis in response to endoplasmic reticulum stress. Mol Biol Cell 1999;10:3787-99.
98. Bertolotti A, Zhang Y, Hendershot LM, et al. Dynamic interaction of BiP and ER stress transducers in the unfolded-protein response. Nat Cell Biol 2000;2:326-32.
99. Chen X, Shen J, Prywes R. The luminal domain of ATF6 senses endoplasmic reticulum (ER) stress and causes translocation of ATF6 from the ER to the Golgi. J Biol Chem 2002;277:13045-52.
100. Shen J, Chen X, Hendershot L, et al. ER stress regulation of ATF6 localization by dissociation of BiP/GRP78 binding and unmasking of Golgi localization signals. Dev Cell 2002;3:99-111.
101. Zhou J, Liu CY, Back SH, et al. The crystal structure of human IRE1 luminal domain reveals a conserved dimerization interface required for activation of the unfolded protein response. Proc Natl Acad Sci U S A 2006;103:14343-8.
102. Harding HP, Novoa I, Zhang Y, et al. Regulated translation initiation controls stress-induced gene expression in mammalian cells. Mol Cell 2000;6:1099-108.
103. Hollien J, Weissman JS. Decay of endoplasmic reticulum-localized mRNAs during the unfolded protein response. Science 2006;313:104-7.
104. Hollien J, Lin JH, Li H, et al. Regulated Ire1-dependent decay of messenger RNAs in mammalian cells. J Cell Biol 2009;186:323-31.
105. Kroemer G, Marino G, Levine B. Autophagy and the integrated stress response. Mol Cell 2010;40:280-93.
106. Vembar SS, Brodsky JL. One step at a time: endoplasmic reticulum-associated degradation. Nat Rev Mol Cell Biol 2008;9:944-57.
107. Friedlander R, Jarosch E, Urban J, et al. A regulatory link between ER-associated protein degradation and the unfolded-protein response. Nat Cell Biol 2000;2:379-84.
108. Okada T, Yoshida H, Akazawa R, et al. Distinct roles of activating transcription factor 6 (ATF6) and double-stranded RNA-activated protein kinase-like endoplasmic reticulum kinase (PERK) in transcription during the mammalian unfolded protein response. Biochem J 2002;366:585-94.
109. Wang XZ, Harding HP, Zhang Y, et al. Cloning of mammalian Ire1 reveals diversity in the ER stress responses. EMBO J 1998;17:5708-17.
110. Yamamoto K, Sato T, Matsui T, et al. Transcriptional induction of mammalian ER quality control proteins is mediated by single or combined action of ATF6alpha and XBP1. Dev Cell 2007;13:365-76.
111. Yoshida H, Haze K, Yanagi H, et al. Identification of the cis-acting endoplasmic reticulum stress response element responsible for transcriptional induction of mammalian glucose-regulated proteins. Involvement of basic leucine zipper transcription factors. J Biol Chem 1998;273:33741-9.

112. Kokame K, Kato H, Miyata T. Identification of ERSE-II, a new cis-acting element responsible for the ATF6-dependent mammalian unfolded protein response. J Biol Chem 2001;276:9199-205.
113. Bruhat A, Jousse C, Carraro V, et al. Amino acids control mammalian gene transcription: activating transcription factor 2 is essential for the amino acid responsiveness of the CHOP promoter. Mol Cell Biol 2000;20:7192-204.
114. Liu XM, Peyton KJ, Ensenat D, et al. Endoplasmic reticulum stress stimulates heme oxygenase-1 gene expression in vascular smooth muscle. Role in cell survival. J Biol Chem 2005;280:872-7.
115. Yoneda T, Imaizumi K, Oono K, et al. Activation of caspase-12, an endoplastic reticulum (ER) resident caspase, through tumor necrosis factor receptor-associated factor 2-dependent mechanism in response to the ER stress. J Biol Chem 2001;276:13935-40.
116. Roy B, Lee AS. The mammalian endoplasmic reticulum stress response element consists of an evolutionarily conserved tripartite structure and interacts with a novel stress-inducible complex. Nucleic Acids Res 1999;27:1437-43.
117. Yoshida H, Okada T, Haze K, et al. ATF6 activated by proteolysis binds in the presence of NF-Y (CBF) directly to the cis-acting element responsible for the mammalian unfolded protein response. Mol Cell Biol 2000;20:6755-67.
118. Ubeda M, Habener JF. CHOP gene expression in response to endoplasmic-reticular stress requires NFY interaction with different domains of a conserved DNA-binding element. Nucleic Acids Res 2000;28:4987-97.
119. Scheuner D, Song B, McEwen E, et al. Translational control is required for the unfolded protein response and in vivo glucose homeostasis. Mol Cell 2001;7:1165-76.
120. Cullinan SB, Zhang D, Hannink M, et al. Nrf2 is a direct PERK substrate and effector of PERK-dependent cell survival. Mol Cell Biol 2003;23:7198-209.
121. Connor JH, Weiser DC, Li S, et al. Growth arrest and DNA damage-inducible protein GADD34 assembles a novel signaling complex containing protein phosphatase 1 and inhibitor 1. Mol Cell Biol 2001;21:6841-50.
122. Brush MH, Weiser DC, Shenolikar S. Growth arrest and DNA damage-inducible protein GADD34 targets protein phosphatase 1 alpha to the endoplasmic reticulum and promotes dephosphorylation of the alpha subunit of eukaryotic translation initiation factor 2. Mol Cell Biol 2003;23:1292-303.
123. Cullinan SB, Diehl JA. Coordination of ER and oxidative stress signaling: the PERK/Nrf2 signaling pathway. Int J Biochem Cell Biol 2006;38:317-32.
124. Vattem KM, Wek RC. Reinitiation involving upstream ORFs regulates ATF4 mRNA translation in mammalian cells. Proc Natl Acad Sci U S A 2004;101:11269-74.
125. Asada R, Kanemoto S, Kondo S, et al. The signalling from endoplasmic reticulum-resident bZIP transcription factors involved in diverse cellular physiology. J Biochem 2011;149:507-18.
126. Haze K, Okada T, Yoshida H, et al. Identification of the G13 (cAMP-response-element-binding protein-related protein) gene product related to activating transcription factor 6 as a transcriptional activator of the mammalian unfolded protein response. Biochem J 2001;355:19-28.
127. Belmont PJ, Chen WJ, San Pedro MN, et al. Roles for endoplasmic reticulum-associated degradation and the novel endoplasmic reticulum stress response gene Derlin-3 in the ischemic heart. Circ Res 2010;106:307-16.
128. Bertolotti A, Wang X, Novoa I, et al. Increased sensitivity to dextran sodium sulfate colitis in IRE1beta-deficient mice. J Clin Invest 2001;107:585-93.
129. Tirasophon W, Welihinda AA, Kaufman RJ. A stress response pathway from the endoplasmic reticulum to the nucleus requires a novel bifunctional protein kinase/endoribonuclease (Ire1p) in mammalian cells. Genes Dev 1998;12:1812-24.
130. Tsuru A, Fujimoto N, Takahashi S, et al. Negative feedback by IRE1beta optimizes mucin production in goblet cells. Proc Natl Acad Sci U S A 2013;110:2864-9.

131. Martino MB, Jones L, Brighton B, et al. The ER stress transducer IRE1beta is required for airway epithelial mucin production. Mucosal Immunol 2013;6:639-54.
132. Shamu CE, Walter P. Oligomerization and phosphorylation of the Ire1p kinase during intracellular signaling from the endoplasmic reticulum to the nucleus. EMBO J 1996;15:3028-39.
133. Liu CY, Wong HN, Schauerte JA, et al. The protein kinase/endoribonuclease IRE1alpha that signals the unfolded protein response has a luminal N-terminal ligand-independent dimerization domain. J Biol Chem 2002;277:18346-56.
134. Yoshida H, Matsui T, Hosokawa N, et al. A time-dependent phase shift in the mammalian unfolded protein response. Dev Cell 2003;4:265-71.
135. Travers KJ, Patil CK, Wodicka L, et al. Functional and genomic analyses reveal an essential coordination between the unfolded protein response and ER-associated degradation. Cell 2000;101:249-58.
136. Lee AH, Iwakoshi NN, Glimcher LH. XBP-1 regulates a subset of endoplasmic reticulum resident chaperone genes in the unfolded protein response. Mol Cell Biol 2003;23:7448-59.
137. Sriburi R, Jackowski S, Mori K, et al. XBP1: a link between the unfolded protein response, lipid biosynthesis, and biogenesis of the endoplasmic reticulum. J Cell Biol 2004;167:35-41.
138. Garcia MA, Gil J, Ventoso I, et al. Impact of protein kinase PKR in cell biology: from antiviral to antiproliferative action. Microbiol Mol Biol Rev 2006;70:1032-60.
139. Harding HP, Zhang Y, Zeng H, et al. An integrated stress response regulates amino acid metabolism and resistance to oxidative stress. Mol Cell 2003;11:619-33.
140. Lu L, Han AP, Chen JJ. Translation initiation control by heme-regulated eukaryotic initiation factor 2alpha kinase in erythroid cells under cytoplasmic stresses. Mol Cell Biol 2001;21:7971-80.
141. de Haro C, Mendez R, Santoyo J. The eIF-2alpha kinases and the control of protein synthesis. FASEB J 1996;10:1378-87.
142. Lee ES, Yoon CH, Kim YS, et al. The double-strand RNA-dependent protein kinase PKR plays a significant role in a sustained ER stress-induced apoptosis. FEBS Lett 2007;581:4325-32.
143. Martinus RD, Garth GP, Webster TL, et al. Selective induction of mitochondrial chaperones in response to loss of the mitochondrial genome. Eur J Biochem 1996;240:98-103.
144. Zhao Q, Wang J, Levichkin IV, et al. A mitochondrial specific stress response in mammalian cells. EMBO J 2002;21:4411-9.
145. Lekstrom-Himes J, Xanthopoulos KG. Biological role of the CCAAT/enhancer-binding protein family of transcription factors. J Biol Chem 1998;273:28545-8.
146. Ubeda M, Wang XZ, Zinszner H, et al. Stress-induced binding of the transcriptional factor CHOP to a novel DNA control element. Mol Cell Biol 1996;16:1479-89.
147. Chitnis NS, Pytel D, Bobrovnikova-Marjon E, et al. miR-211 is a prosurvival microRNA that regulates chop expression in a PERK-dependent manner. Mol Cell 2012;48:353-64.
148. Ubeda M, Schmitt-Ney M, Ferrer J, et al. CHOP/GADD153 and methionyl-tRNA synthetase (MetRS) genes overlap in a conserved region that controls mRNA stability. Biochem Biophys Res Commun 1999;262:31-8.
149. Jousse C, Bruhat A, Carraro V, et al. Inhibition of CHOP translation by a peptide encoded by an open reading frame localized in the chop 5'UTR. Nucleic Acids Res 2001;29:4341-51.
150. Ubeda M, Habener JF. CHOP transcription factor phosphorylation by casein kinase 2 inhibits transcriptional activation. J Biol Chem 2003;278:40514-20.
151. Wang XZ, Ron D. Stress-induced phosphorylation and activation of the transcription factor CHOP (GADD153) by p38 MAP Kinase. Science 1996;272:1347-9.

152. Hattori T, Ohoka N, Inoue Y, et al. C/EBP family transcription factors are degraded by the proteasome but stabilized by forming dimer. Oncogene 2003;22:1273-80.
153. Ohoka N, Hattori T, Kitagawa M, et al. Critical and functional regulation of CHOP (C/EBP homologous protein) through the N-terminal portion. J Biol Chem 2007;282:35687-94.
154. Zimmermann J, Erdmann D, Lalande I, et al. Proteasome inhibitor induced gene expression profiles reveal overexpression of transcriptional regulators ATF3, GADD153 and MAD1. Oncogene 2000;19:2913-20.
155. Chen BP, Wolfgang CD, Hai T. Analysis of ATF3, a transcription factor induced by physiological stresses and modulated by gadd153/Chop10. Mol Cell Biol 1996;16:1157-68.
156. Chiribau CB, Gaccioli F, Huang CC, et al. Molecular symbiosis of CHOP and C/EBP beta isoform LIP contributes to endoplasmic reticulum stress-induced apoptosis. Mol Cell Biol 2010;30:3722-31.
157. Su N, Kilberg MS. C/EBP homology protein (CHOP) interacts with activating transcription factor 4 (ATF4) and negatively regulates the stress-dependent induction of the asparagine synthetase gene. J Biol Chem 2008;283:35106-17.
158. Fornace AJ, Jr., Nebert DW, Hollander MC, et al. Mammalian genes coordinately regulated by growth arrest signals and DNA-damaging agents. Mol Cell Biol 1989;9:4196-203.
159. Luethy JD, Fargnoli J, Park JS, et al. Isolation and characterization of the hamster gadd153 gene. Activation of promoter activity by agents that damage DNA. J Biol Chem 1990;265:16521-6.
160. Barone MV, Crozat A, Tabaee A, et al. CHOP (GADD153) and its oncogenic variant, TLS-CHOP, have opposing effects on the induction of G1/S arrest. Genes Dev 1994;8:453-64.
161. Prasanthi JR, Larson T, Schommer J, et al. Silencing GADD153/CHOP gene expression protects against Alzheimer's disease-like pathology induced by 27-hydroxycholesterol in rabbit hippocampus. PLoS One 2011;6:e26420.
162. Kumar R, Azam S, Sullivan JM, et al. Brain ischemia and reperfusion activates the eukaryotic initiation factor 2alpha kinase, PERK. J Neurochem 2001;77:1418-21.
163. Kumar R, Krause GS, Yoshida H, et al. Dysfunction of the unfolded protein response during global brain ischemia and reperfusion. J Cereb Blood Flow Metab 2003;23:462-71.
164. Treton X, Pedruzzi E, Cazals-Hatem D, et al. Altered endoplasmic reticulum stress affects translation in inactive colon tissue from patients with ulcerative colitis. Gastroenterology 2011;141:1024-35.
165. Bogaert S, De Vos M, Olievier K, et al. Involvement of endoplasmic reticulum stress in inflammatory bowel disease: a different implication for colonic and ileal disease? PLoS One 2011;6:e25589.
166. Namba T, Tanaka K, Ito Y, et al. Positive role of CCAAT/enhancer-binding protein homologous protein, a transcription factor involved in the endoplasmic reticulum stress response in the development of colitis. Am J Pathol 2009;174:1786-98.
167. Lozon TI, Eastman AJ, Matute-Bello G, et al. PKR-dependent CHOP induction limits hyperoxia-induced lung injury. Am J Physiol Lung Cell Mol Physiol 2011;300:L422-9.
168. Jauhiainen A, Thomsen C, Strombom L, et al. Distinct cytoplasmic and nuclear functions of the stress induced protein DDIT3/CHOP/GADD153. PLoS One 2012;7:e33208.
169. Arai N, Mitomi H, Ohtani Y, et al. Enhanced epithelial cell turnover associated with p53 accumulation and high p21WAF1/CIP1 expression in ulcerative colitis. Mod Pathol 1999;12:604-11.
170. Iwamoto M, Koji T, Makiyama K, et al. Apoptosis of crypt epithelial cells in ulcerative colitis. J Pathol 1996;180:152-9.

171. Maytin EV, Ubeda M, Lin JC, et al. Stress-inducible transcription factor CHOP/gadd153 induces apoptosis in mammalian cells via p38 kinase-dependent and -independent mechanisms. Exp Cell Res 2001;267:193-204.
172. Wang XZ, Kuroda M, Sok J, et al. Identification of novel stress-induced genes downstream of chop. EMBO J 1998;17:3619-30.
173. McCullough KD, Martindale JL, Klotz LO, et al. Gadd153 sensitizes cells to endoplasmic reticulum stress by down-regulating Bcl2 and perturbing the cellular redox state. Mol Cell Biol 2001;21:1249-59.
174. Ishikawa F, Akimoto T, Yamamoto H, et al. Gene expression profiling identifies a role for CHOP during inhibition of the mitochondrial respiratory chain. J Biochem 2009;146:123-32.
175. Ohoka N, Yoshii S, Hattori T, et al. TRB3, a novel ER stress-inducible gene, is induced via ATF4-CHOP pathway and is involved in cell death. EMBO J 2005;24:1243-55.
176. Yamaguchi H, Wang HG. CHOP is involved in endoplasmic reticulum stress-induced apoptosis by enhancing DR5 expression in human carcinoma cells. J Biol Chem 2004;279:45495-502.
177. Cheng EH, Wei MC, Weiler S, et al. BCL-2, BCL-X(L) sequester BH3 domain-only molecules preventing BAX- and BAK-mediated mitochondrial apoptosis. Mol Cell 2001;8:705-11.
178. Puthalakath H, O'Reilly LA, Gunn P, et al. ER stress triggers apoptosis by activating BH3-only protein Bim. Cell 2007;129:1337-49.
179. Tavender TJ, Bulleid NJ. Molecular mechanisms regulating oxidative activity of the Ero1 family in the endoplasmic reticulum. Antioxid Redox Signal 2010;13:1177-87.
180. Li G, Scull C, Ozcan L, et al. NADPH oxidase links endoplasmic reticulum stress, oxidative stress, and PKR activation to induce apoptosis. J Cell Biol 2010;191:1113-25.
181. Brush MH, Shenolikar S. Control of cellular GADD34 levels by the 26S proteasome. Mol Cell Biol 2008;28:6989-7000.
182. Han J, Back SH, Hur J, et al. ER-stress-induced transcriptional regulation increases protein synthesis leading to cell death. Nat Cell Biol 2013;15:481-90.
183. Roucou X, Martinou JC. Conformational change of Bax: a question of life or death. Cell Death Differ 2001;8:875-7.
184. Jiang X, Wang X. Cytochrome C-mediated apoptosis. Annu Rev Biochem 2004;73:87-106.
185. Elmore S. Apoptosis: a review of programmed cell death. Toxicol Pathol 2007;35:495-516.
186. Creamer B, Shorter RG, Bamforth J. The turnover and shedding of epithelial cells. I. The turnover in the gastro-intestinal tract. Gut 1961;2:110-8.
187. van der Flier LG, Clevers H. Stem cells, self-renewal, and differentiation in the intestinal epithelium. Annu Rev Physiol 2009;71:241-60.
188. Barker N, van Es JH, Kuipers J, et al. Identification of stem cells in small intestine and colon by marker gene Lgr5. Nature 2007;449:1003-7.
189. Sato T, van Es JH, Snippert HJ, et al. Paneth cells constitute the niche for Lgr5 stem cells in intestinal crypts. Nature 2011;469:415-8.
190. Munoz J, Stange DE, Schepers AG, et al. The Lgr5 intestinal stem cell signature: robust expression of proposed quiescent '+4' cell markers. EMBO J 2012;31:3079-91.
191. Brewer JW, Diehl JA. PERK mediates cell-cycle exit during the mammalian unfolded protein response. Proc Natl Acad Sci U S A 2000;97:12625-30.
192. Hamanaka RB, Bennett BS, Cullinan SB, et al. PERK and GCN2 contribute to eIF2alpha phosphorylation and cell cycle arrest after activation of the unfolded protein response pathway. Mol Biol Cell 2005;16:5493-501.
193. Brewer JW, Hendershot LM, Sherr CJ, et al. Mammalian unfolded protein response inhibits cyclin D1 translation and cell-cycle progression. Proc Natl Acad Sci U S A 1999;96:8505-10.

194. Horndasch M, Lienkamp S, Springer E, et al. The C/EBP homologous protein CHOP (GADD153) is an inhibitor of Wnt/TCF signals. Oncogene 2006;25:3397-407.
195. Korinek V, Barker N, Moerer P, et al. Depletion of epithelial stem-cell compartments in the small intestine of mice lacking Tcf-4. Nat Genet 1998;19:379-83.
196. Clevers H. Wnt/beta-catenin signaling in development and disease. Cell 2006;127:469-80.
197. Dang CV. c-Myc target genes involved in cell growth, apoptosis, and metabolism. Mol Cell Biol 1999;19:1-11.
198. Fu M, Wang C, Li Z, et al. Minireview: Cyclin D1: normal and abnormal functions. Endocrinology 2004;145:5439-47.
199. Pinto D, Gregorieff A, Begthel H, et al. Canonical Wnt signals are essential for homeostasis of the intestinal epithelium. Genes Dev 2003;17:1709-13.
200. Kuhnert F, Davis CR, Wang HT, et al. Essential requirement for Wnt signaling in proliferation of adult small intestine and colon revealed by adenoviral expression of Dickkopf-1. Proc Natl Acad Sci U S A 2004;101:266-71.
201. Araki Y, Mukaisyo K, Sugihara H, et al. Increased apoptosis and decreased proliferation of colonic epithelium in dextran sulfate sodium-induced colitis in mice. Oncol Rep 2010;24:869-74.
202. Wang J, Duncan D, Shi Z, et al. WEB-based GEne SeT AnaLysis Toolkit (WebGestalt): update 2013. Nucleic Acids Res 2013;41:W77-83.
203. Saeed AI, Bhagabati NK, Braisted JC, et al. TM4 microarray software suite. Methods Enzymol 2006;411:134-93.
204. Whitehead RH, Robinson PS. Establishment of conditionally immortalized epithelial cell lines from the intestinal tissue of adult normal and transgenic mice. Am J Physiol Gastrointest Liver Physiol 2009;296:G455-60.
205. Katakura K, Lee J, Rachmilewitz D, et al. Toll-like receptor 9-induced type I IFN protects mice from experimental colitis. J Clin Invest 2005;115:695-702.
206. el Marjou F, Janssen KP, Chang BH, et al. Tissue-specific and inducible Cre-mediated recombination in the gut epithelium. Genesis 2004;39:186-93.
207. Manta C, Heupel E, Radulovic K, et al. CX(3)CR1(+) macrophages support IL-22 production by innate lymphoid cells during infection with Citrobacter rodentium. Mucosal Immunol 2012.
208. Murthy SN, Cooper HS, Shim H, et al. Treatment of dextran sulfate sodium-induced murine colitis by intracolonic cyclosporin. Dig Dis Sci 1993;38:1722-34.
209. Neurath MF, Wittkopf N, Wlodarski A, et al. Assessment of tumor development and wound healing using endoscopic techniques in mice. Gastroenterology 2010;139:1837-1843 e1.
210. Donnenberg MS, Tacket CO, James SP, et al. Role of the eaeA gene in experimental enteropathogenic Escherichia coli infection. J Clin Invest 1993;92:1412-7.
211. Moon HW, Whipp SC, Argenzio RA, et al. Attaching and effacing activities of rabbit and human enteropathogenic Escherichia coli in pig and rabbit intestines. Infect Immun 1983;41:1340-51.
212. Rothbaum RJ, Partin JC, Saalfield K, et al. An ultrastructural study of enteropathogenic Escherichia coli infection in human infants. Ultrastruct Pathol 1983;4:291-304.
213. van Ampting MT, Loonen LM, Schonewille AJ, et al. Intestinally secreted C-type lectin Reg3b attenuates salmonellosis but not listeriosis in mice. Infect Immun 2012;80:1115-20.
214. Luperchio SA, Schauer DB. Molecular pathogenesis of Citrobacter rodentium and transmissible murine colonic hyperplasia. Microbes Infect 2001;3:333-40.
215. Wiles S, Clare S, Harker J, et al. Organ specificity, colonization and clearance dynamics in vivo following oral challenges with the murine pathogen Citrobacter rodentium. Cell Microbiol 2004;6:963-72.

216. Okayasu I, Hatakeyama S, Yamada M, et al. A novel method in the induction of reliable experimental acute and chronic ulcerative colitis in mice. Gastroenterology 1990;98:694-702.
217. Cooper HS, Murthy SN, Shah RS, et al. Clinicopathologic study of dextran sulfate sodium experimental murine colitis. Lab Invest 1993;69:238-49.
218. Taupin D, Podolsky DK. Trefoil factors: initiators of mucosal healing. Nat Rev Mol Cell Biol 2003;4:721-32.
219. Monaco SE, Angelastro JM, Szabolcs M, et al. The transcription factor ATF5 is widely expressed in carcinomas, and interference with its function selectively kills neoplastic, but not nontransformed, breast cell lines. Int J Cancer 2007;120:1883-90.
220. Nenci A, Becker C, Wullaert A, et al. Epithelial NEMO links innate immunity to chronic intestinal inflammation. Nature 2007;446:557-61.
221. Gunther C, Neumann H, Neurath MF, et al. Apoptosis, necrosis and necroptosis: cell death regulation in the intestinal epithelium. Gut 2013;62:1062-71.
222. Kwok SC, Daskal I. Brefeldin A activates CHOP promoter at the AARE, ERSE and AP-1 elements. Mol Cell Biochem 2008;319:203-8.
223. Hall PA, Levison DA. Review: assessment of cell proliferation in histological material. J Clin Pathol 1990;43:184-92.
224. Gregorieff A, Clevers H. Wnt signaling in the intestinal epithelium: from endoderm to cancer. Genes Dev 2005;19:877-90.
225. Sipos F, Molnar B, Zagoni T, et al. Growth in epithelial cell proliferation and apoptosis correlates specifically to the inflammation activity of inflammatory bowel diseases: ulcerative colitis shows specific p53- and EGFR expression alterations. Dis Colon Rectum 2005;48:775-86.
226. Iizuka M, Konno S. Wound healing of intestinal epithelial cells. World J Gastroenterol 2011;17:2161-71.
227. Miyoshi H, Ajima R, Luo CT, et al. Wnt5a potentiates TGF-beta signaling to promote colonic crypt regeneration after tissue injury. Science 2012;338:108-13.
228. Topol L, Jiang X, Choi H, et al. Wnt-5a inhibits the canonical Wnt pathway by promoting GSK-3-independent beta-catenin degradation. J Cell Biol 2003;162:899-908.
229. Iwata Y, Yoshizaki A, Komura K, et al. CD19, a response regulator of B lymphocytes, regulates wound healing through hyaluronan-induced TLR4 signaling. Am J Pathol 2009;175:649-60.
230. Savage DC, Siegel JE, Snellen JE, et al. Transit time of epithelial cells in the small intestines of germfree mice and ex-germfree mice associated with indigenous microorganisms. Appl Environ Microbiol 1981;42:996-1001.
231. Brown JB, Cheresh P, Goretsky T, et al. Epithelial phosphatidylinositol-3-kinase signaling is required for beta-catenin activation and host defense against Citrobacter rodentium infection. Infect Immun 2011;79:1863-72.
232. Sellin JH, Wang Y, Singh P, et al. beta-Catenin stabilization imparts crypt progenitor phenotype to hyperproliferating colonic epithelia. Exp Cell Res 2009;315:97-109.
233. Song B, Scheuner D, Ron D, et al. Chop deletion reduces oxidative stress, improves beta cell function, and promotes cell survival in multiple mouse models of diabetes. J Clin Invest 2008;118:3378-89.
234. Munkholm P. Review article: the incidence and prevalence of colorectal cancer in inflammatory bowel disease. Aliment Pharmacol Ther 2003;18 Suppl 2:1-5.
235. Park MT, Lee SJ. Cell cycle and cancer. J Biochem Mol Biol 2003;36:60-5.
236. Corvinus FM, Orth C, Moriggl R, et al. Persistent STAT3 activation in colon cancer is associated with enhanced cell proliferation and tumor growth. Neoplasia 2005;7:545-55.
237. Rong R, Montalbano J, Jin W, et al. Oncogenic Ras-mediated downregulation of Gadd153/CHOP is required for Ras-induced cellular transformation. Oncogene 2005;24:4867-72.

238. Singh VK, Pacheco I, Uversky VN, et al. Intrinsically disordered human C/EBP homologous protein regulates biological activity of colon cancer cells during calcium stress. J Mol Biol 2008;380:313-26.
239. Song JH, Park JK, Yoon JW, et al. Genetic alterations of the CHOP gene in gastric cancers. Molecular & Cellular Toxicology 2011;7:1-6.
240. Moriya S, Miyazawa K, Kawaguchi T, et al. Involvement of endoplasmic reticulum stress-mediated CHOP (GADD153) induction in the cytotoxicity of 2-aminophenoxazine-3-one in cancer cells. Int J Oncol 2011;39:981-8.
241. Woo KJ, Lee TJ, Lee SH, et al. Elevated gadd153/chop expression during resveratrol-induced apoptosis in human colon cancer cells. Biochem Pharmacol 2007;73:68-76.
242. Scott DW, Loo G. Curcumin-induced GADD153 gene up-regulation in human colon cancer cells. Carcinogenesis 2004;25:2155-64.

ACKNOWLEDGEMENTS

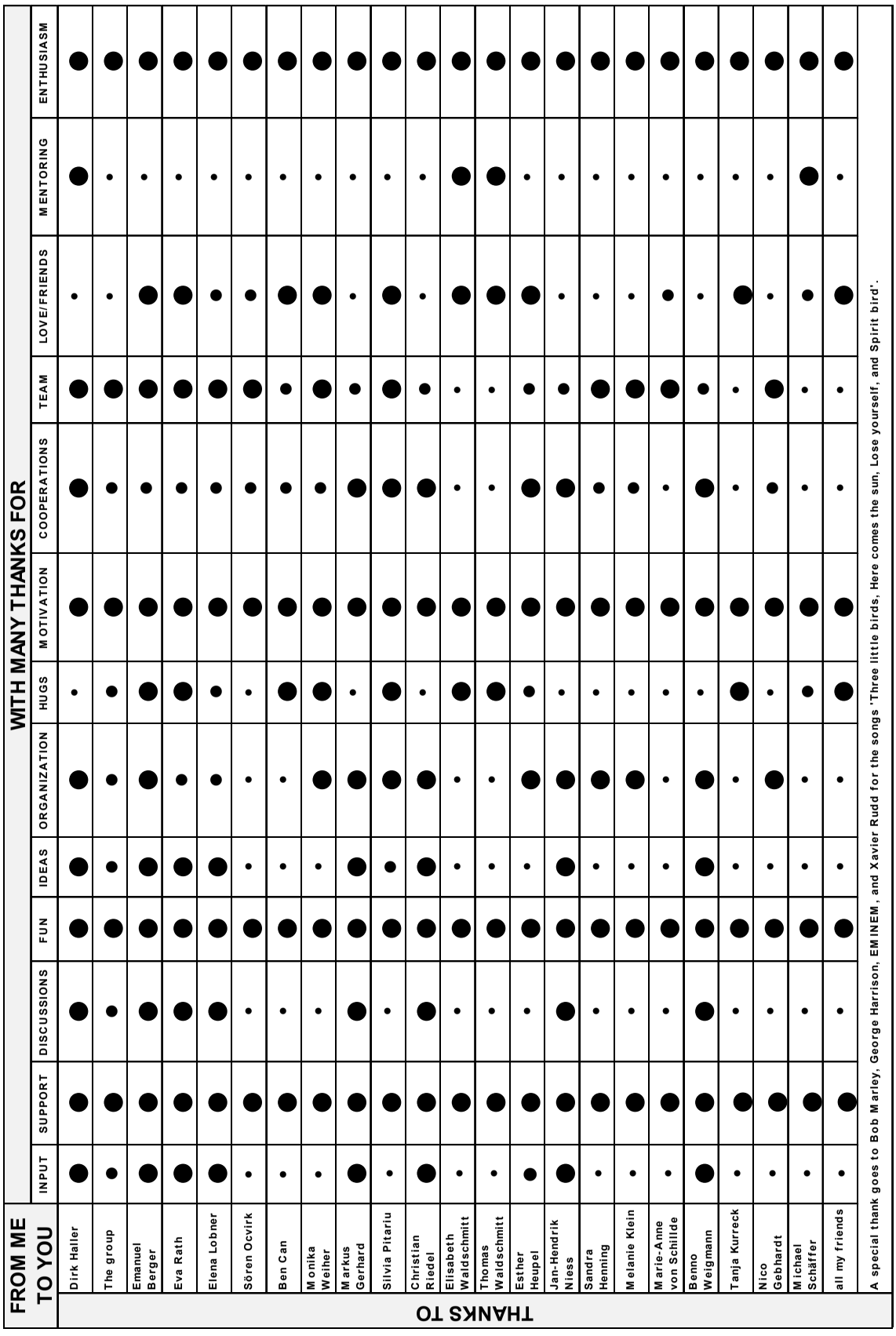

FROM ME TO YOU	WITH MANY THANKS FOR											
THANKS TO	INPUT	SUPPORT	DISCUSSIONS	FUN	IDEAS	ORGANIZATION	HUGS	MOTIVATION	COOPERATIONS	TEAM	LOVE/FRIENDS	MENTORING	ENTHUSIASM
Dirk Haller	●	●	●	●	●	●	•	●	●	●	•	●	●
The group	●	●	●	●	●	●	●	●	●	●	•	•	●
Emanuel Berger	●	●	●	●	●	●	●	●	●	●	●	•	●
Eva Rath	●	●	●	●	●	●	●	●	●	●	●	•	●
Elena Lobner	●	●	●	●	●	●	●	●	●	●	●	•	●
Sören Ocvirk	•	●	•	●	•	•	•	●	●	●	●	•	●
Ben Can	•	●	•	●	•	•	●	●	●	•	●	•	●
Monika Weiher	•	●	•	●	•	●	●	●	●	●	●	•	●
Markus Gerhard	●	●	●	●	●	●	•	●	●	•	•	•	●
Silvia Pitariu	•	●	•	●	●	●	●	●	●	●	●	•	●
Christian Riedel	●	●	●	●	●	●	•	●	●	•	•	•	●
Elisabeth Waldschmitt	•	●	•	●	•	•	●	●	•	•	●	●	●
Thomas Waldschmitt	•	●	•	●	•	•	●	●	•	•	●	●	●
Esther Heupel	●	●	•	●	•	●	●	●	●	•	●	•	●
Jan-Hendrik Niess	●	●	●	●	●	●	•	●	●	•	•	•	●
Sandra Henning	•	●	•	●	•	●	•	●	•	●	•	•	●
Melanie Klein	•	●	•	●	•	●	•	●	•	●	•	•	●
Marie-Anne von Schilde	•	●	•	●	•	•	•	●	•	●	●	•	●
Benno Weigmann	●	●	●	●	●	●	•	●	●	●	•	•	●
Tanja Kurreck	•	●	•	●	•	•	●	●	•	•	●	•	●
Nico Gebhardt	•	●	•	●	•	●	•	●	●	●	•	•	●
Michael Schäffer	•	●	•	●	•	•	●	●	•	•	●	●	●
all my friends	•	●	•	●	•	•	●	●	•	•	●	•	●

A special thank goes to Bob Marley, George Harrison, EMINEM, and Xavier Rudd for the songs 'Three little birds, Here comes the sun, Lose yourself, and Spirit bird'.

CURRICULUM VITAE

Personal data **Nadine Waldschmitt**

M.Sc. Molecular Biotechnology (TUM)

Birth 10-24-1979

Education

12/2009 – 11/2013	**PhD candidate**, Dissertation topic: Tissue-specific overexpression of UPR-related C/EBP homologous protein impairs mucosal repair in *Chop*$^{IEC\ Tg/Tg}$ mice *Chair of Nutrition and Immunology, Technische Universität München (TUM), Prof. Dr. Dirk Haller*
10/2007 – 09/2009	**Master of Science, Molecular Biotechnology (TUM)** passed with high distinction (1.0) Thesis topic: Examination of oxidative stress resistance of lactic acid bacteria in starter cultures *Chair of Technical Microbiology,TUM,* *Prof. Dr. Rudi F. Vogel*
10/2004 – 09/2007	**Bachelor of Science, Molecular Biotechnology (TUM)** passed with merit (1,6) Thesis topic: Role of GM-CSF in bovine uteri during implantation *Chair of Molecular Physiology, TUM, Prof. Dr. H.H. Meyer*
08/2000 – 12/2002	**Biological laboratory technician**, *Paul-Ehrlich Institut, Langen in cooperation with Merck KGaA, Darmstadt* awarded for the best exam in 2002, IHK Offenbach
10/1990 – 07/1999	**Abitur**, *Immanuel-Kant Gymnasium, Tuttlingen*

Work experience

01/2014 – current	**Postdoctoral researcher**, *NODS-Like receptors in infection and immunity, Pasteur Institut Lille, Dr. Mathias Chamaillard*
12/2009 – 11/2013	**PhD candidate**, *Chair of Nutrition and Immunolgy, TUM, Prof. Dr. Dirk Haller*
02/2008 – 10/2008	**Research Associate** (20 hours/week), *Chair of Molecular Physiology, TUM,* *Prof. Dr. H.H. Meyer*
04/2006 – 01/2007	**Lab technician** (20 hours/week), *Chair of Molecular Physiology, TUM, Prof. Dr. H.H. Meyer*
10/2004 – 07/2005	**Student assistant***, Sirenade Pharmaceuticals, Martinsried*
01/2003 – 09/2004	**Lab technician***, SiREEN AG, Martinsried*

Additional education

10/2012 – 03/2013	**Lecture Quality Management (distance study) with QMB (TÜV) certification,** *Internationales Hochschulinstitut Zittau, Prof. Dr. R. Förster*

08/2007 – 12/2007	**Practical training** (4 month), *Chair of Reproductive Physiology, Universidad de Murcia, Spain, Prof. Dr. Pilar Coy,* Fellowship Erasmus Praktikum
2008	**Ausbilder-Eignungsschein** (AEVO)
2003	**Trained assistant for molecular biology, molecular medicine, and gene technology**, *Rheinisches Bildungszentrum e.V. Köln, Institute for Biology and Medicine*

Activities

- voluntary work Lebenshilfe, e.V., Freising (2009-2010)
- participation in E-Mentoring-Program CyberMentor for girls and women with scientific interests, University of Regensburg (2010-2012)

Freising, 2014

PUBLICATIONS AND PRESENTATIONS

Peer-reviewed original manuscripts

Waldschmitt N, Berger E, Rath E, Sartor RB, Weigmann B, Heikenwälder M, Gerhard M, Janssen KP, Haller D. *C/EBP homologous protein inhibits tissue repair in response to gut injury and is inversely regulated with chronic inflammation.* MUCOSAL IMMUNOLOGY (2014) 7 (6): 1452-1466

Mapesa JO, Waldschmitt N, Schmoeller I, Blume C, Hofmann T, Mahungu S, Clavel T, Haller D. *Catechols in caffeic acid phenethyl ester are essential for inhibition of TNF-mediated IP-10 expression through NF-κB-dependent but HO-1-and p38-independent mechanisms in mouse intestinal epithelial cells.* MOLECULAR NUTRITION & FOOD RESEARCH (2011) Volume: 55 Issue: 12 Pages: 1850-1861

Ulbrich SE, Frohlich T, Schulke K, Englberger E, Waldschmitt N, Arnold GJ, Reichenbach HD, Reichenbach M, Wolf E, Meyer HHD, Bauersachs S. *Evidence for Estrogen-Dependent Uterine Serpin (SERPINA14) Expression During Estrus in the Bovine Endometrial Glandular Epithelium and Lumen.* BIOLOGY OF REPRODUCTION (2009) Volume: 81 Issue: 4

Published abstacts

Waldschmitt N, Rath E, Berger E, Haller D. *Expression of C/EBP Homologous Protein in Intestinal Epithelial Cells is Not Associated With the Development of Chronic Inflammation: A Transgenic Approach.* Gastroenterology (2012) Volume: 142 Issue 5, Supplement 1 Page S-124

Schulke K, Groebner AE, Waldschmitt N, Ulbrich SE, Meyer HH. *Increased fibroblast growth factor 2 protein in the bovine endometrium coincides with beginning trophoblast elongation during preimplantation development.* REPRODUCTION IN DOMESTIC ANIMALS (2009) Volume: 44, Pages 33-33

Grullon L, Saavedra MD, Waldschmitt N, Coy P. *Effect of Plasminogen on Zona Pellucida Resistance to Proteolysis and In Vitro Fertilization Results in Pig.* REPRODUCTION IN DOMESTIC ANIMALS (2008) Volume: 43, Supplement: 5 Pages 80-80

Oral presentations

Waldschmitt N, Berger E, Rath E, Weigmann B, Janssen K-P, Haller D. *Tissue-specific overexpression of UPR-related C/EBP homologous protein impairs mucosal repair in Chop$^{IEC\ Tg/Tg}$ mice.* 50. Wissenschaftlicher Kongress der Deutschen Gesellschaft für Ernährung (German Nutrition Society), March 20-22, 2013, Bonn, Germany

Waldschmitt N, Rath E, Berger E, Haller D. *Association of C/EBP homologous protein in intestinal epithelial cells with the development of chronic inflammation: a transgenic approach.* 5th Seeon Conference (German Society for Hygiene and Microbiology), June 15-17, 2012, Kloster Seeon, Germany

Waldschmitt N, Rath E, Berger E, Haller D.*Expression of C/EBP Homologous Protein in Intestinal Epithelial Cells is Not Associated With the Development of Chronic Inflammation: A Transgenic Approach.* Digestive Disease Week, May 19-22, 2012, San Diego, US

Poster presentations

Waldschmitt N, Berger E, Rath E, Sartor RB, Weigmann B, Gerhard M, Janssen K-P, Haller D. *Tissue-specific overexpression of UPR-related C/EBP homologous protein impairs mucosal tissue repair.* 21st United European Gastroenterology Week, 12-16 October 2013, Berlin, Germany (Poster of Excellence)

Waldschmitt N, Berger E, Heupel E, Rath E, Boekschoten MV, Riedel CU, Weigmann B, Niess JH, Janssen K-P, Haller D. *Tissue-specific overexpression of UPR-related C/EBP homologous protein impairs mucosal tissue repair*. 10th NuGOweek, 9-12 September 2013, Freising-Weihenstephan, Germany

Waldschmitt N, Berger E, Heupel E, Rath E, Boekschoten MV, Riedel CU, Weigmann B, Niess JH, Janssen K-P, Haller D. *Tissue-specific overexpression of UPR-related C/EBP homologous protein impairs mucosal tissue repair*. 16th International Congress of Mucosal Immunology, 17-20 July 2013, Vancouver, Canada

Waldschmitt N, Berger E, Rath E, Haller D. *Association of C/EBP homologous protein in intestinal epithelial cells with the development of chronic inflammation: a transgenic approach.* 50. Wissenschaftlicher Kongress der Deutschen Gesellschaft für Ernährung (German Nutrition Society), March 20-22, 2013, Bonn, Germany

Berger E, Yuan D, Waldschmitt N, Simonavicius N, Janssen K-P, Heikenwälder M, Haller D. *Tissue-specific knock out mouse models reveal a crucial role of mitochondrial HSP60 for maintaining homeostasis in intestinal epithelial cells.* 50. Wissenschaftlicher Kongress der Deutschen Gesellschaft für Ernährung (German Nutrition Society), March 20-22, 2013, Bonn, Germany

Waldschmitt N, Berger E, Rath E, Haller D. *The Ambivalent Role of CHOP Signaling in IBD.* 49. Wissenschaftlicher Kongress der Deutschen Gesellschaft für Ernährung (German Nutrition Society), March 14-16, 2012, Freising-Weihenstephan, Germany

Waldschmitt N, Berger E, Rath E, Haller D. *Transgenic and knock-out mouse models – A tool to study inflammatory stress responses.* 4th Seeon Conference (German Society for Hygiene and Microbiology), April 15-17, 2011, Kloster Seeon, Germany

Grants

Travel Grant, GlaxoSmithKline foundation
(21st United European Gastroenterology Week, 12-16 October 2013, Berlin, Germany)

Erasmus Placement Scholarship, 2007
(four-month research period at the University of Murcia, Spain)

Vocational Training Programme for the Highly Talented (Begabtenförderung Berufliche Bildung), Industrie- und Handelskammer Darmstadt, 2003

ERKLÄRUNG

Hiermit erkläre ich, dass ich die vorliegende Doktorarbeit selbstständig angefertigt habe. Es wurden nur die in der Arbeit ausdrücklich benannten Quellen und Hilfsmittel benutzt. Wörtlich oder sinngemäß übernommenes Gedankengut habe ich als solches kenntlich gemacht.

Ort, Datum

Unterschrift